WIDE-BAND, QUASI-ISOTROPIC, KM-RANGE RF ENERGY HARVESTERS FOR PERPETUAL IOT

A Dissertation
Presented to
The Academic Faculty

By

Eui Min Jung

In Partial Fulfillment
of the Requirements for the Degree
Doctor of Philosophy in the
School of Electrical and Computer Engineering

Georgia Institute of Technology

December 2021

WIDE-BAND, QUASI-ISOTROPIC, KM-RANGE RF ENERGY HARVESTERS FOR PERPETUAL IOT

Approved by:

Dr. Manos M. Tentzeris, Advisor
School of Electrical Engineering
Georgia Institute of Technology

Dr. Andrew F. Peterson
School of Electrical Engineering
Georgia Institute of Technology

Dr. Gregory D. Durgin
School of Electrical Engineering
Georgia Institute of Technology

Dr. Saibal Mukhopadhyay
School of Electrical Engineering
Georgia Institute of Technology

Dr. Wang-Sang Lee
Department of Electrical Engineering / Engineering Research Institute
Gyeongsang National University

Date Approved: December 17, 2021

ever wandering, upon a wave not leading to any path

the boat moves along, while simply drifting

live on like so, now as two people

destination is unknown

aimerrhythm

Credit goes to my family.

ACKNOWLEDGEMENTS

Special mention goes to the dissertation committee members, colleagues, Dr. Rushi J. Vyas (University of Calgary), Dr. Yogesh B. Gianchandani (University of Michigan), Dr. Keith Riles (University of Michigan), Dr. Stella W. Peng (City University of Hong Kong), Dr. Il-Joo Cho (Korea Institute of Science and Technology), Dr. In-Cheol Park (Korea Advanced Institute of Science and Technology), Dr. Amanda M. Holland-Minkley (Washington & Jefferson College), Dr. Daniela Staiculescu (Georgia Institute of Technology), and Christina M. Bourgeois (Georgia Institute of Technology).

TABLE OF CONTENTS

LIST OF TABLES

LIST OF FIGURES

SUMMARY

This research demonstrates, through real-world field-tests, an ambient RF (radio frequency) energy harvesting system, fabricated on low cost FR4 (flame retardant 4), capable of harvesting from all surrounding UHF-TV (ultra high frequency television) and FM (frequency modulation) towers across km ranges in all UHF-TV and FM frequencies simultaneously to perpetually power a WSN (wireless sensor node). The broader impact of this research is to encourage researchers in the field to focus their efforts on real-world usability, thereby advancing ambient RF energy harvesting towards widespread adoption.

The system achieves -10 dB matching across the entire frequency bands. The FBW (fractional bandwidth) is as wide as 31 % for the UHF-TV portion and 23 % for the FM portion. For UHF-TV, front and rear antenna gains combined is 1 or greater across all θ and ϕ, allowing isotropic harvesting (omnidirectional for FM). The RF-dc efficiency is as high as 70 % (56 % for FM). The system is as sensitive as -18 dBm (-17 dBm for FM). The UHF-TV portion harvested as much as 231 μW across 5.83 km (885 μW across 1.53 km for FM). The alignment-free, channel-agnostic nature demonstrates potential for ambient RF energy harvesting's adaption by users outside of the RF community who are not expected to be familiar with antenna alignment and frequency selection.

CHAPTER 1
INTRODUCTION

1.1 Introduction

Energy harvesting saves labor costs associated with replacing batteries of WSNs and internet-of-things (IoT) devices and allows them to be deployed in hard-to-reach places (e.g., hazardous areas, complex structures, sealed systems, etc.) where replacing batteries would be impractical. It reduces the environmental impact associated with battery production and disposal. RF harvesting is available day and night [1] and can be implemented in tandem with photovoltaic harvesting to complement each other [2, 3, 4, 5]. Long wavelengths (sub-GHz) of UHF-TV and FM broadcast signals allow less attenuation through mediums and enable appropriately sized antennas to harvest more energy without needing to form arrays [6]. They are widely available especially in urban areas.

This document proceeds with Chapter 2 to discuss previously published efforts by researchers in the field of ambient RF energy harvesting and outlines current challenges. Chapter 3 explains how this research overcomes these challenges by presenting a full-FM-band, omnidirectional, km-range ambient RF energy harvesting system. Chapter 4 describes the extension of the FM harvester work including an antenna printed on a window glass. Chapter 5 presents a further advancement which combines the FM harvester with a full-UHF-TV-band, quasi-isotropic, km-range ambient RF energy harvesting system. Chapter 6 discusses the UHF-TV harvester portion in more detail, diving into the design strategy and future work. Chapter 7 recapitulates the outcome of this research.

CHAPTER 2

PREVIOUS EFFORTS IN THE FIELD OF RF ENERGY HARVESTING

2.1 Antennas

Maximizing the amount of harvested energy has been a common goal of RF energy harvesting efforts especially with far-field ambient RF power density being relatively low at around 1 μW/cm^2 compared to other sources such as sun light at around 100 mW/cm^2 [7]. Antenna is the first building block of an RF energy harvesting system and converts incident wave into electric current. It is difficult to design an antenna that simultaneously achieves wide bandwidth, wide beam-width, high efficiency, and compact size [8, 6]. Aspects of the antenna must be prioritized according to one's strategy for maximizing the amount of harvested energy.

Prioritizing wide bandwidth is one way to maximize the amount of harvested energy, as a wider spectrum allows the transmitter signal to carry more power. Such antenna can also receive power from multiple transmitters broadcasting in different frequencies within the frequency band of interest. This ability becomes especially useful for ambient harvesting when the antenna is designed to have wide beam-width or even omnidirectional/isotropic reception. An omnidirectional antenna would be able to harvest energy from all surrounding broadcasting towers. [9] proposed a crossed bow-tie directional antenna for wide-band energy harvesting. [2] incorporated a wide-band monopole with wide beam-width, albeit not omnidirectional. [10] utilized a relatively wide (210×36 mm^2) dipole to achieve a bandwidth of 512–566 MHz, although it functioned as a directional antenna due to it being horizontally orientated to receive horizontally polarized UHF-TV broadcasting signals. Similarly, the omnidirectional antenna of [11] functions as a directional antenna due to polarization. It should be noted that the antenna's -10 dB matching band does not coincide

with the intended operation frequencies, contradicting its wide-band claim. A wide-band antenna must be accompanied by a wide-band matching circuit to take advantage of its wide-band harvesting ability. The work mentioned here were unfortunately not accompanied by matching circuits that can fully utilize the bandwidths of the antennas. [12, 13] provided matching that accommodates the bandwidth of their antenna, but they did not achieve -10 dB matching across their entire claimed frequency band of 0.47–0.88 GHz.

Prioritizing high-gain can maximize the amount of power received from a single source. This approach has the advantage of being able to receive higher amount of power at further distances from the source. Characterization is more straightforward as it only involves receiving power from a single tower. Design is also less challenging because it does not need to be accompanied by a wide-band matching circuit. However, carefully aligning the antenna with calibration equipment during every installation can be impractical when deploying in mass scale, when the broadcasting tower is visually obstructed, or when it is unknown which of the surrounding towers provide the most power to each harvester location [1, 14, 15]. Careful installation process must be repeated every time an antenna becomes out-of-alignment, which may defeat the purpose of not having to replace batteries.

LPDA (log-periodic dipole array) is a popular choice because it can be designed to have high directivity and wide bandwidth [16]. [17] designed an LPDA with a peak gain of 7.3 dBi and bandwidth of 512–566 MHz, which was suitable for receiving 17 μW from a single tower broadcasting on multiple channels at 6.3 km away. [18, 19] designed an LPDA to receive 62.5 μW from a tower broadcasting a 539 MHz signal at 4.2 km away. [20] used a commercial LPDA with 5 dBi gain to receive 60 μW from a tower broadcasting on channel 48 (674–680 MHz) at 4.1 km away. As with the case of those antennas that focus more on wide bandwidth, these LPDAs were not accompanied by matching that can fully utilize their bandwidth. Other highly directional choices of antennas include patch antennas [5, 21] and loop antennas [22, 15].

Prioritizing compactness is often for practical reasons. The size of the antenna may be limited by usability concerns or by manufacturing capabilities. Miniaturizing antenna naturally compromises bandwidth and efficiency [8, 6]. Compact antennas designed to harvest in the AM broadcast band are good examples as the relatively long wavelengths of the band pose usability and manufacturing challenges. [23, 24] incorporate ferrite to miniaturize their long-wavelength antennas. When size is less of a concern, the larger apertures of longer-wavelength antennas allow more power to be received in an environment with an equal amount of power-density. For shorter wavelengths, forming arrays can mitigate the effect of decreased aperture [25, 26].

Multi-band antennas garnered significant interest as a method to combine power from multiple frequency bands. Multi-band solutions can be more practical than wide-band solutions depending on the required bandwidth, especially considering the fact that they do not need to be accompanied by wide-band matching (although they do require multi-band matching). Similarly to wide-band antennas, multi-band antenna configurations often compromise efficiency due to the need to accommodate multiple frequency bands within their apertures. Multi-band antenna examples include [27, 28, 29].

Polarization is another concern in designing antennas for ambient RF energy harvesting. FM broadcasting signals are horizontally and vertically polarized in general. A vertical dipole with full bandwidth coverage can receive power from all surrounding FM towers (as this research demonstrates [30, 31, 32]). Addition of horizontal polarization would capture additional power. UHF-TV broadcasting signals on the other hand are typically horizontally polarized. Most UHF-TV harvesting antennas are thus horizontally polarized. Addition of vertical polarization would allow reflected waves to be captured. North-south and east-west polarized antenna with full bandwidth coverage would receive power from all surrounding UHF-TV towers. The idea of two crossed dipole antennas operating independently has been discussed [33]. This research demonstrates combining power from north-south and east-west polarized antennas to achieve quasi-isotropic harvesting [34].

2.2 Matching Networks

An antenna converts incident wave into electric current. The rectifier connected to the antenna converts the RF electric current to dc. When an RF signal encounters an interface between two different impedances, a portion of the signal is reflected back to the source rather than being fully transmitted. This loss of energy degrades the harvester's efficiency. Impedance matching the antenna and the rectifier is critical to maximizing power transfer.

Matching at a single frequency can be achieved by a single element or a two-element network [35, 36]. Previous RF energy harvesting efforts largely focus on single individual frequencies, and therefore resort to such simple matching schemes [5, 22, 14, 15, 21, 23, 25, 26, 37, 38, 39], including those that incorporated relatively wide-band antennas [2, 10, 17, 20]. It is even possible to forgo matching by designing an antenna to have an intrinsic impedance that matches to the rectifier [40], although it can alternatively be perceived as the antenna feed serving as the matching network.

Multi-band harvesters require multi-band matching in addition to multi-band antennas. These typically make use of matching networks that resonate at multiple frequencies [27, 11, 28, 29, 41]. Their main focus is on increasing the number of single-tone frequencies at which matching is achieved rather than widening the bandwidth.

[12, 13] provided matching that accommodates their wide-band antenna, but they achieved -10 dB matching within their claimed frequency band of 0.47 GHz - 0.88 GHz at -1 dBm of input power, which is over 2500 times higher than the average ambient power they measured at the test location (-35 dBm). [42, 43] presented rectifiers that achieve approximate -5 dB octave matching (470 MHz - 990MHz) at -10 dBm and approximate -2 dB decade matching (250 MHz - 3 GHz) at 10 dBm. The high level of S_{11} threshold and input power required to achieve wide-band matching highlight the difficulty of wide-band matching.

2.3 Rectifiers

The rectifier receives, through the matching network, the RF electric current generated by the antenna and converts to dc. Most electronics in WSNs and IoT devices require dc to operate. If they need regulated power, power management circuitry is placed between the rectifier and the load device.

The principle of rectifiers typically used for RF energy harvesting is RF-to-dc conversion using diodes, so the choice of diodes greatly affects the performance of the rectifier. Schottky diodes have been the dominant choice for low power ambient RF energy harvesting due to their low forward voltage compared to PN diodes as well as process maturation resulting in low cost and wide availability. Low junction capacitance and turn-on voltage are favored for high-frequency and low-power applications when choosing Schotty diodes, respectively. The maximum responsivity of Schottky diodes due to thermal voltage limitation has been reached in as early as the 1960s. Emerging diode technologies such as tunnel diodes have potential to surpass Schottky diodes once the process matures as they can achieve higher responsivity and lower junction capacitance [44, 45].

One of the most simple forms of rectifier topology is a series diode accompanied by a capacitor (or inductor) filter, examples of which are featured in [2, 5, 11, 15, 23, 37, 41]. A single shunt-diode configuration is an alternative as seen in [14, 40]. Voltage multiplier is a popular choice as it rectifies RF-to-dc and also increases the output potential. This is useful because the output potential may otherwise be too low to drive the device connected to the output of the rectifier. [22, 12, 21, 28, 38, 43] are examples of previous work that incorporate voltage multipliers. Cascading voltage multiplier stages further increases the output potential to meet the requirement of the device connected to the output of the rectifier, but the additional components increase leakage and insertion loss, compromising efficiency [1, 44]. The examples of previous work that utilize cascaded voltage multipliers include [10, 17, 18, 19, 20, 29, 39, 42].

2.4 Power Management Units

The rectifier output potential of an RF energy harvester typically varies depending on factors such as moving obstruction between the signal source and the harvester antenna. WSNs and IoT devices typically require more stable input potential. Few devices can inherently feed on widely varying potential, and some integrate power management circuitry. In most cases, a PMU (power management unit), which regulates the potential received from the rectifier, is necessary.

PMUs can also be used to effectively lower the potential requirement of the load device by boosting the rectifier output potential to the level required by the load device. It can be an alternative solution to voltage multipliers and can keep the rectifier design simpler. [4, 27, 11, 15, 23, 37, 46, 47] feature PMUs in their systems, all of which are capable of boosting potential.

The load device would not be able to operate if the power received by the antenna and transferred to the output of the PMU is consistently lower than the amount required by the load device. With charge cycling, the PMU stores the harvested energy (for example, in a reserve capacitor) and releases to the load device when enough energy is collected. When the energy is depleted, the PMU stops supplying power to the load device and the cycle repeats, allowing the load device to operate periodically. These "enough" and "depleted" thresholds are typically determined by the reserve capacitor potential. Charge cycling allows devices to operate in lower-power-density environments or at further distances from their energy sources as long as the available power is enough to operate the circuitry responsible for charge cycling. It also serves to maintain stable power delivery during momentary interruptions. [27, 15, 46] utilize the charge cycling ability of the Texas Instruments BQ25504 commercial solution, and [17, 23] implement charge cycling in their custom power management systems.

Commercial power management solutions offer reliability as they have undergone testing for quality control and allow researchers to focus their effort and time in innovating other parts of the harvesting system. They may support a wide range of operating conditions and multiple energy sources including photovoltaic, thermoelectric, and piezoelectric energy. Custom-designed PMUs on the other hand allow researchers to specifically tailor the PMU characteristics to be optimized for their targeted testing scenarios, often able to increase efficiency under their operating conditions [1]. [11, 17, 23, 37, 38, 47] feature specifically designed power management system in their work. [48] was able to achieve -25 dBm sensitivity largely due to their custom-designed PMU which has low input power and potential requirements.

2.5 Field Tests

Relatively few reports provide detailed field-testing results. Sometimes, it is because their work focus on individual harvester building blocks and they do not have complete systems required to conduct field testing. Other times, it may be because they consider detailed field testing to be outside of their scope of work. There are countless examples of previous efforts that only provide laboratory testing results. Some researchers only provide simple proof-of-concept field-test results, such as reporting the rectifier output potential across a capacitor [22, 23, 28, 49], a resistor [12, 18, 50], or an open load [16]. [24] simply claimed that their test was successful.

Few research efforts provide more detailed field-testing results. These details may include the exact locations of the harvester and the broadcasting tower(s), the power spectrum at the harvester location, the amount of power harvested throughout a day, the amount of outside ambient RF energy harvested while being indoors, and device uptime and downtime due to charge cycling. Conducting field tests while powering a WSN/IoT device adds to the complexity. Powering such device is usually not as simple as quoting the instantaneous peak power measured at the rectifier output, because such device typically requires stable supply of power for an extended period of time and its power consumption may fluctuate in time. Confirmation must be provided as to whether such device functions as intended while being powered by the harvester in the field. Powering such device, with or without PMU, imposes requirements in terms of the minimum power and voltage that the harvester must supply. High figure-of-merits achieved without these constraints have little significance, and such systems are unlikely to provide useful function.

[17] harvested 17 μW from a UHF-TV tower broadcasting on nine UHF-TV channels at 6.3 km away and powered an MCU (micro-controller unit) with 60 s downtime for every 2 s uptime. [20] harvested 60 μW from a 960 kW UHF-TV tower at 4.1 km away and continuously powered a wired temperature/humidity meter. [19] powered a WSN at 4.2 km away from a 1 MW UHF-TV tower to measure temperature and light level "at a rate of nearly 1 Hz over a 5.5 hour interval." The collected power was 62.5 μW, albeit using a different harvesting system [18]. [15] harvested a maximum of 5.5 μW from the GSM900 band inside of a building at Imperial College London and powered an LED with 8 s downtime for every 13 s uptime.

2.6 Challenges

Following challenges currently faced by the field of ambient RF energy harvesting are apparent from the preceding review of previous efforts.

- Wide-band antennas and matching networks of compatible bandwidths are rarely mated together and thus unable to take advantage of more power being carried through a wider spectrum. Previous work that achieved wide-band matching did so at high input power or at high S_{11} level.
- The standard high-directivity/narrow-beam-width approach requires meticulous alignment for every installation and maintenance. The ability to harvest from multiple broadcasting towers is limited by narrow beam-width and narrow bandwidth.
- Without detailed field testing, whether the presented solutions will operate as intended in the real world is questionable. The lack of operability/usability validation through field testing may be one of the causes hindering widespread adoption of ambient RF energy harvesting despite the abundance of publications being produced in the field.

The following chapters demonstrate how this research overcomes these challenges.

CHAPTER 3
THE FULL-FM-BAND, OMNIDIRECTIONAL, AMBIENT RF ENERGY HARVESTER

3.1 The FM Energy Harvester Antenna Design

Gain of a wide-band antenna is limited by its dimensions [6], requiring a full-bandwidth FM harvesting antenna to have an appropriate size. The relatively long wavelengths of FM broadcasting signals enable appropriately sized antennas to harvest more energy without needing to form arrays. More compact antennas exist for listening to FM radio broadcasts, but these audio systems typically require a separate power source to boost the received signal. These ESAs (electrically small antennas) would be counter-intuitive in an energy harvesting system.

Fig. 3.1 shows three bow-tie antenna designs. A classic bow-tie antenna (design1) has a shorter segment a, a longer segment b, and infinitesimal segments of intermediate sizes between a and b. These segments resonate at different frequencies, allowing broadband operation. The bandwidth of the bow-tie antenna can be increased by increasing the thickness of the antenna at its ends, additionally creating segments between b and c (design2). However, its S_{11} becomes less steep in the frequency band of interest as its current distribution becomes less focused. The difference between the simulated S_{11} of the two antennas can be seen in Fig. 3.2. A full-wave electromagnetic simulation tool (CST Microwave Studio) was used for simulation. Such wide-band antenna is more resilient to influences from nearby objects and better retains the ability to operate at the desired frequencies.

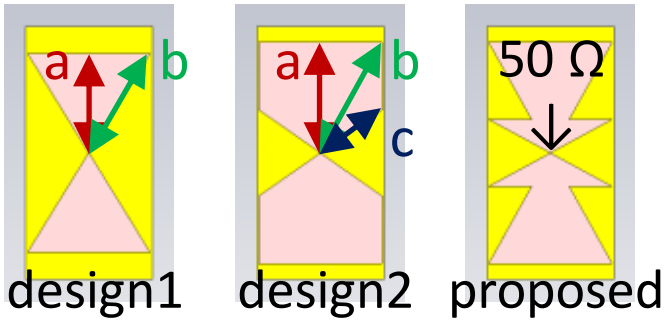

Figure 3.1: The FM harvester antenna in comparison to more traditional triangular sheet antennas.

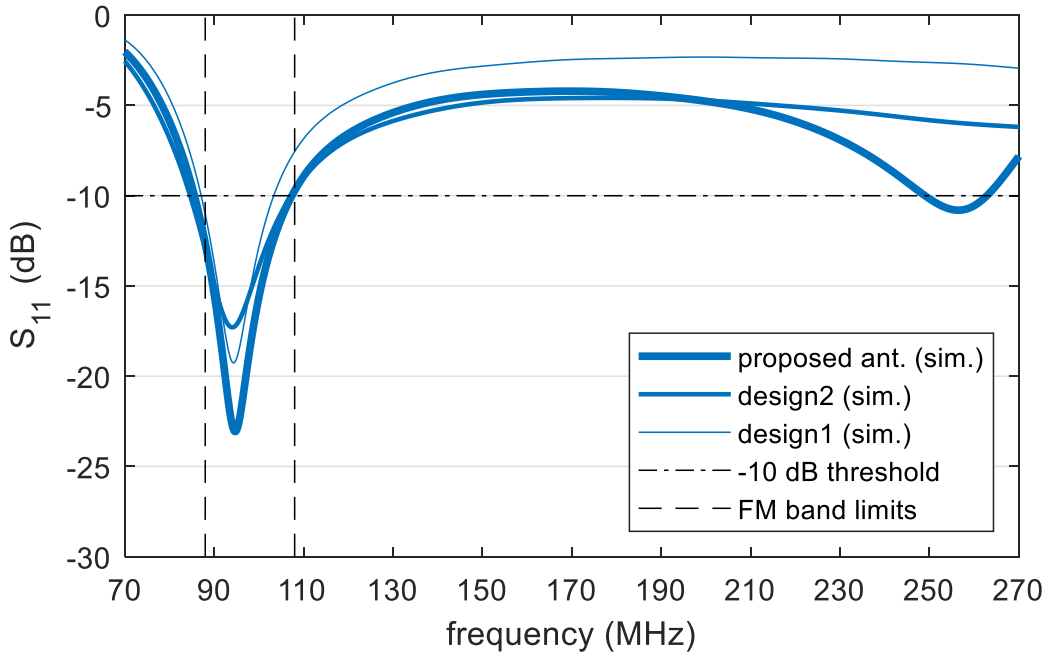

Figure 3.2: Simulated S_{11} of the FM harvester antenna in comparison to more traditional triangular sheet antennas.

To widen the bandwidth while simultaneously preserving the steep S_{11}, the proposed antenna creates another resonance point outside of the frequency band of interest by transposing a smaller bow-tie on top of the classic bow-tie antenna (Fig. 3.1). Fig. 3.2 shows the two resonance points in the S_{11} simulation result for the proposed antenna. The resonance point at higher frequencies stretches the original S_{11} dip to be wider and deeper.

Eight panels of MG Chemicals 521 FR4 substrates (35 μm single-sided copper cladding, $304 \times 304 \times 1.6\,\text{mm}^3$ per panel FR4, $\epsilon = 4.2$ and $\delta = 0.015$ at 1 GHz) were joined together to fabricate the proposed antenna. The panels were individually drawn by hand using a masking pen. The copper layer pattern was etched in ferric chloride baths. The masking layer was subsequently removed. Electrical connection between panels were formed using solder. An SMA (sub-miniature version A) connector was soldered at the feed point of the antenna. The overall metal outline is $1064 \times 592\,\text{mm}^2$ ($0.35 \times 0.19\,\lambda^2$). Fig. 3.3 shows detailed dimensions of the proposed antenna. A $4 \times 4\,\text{mm}^2$ area was subtracted from the otherwise two touching vertices of metal triangles to form the 4 mm-gap feed point. Impedance value of $50\,\Omega$ was chosen to allow the system to be compatible with characterization equipment designed to work with $50\,\Omega$ devices. Selecting a value that optimizes the RF-dc η (efficiency) and bandwidth would be another option.

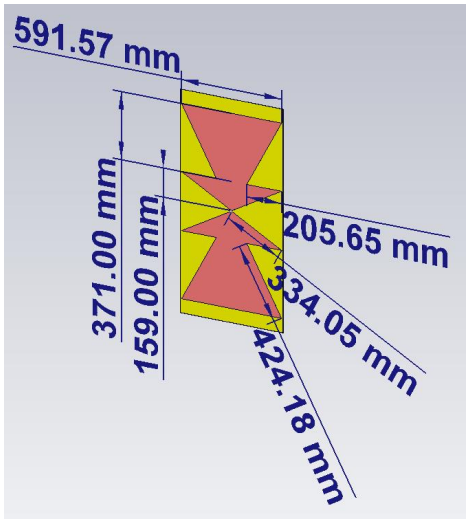

Figure 3.3: The dimensions of the FM harvester antenna.

Keysight N9923A was used to measure the S_{11} of the proposed antenna in an anechoic chamber. The result is shown in Fig. 3.4. For comparison, the figure includes measurement results for a commercial reference antenna (Diamond SRH789) as well as the simulation results for the three antenna design variations. The measured S_{11} of the proposed antenna achieves $<$ -10 dB across the entire FM broadcasting band. The -10 dB matching FBW for the antenna is 29 %. In comparison, the measured S_{11} of the reference antenna achieves $<$ -10 dB in only about half of the FM broadcasting band. Anritsu MS46522B VNA (vector network analyzer) was used to measure the realized gain of the proposed antenna. The results are shown in Fig. 3.5. The proposed antenna has higher measured gain across the entire FM broadcasting band (2.0 dBi) than the reference antenna.

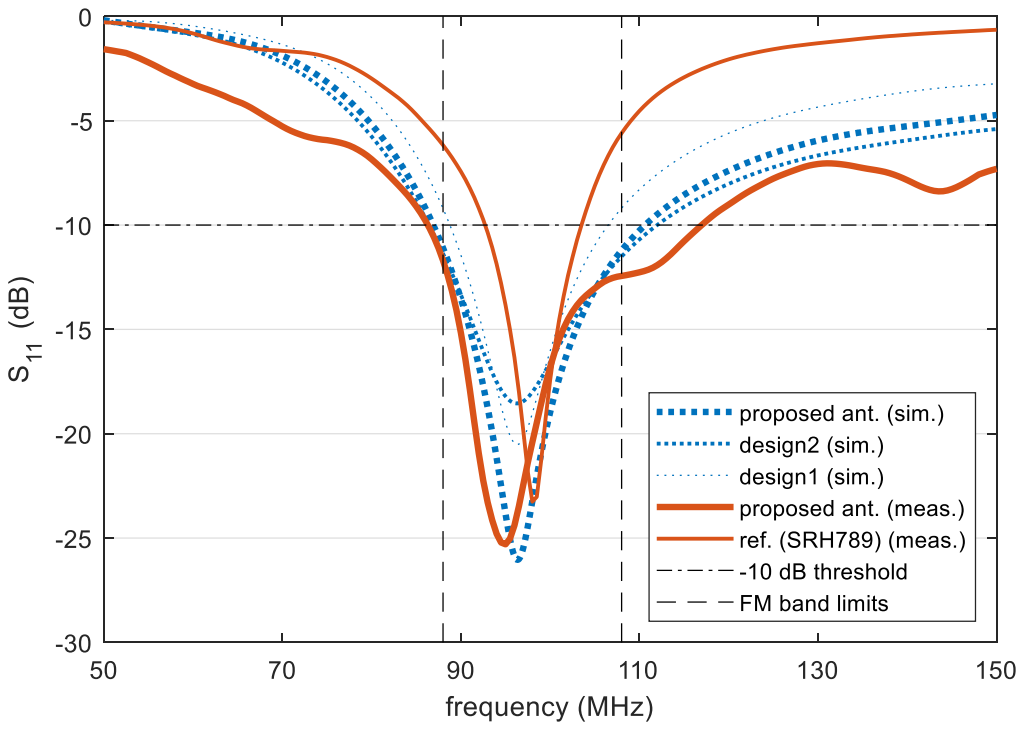

Figure 3.4: Simulated and measured S_{11} of the harvester antenna across the FM band.

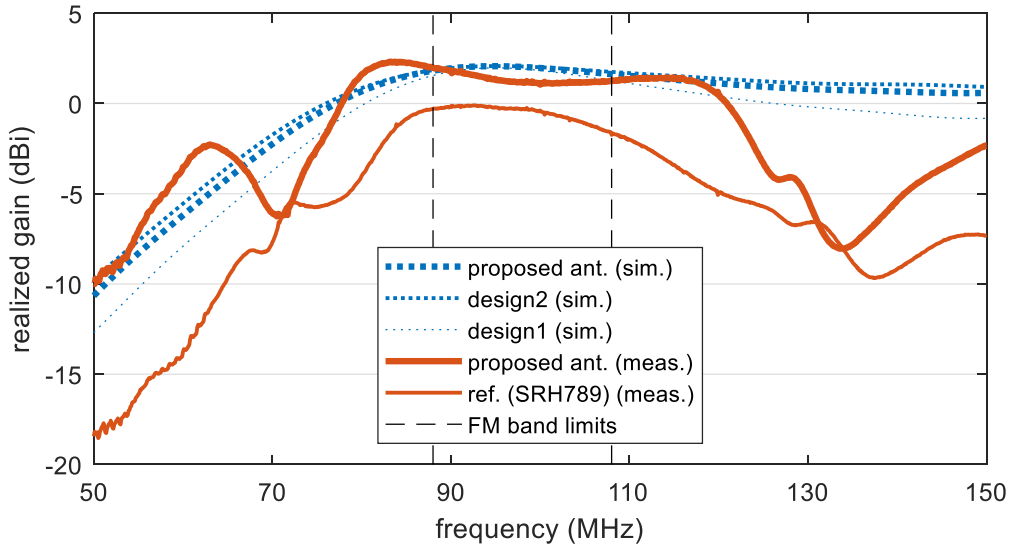

Figure 3.5: Simulated and measured realized gain of the harvester antenna across the FM band.

Fig. 3.6 shows simulated (top) and measured (bottom) realized gain of the proposed antenna. Gain is in dBi and angle is in degrees. Omnidirectional reception is achieved when realized gain ≥ 0 dBi in the azimuth plane, i.e., the antenna is capable of harvesting energy from all surrounding broadcast towers. The simulation and the measurement results show the omnidirectional pattern of the proposed antenna, with the realized gain in the azimuth plane > 0 dBi in all directions across the entire FM broadcasting band.

3.2 The Matching Circuit Design

Lumped-element matching rather than transmission-line or stub matching is used, because the relatively long wavelengths of the FM broadcasting band (approximately 3.4 m for the lowest frequency) may otherwise result in metal trace sizes that are not practical for sample fabrication. A combination of alternating series inductors and shunt capacitors is used as it can theoretically match an impedance that is anywhere on the Smith chart [35, 36]. With fixed pad layout and component types, the component values can be iteratively optimized while taking into account the parasitic effects of the pad layout.

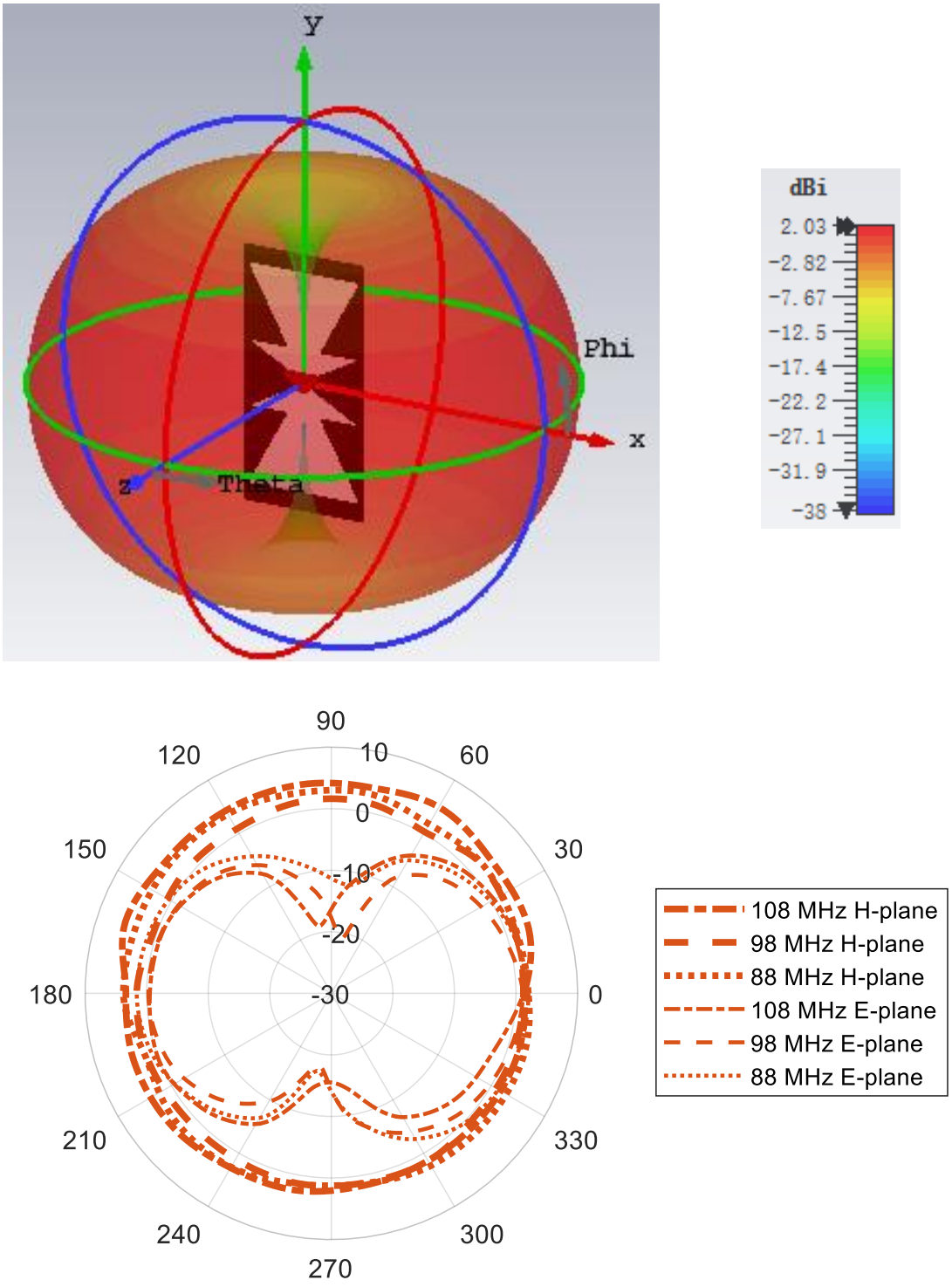

Figure 3.6: Simulated and measured realized gain radiation pattern of the FM harvester antenna.

Keysight ADS (Advanced Design System) was used for simulation. The pad layout for the lumped components were drawn based on the dimensions of the lumped components. The gap between the pads is 0.3 mm, and the overall board dimension is 51.8×11 mm^2. The width of the metal trace was set to be 3 mm to yield 50 Ω impedance, although the entire matching network assembly is electrically small compared to the wavelengths of the FM broadcasting band. Vias connect the ground pads to the backside copper layer which covers the entire backside of the board. A model representing the parasitic effects of the board layout was generated and was incorporated into the simulations. The lumped-element values were first determined by mathematically solving for the series and shunt reactance values. These were used as initial values for the optimization algorithm. The optimization algorithm of the simulation software was configured to select among the manufacturer provided S-parameter files representing the lumped elements. Optimization was performed while the input power level was set to -20 dBm, which represents the relatively low power density of ambient RF energy [7]. The load at the output of the rectifier was set to 3.3 kΩ to represent the PMU. This is because the input resistance of the PMU was measured to fluctuate around 3.3 kΩ during cold-start and initial charge-discharge cycles. The number of L-network stages was determined empirically through simulation.

The S_{11} simulation results for the matching network are shown in Fig. 3.7 and Fig. 3.8. At an input power level of -20 dBm, the S_{11} is $<$ -17 dB across the FM broadcasting band. At -10 dBm, the S_{11} is $<$ -13 dB within the band. Even at 0 dBm, the maximum S_{11} is approximately -10 dB within the band.

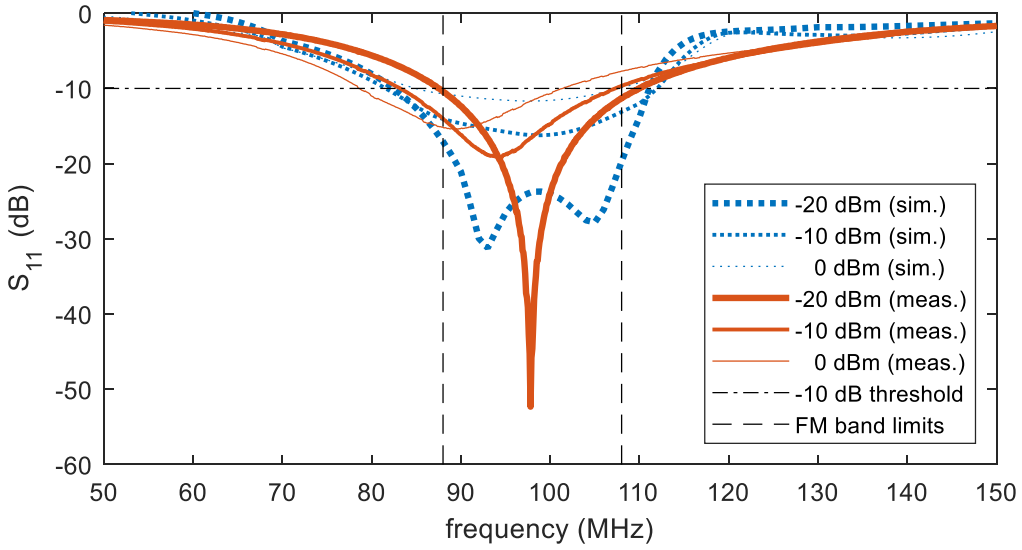

Figure 3.7: Simulated and Measured S_{11} of the FM harvester matching network.

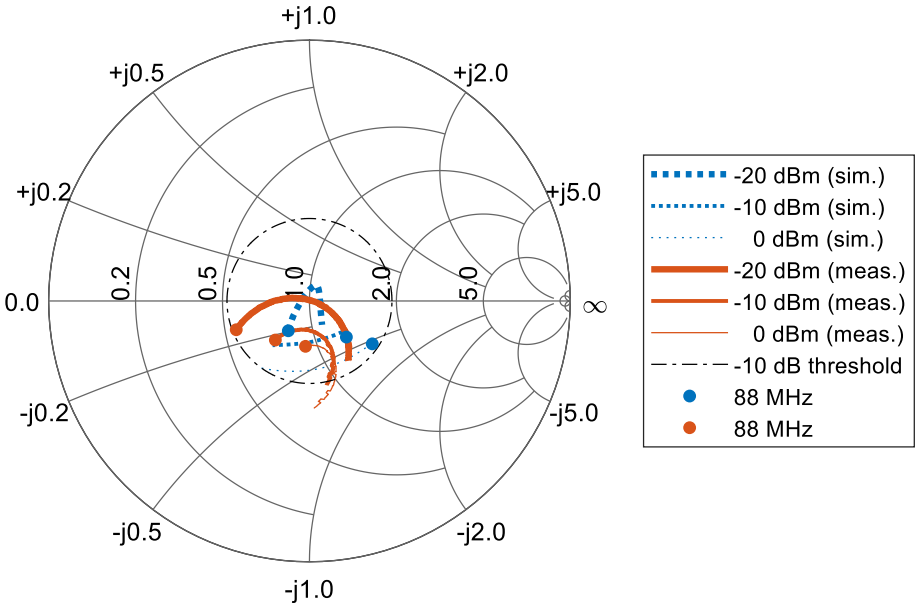

Figure 3.8: Simulated and Measured S_{11} of the FM harvester matching network from 88 MHz to 108 MHz.

The physical sample of the matching network was fabricated using an MG Chemicals 555 substrate. It has double-sided copper-cladding but is otherwise equivalent to the MG Chemicals 521 substrate. SU8 photoresist was inkjet printed using a Fujifilm DMP-2850 printer to form a masking layer for the pad layout. The pattern was etched in a ferric chloride bath. The backside copper was protected to form a ground plane. Via holes were drilled and copper rings were inserted to form connections. Components were soldered on to the board. Anritsu MS46522B VNA was used to measure the S_{11} of the matching network. Two of the lumped elements were replaced with ones that have different values after this initial measurement in order to shift the S_{11} dip from lower to higher frequencies so that it aligns with the FM broadcasting band. Using impedance measurement of diodes in simulation rather than diode model can reduce simulation-measurement discrepancy and the need for post-fabrication adjustments. Further advancement of the harvesting system discussed in Chapter 5 uses this technique. Fig. 3.9 shows a fabricated sample of the matching network. The 510 nH inductor replaced a 680 nH inductor after the initial measurement. A 0.5 pF capacitor was removed from the now vacant space between the 10 pF and 0.3 pF capacitors.

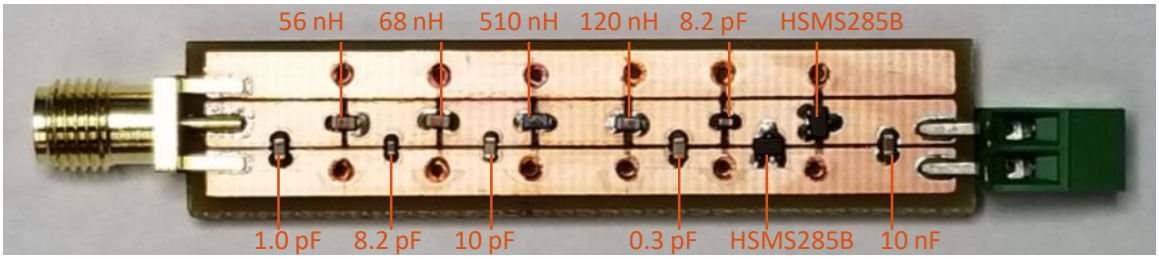

Figure 3.9: The FM harvester matching and rectifying circuit.

The measured S_{11} of the matching network is shown on Fig. 3.7. At an input power level of -20 dBm, the S_{11} is $<$ -10 dB across the entire FM broadcasting band. The -10 dB matching FBW for the matching network is 23 % at -20 dBm. Even at -10 dBm, the maximum S_{11} is approximately -10 dB within the band. At 0 dBm, the S_{11} is $<$ -10 dB for the majority of the band, and the maximum S_{11} is approximately -8 dB within the band. A 3.3 kΩ resistor was connected to the output of the rectifier to represent the PMU.

3.3 The Rectifying Circuit Design

Schottky diodes were chosen for their low cost and wide availability (that result from process maturation) as well as for their performance (low forward voltage). Avago HSMS285B was chosen even though Skyworks SMS7630 has lower series resistance, zero-bias junction capacitance, and ideality factor [44], because simulation results with HSMS285B yielded impedance matching results with wider bandwidth in the FM broadcasting band.

Voltage multiplier topology was chosen to take advantage of the increase in output potential. Fano limit determines the lowest return loss theoretically possible for wide-band matching [51]. The input impedance of the rectifier with varying number of stages was found from simulation while taking into account the varying parasitic effects of the pad layout. The resulting theoretical return loss according to Fano limit indicated that matching is not significantly improved by varying the number of stages. To minimize leakage and insertion loss, a single voltage multiplier stage was used [1, 44].

The rectifier was fabricated together with the matching network. Rectifier measurements were performed by connecting a Rohdes & Schwarz SMJ100A vector signal generator to the input of the matching network, connecting a resistor to the output of the rectifier, and measuring the potential across the resistor with an Agilent 34401A multimeter.

Fig. 3.10 shows the RF-dc η of the matching and rectifying circuit with respect to frequency. The evenness of the curves indicate the consistency of the circuit's performance across the FM frequency band. Maximum RF-dc η of 17 %, 40 %, and 56 % are respectively achieved at -20 dBm, -10 dBm, and 0 dBm. (The minimum RF-dc η are respectively 14 %, 31 %, and 42 %.) Discrepancies between the simulation and measurement results primarily originate from the simulation-measurement discrepancies in the matching network, since the input power to the rectifying circuit is fed through the matching network.

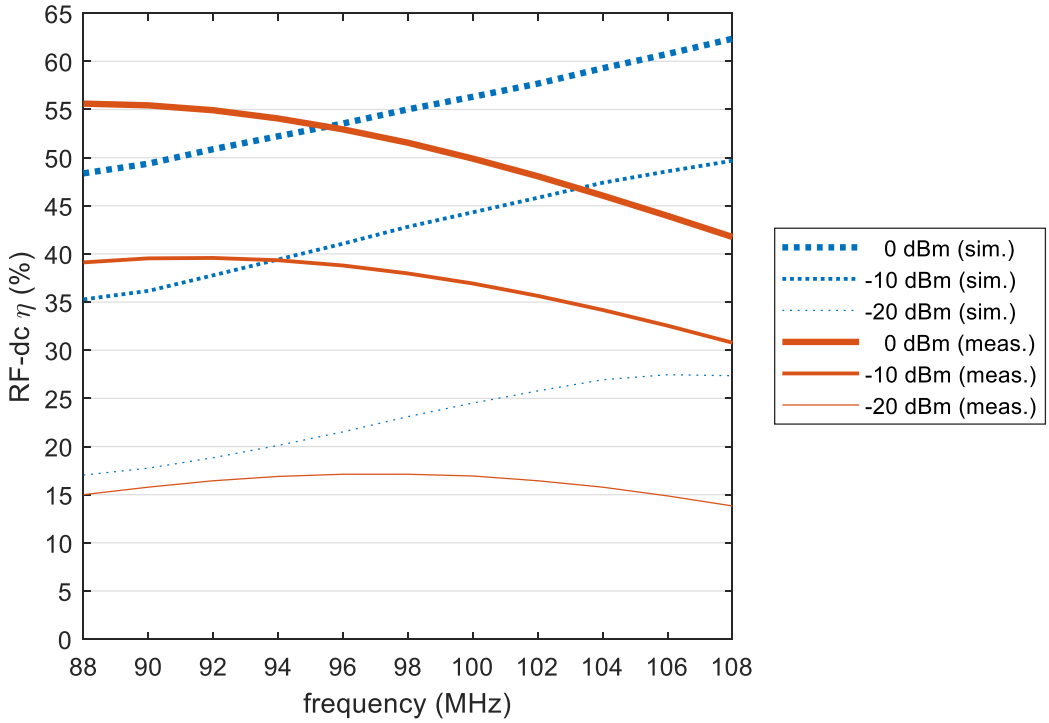

Figure 3.10: Measured RF-dc η of the matching and rectifying circuit in the FM frequency band.

Fig. 3.11 shows the sensitivity of the matching and rectifying circuit in the FM frequency band. The input requirement to operate the PMU is 100 mV and 5 μW (330 mV and 15 μW for cold-start). With a 3.3 kΩ resistor connected to the output of the rectifying circuit, this requirement translates to 129 mV (330 mV for cold-start). Sensitivity was measured by finding the input power level which produces this output potential. The best and worst sensitivity were respectively measured to be -17 dBm and -16 dBm (-11 dBm and -10 dBm for cold-start).

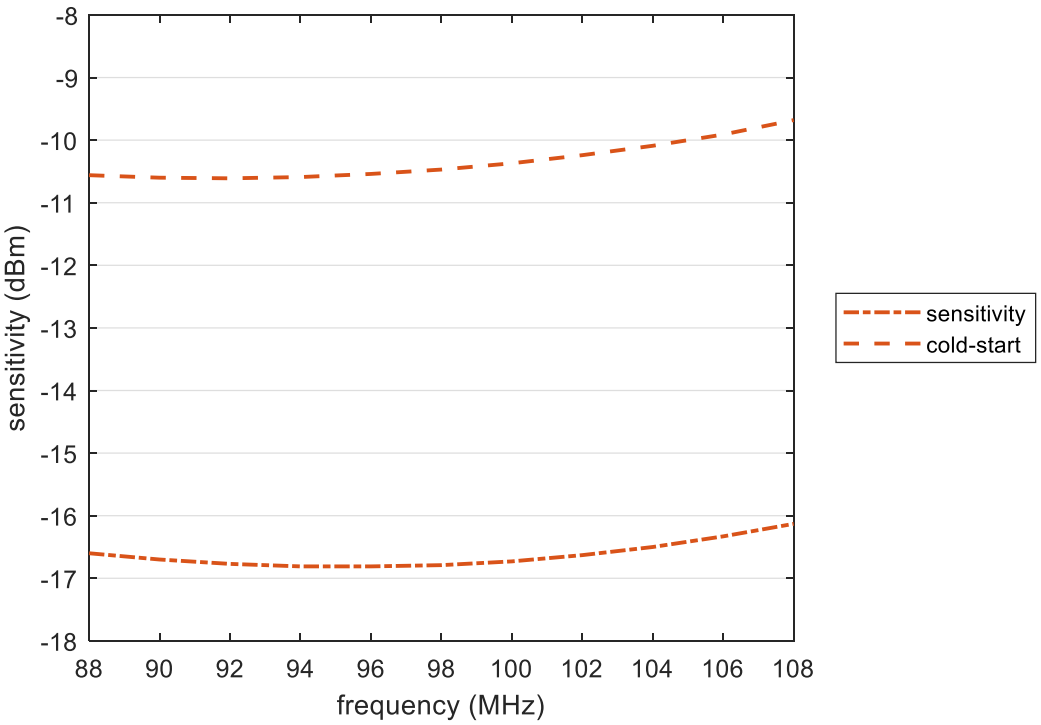

Figure 3.11: Measured sensitivity and cold-start sensitivity of the matching and rectifying circuit in the FM frequency band.

Fig. 3.12 shows the RF-dc η of the matching and rectifying circuit with varying amount of matching network input power. The RF-dc η increases as the input power increases, because the efficiency of HSMS285B improves from -20 dBm to 0 dBm [52]. Optimizing the matching network while setting the input power to 0 dBm instead of -20 dBm would further improve the RF-dc η beyond 56 % but would compromise sensitivity. Fig. 3.13 shows the output potential of the matching and rectifying circuit with varying amount of matching network input power.

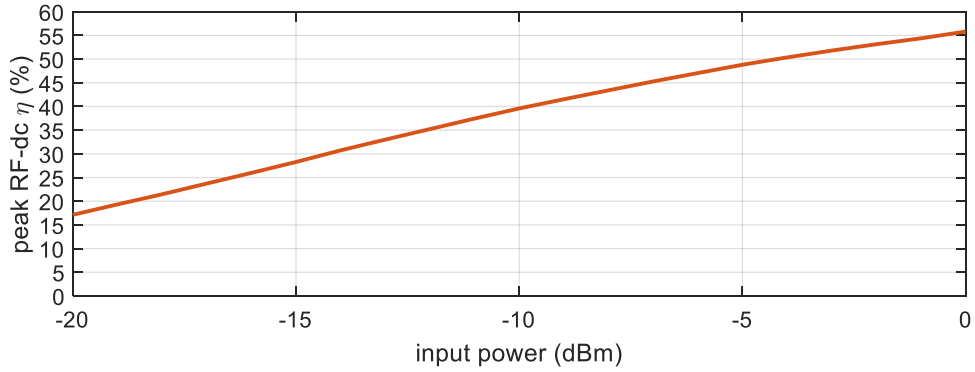

Figure 3.12: Measured peak RF-dc η of the FM harvester with varying power.

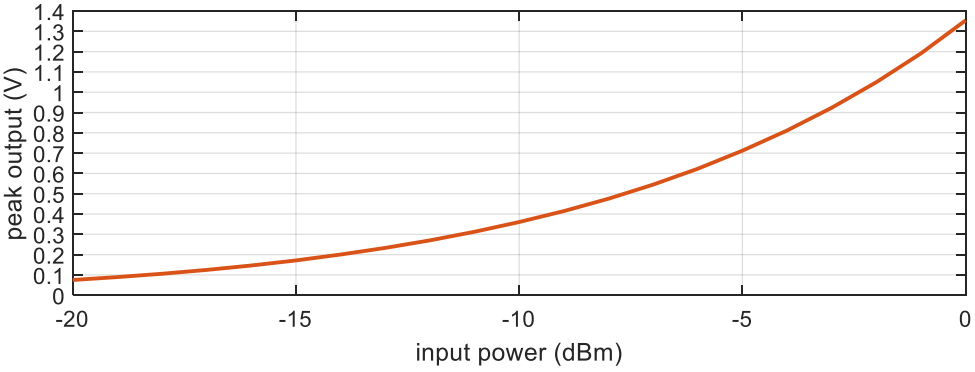

Figure 3.13: Measured output potential of the FM harvester with varying power.

Fig. 3.14 shows the RF-dc η of the matching and rectifying circuit with varying load. It indicates the matching and rectifying circuit's ability to cope with fluctuating load. The highest RF-dc η are achieved with 3.3 kΩ and 10 kΩ. The RF-dc η starts to decrease with 1 kΩ and 33 kΩ but still maintains double-digit values at -10 dBm and 0 dBm.

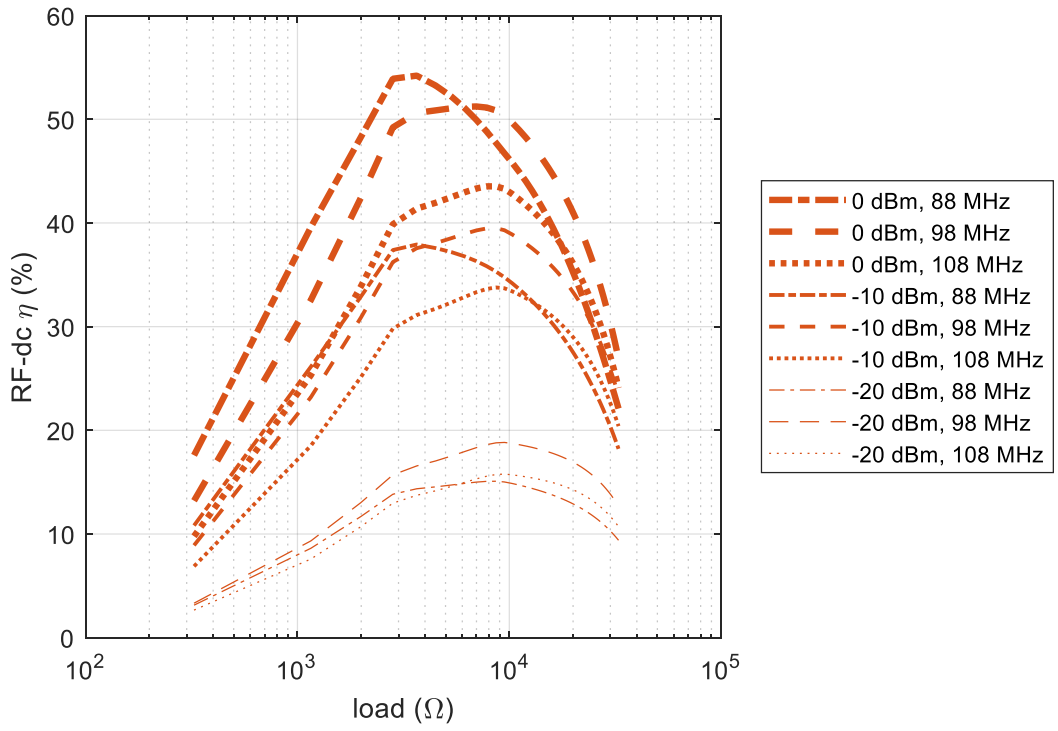

Figure 3.14: Measured RF-dc η of the FM harvester with varying load.

3.4 The Power Management Unit

The PMU is Texas Instruments BQ25570EVM-206. It features charge cycling. The upper and lower thresholds of the reserve capacitor potential were respectively set to 3.2 V and 2.1 V. All other configurations for the PMU were set to default. Three Seiko CPH3225A in parallel were used as the reserve capacitor. When the available ambient RF power density is high enough to power the WSN without needing to periodically shut down, the PMU's charge cycling capability serves to maintain stable power output during interruptions such as momentary obstructions between the broadcasting towers and the harvesting antenna. Otherwise, charge cycling allows the WSN to operate by powering it down periodically. The PMU charges the reserve capacitor during the WSN downtime and uses the stored charge to turn on the WSN. The amount of power available to the PMU must still be enough for the PMU to operate its charge cycling capability.

The WSN is Kontakt.io S18-3. It communicates its temperature and orientation information via Bluetooth. It is connected to the 1.8 V output of the PMU. (It was originally designed to be powered by a 3 V battery.) Its average power consumption during operation was measured to be 141 μW.

Integration of the components from the antenna to the WSN on a single substrate is discussed as a future work in section 6.5.

3.5 System Demonstration

The test site is located at (33.7759, -84.3898) and has both outdoor and indoor areas. The outdoor area is a rooftop. The indoor area has closed walls, windows, doors, a floor and a ceiling. Fig. 3.15 shows the power spectrum measured using the proposed antenna and a Tektronix RSA3408A real-time spectrum analyzer on the rooftop of the test site. The highest contribution (2 dBm) came from 91.1 MHz located 1.54 km away. The full-FM-band, omnidirectional nature of the harvester aggregates power from the entire spectrum, but the fact that the 91.1 MHz signal serves as the prominent source of power allows the harvester's performance to be characterized in terms of the distance from the 91.1 MHz tower. (The second highest peak was 6 dBm less.) The situation is similar indoors. Fig. 3.16 shows the power spectrum measured indoors using the proposed antenna and the same real-time spectrum analyzer at the test site. The highest amount of power received indoors was -4 dBm at 91.1 MHz, and the second highest peak was -11 dBm at 100.5 MHz (a 7 dBm difference).

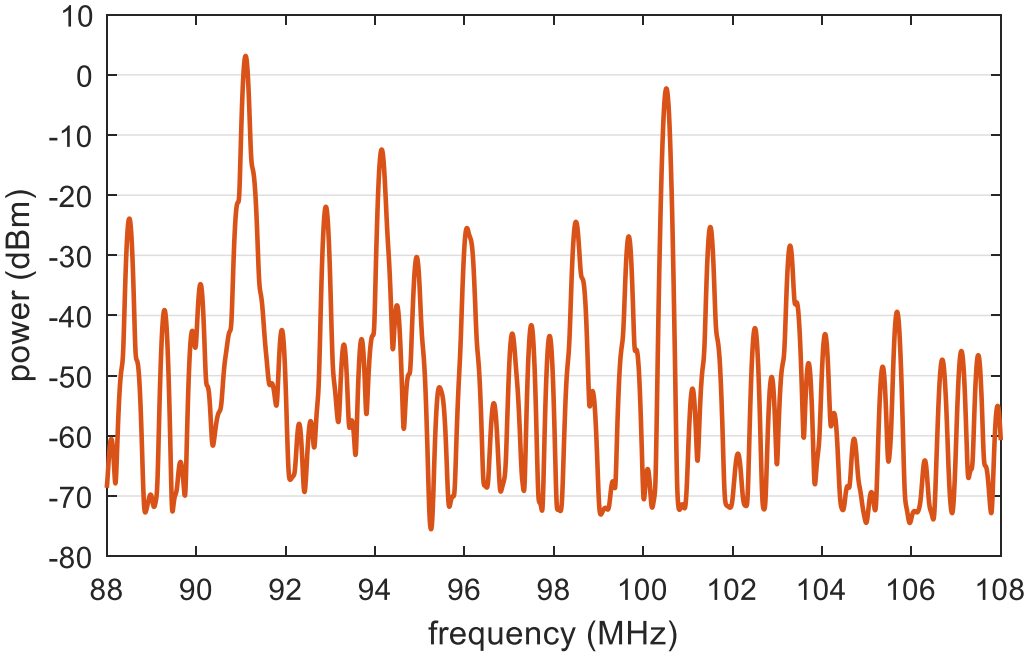

Figure 3.15: Rooftop spectrum measured using the FM harvester antenna at the test site.

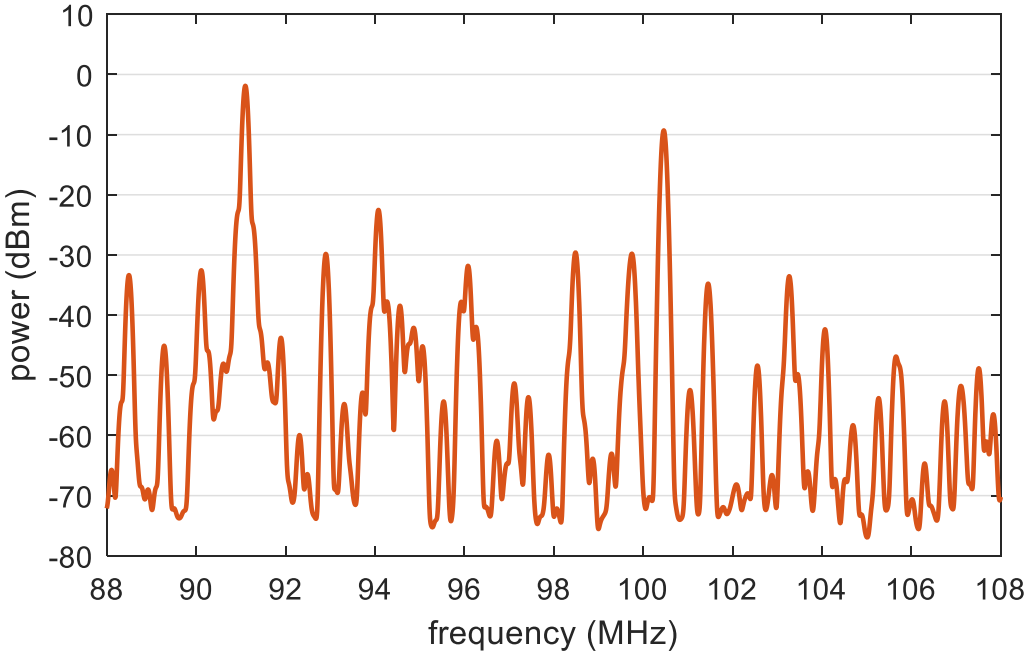

Figure 3.16: Indoor spectrum measured using the FM harvester antenna at the test site.

According to Friis formula, the theoretical amount of power to be received without considering real-world factors (e.g., obstruction) can be calculated from the transmitting power, directivity, wavelength, and distance [53]. This value is 9.8 dBm for the 91.1 MHz 100 kW ERP signal received on the rooftop at 1.54 km away. The directivity of the proposed antenna was taken from simulation to be approximately 2 dBi.

The amount of power harvested by the PMU on the rooftop was measured throughout a day to evaluate the consistency of the harvester performance and to observe any variation in the harvesting environment. Measurements were taken from 10:00 in the morning to 22:30 at night in 2.5-hour intervals. Each time, the system harvested ambient FM energy to charge the reserve capacitor to the upper voltage threshold and to power the WSN. The matching network was then disconnected from the antenna to drain the reserve capacitor to the lower voltage threshold. The matching network was reconnected to the antenna to resume harvesting. While the reserve capacitor was being charged, a multimeter (Fluke 15B+) measured the potential across the input of the PMU and another multimeter (Fluke 17B+) measured the current flowing into the PMU. The voltage and current measurements were used to calculate the amount of power being delivered to the PMU.

Once the reserve capacitor reached the upper voltage threshold again and power was supplied to the WSN, the matching network was disconnected until the reserve capacitor was drained to the lower voltage threshold. This time, the two multimeters were relocated, and then the matching network was reconnected to resume harvesting. The first multimeter measured the potential between the BAT_OK and GND pins. The potential across these pins switches from low to the reserve capacitor potential when the reserve capacitor reaches the upper threshold, allowing the charging duration to be timed. This information was used to calculate the amount of power which was charging the reserve capacitor. The second multimeter measured the potential across the reserve capacitor to monitor the charging progress. The power calculated from the two different methods were averaged to determine the amount of power being harvested by the PMU each time in 2.5-hour intervals.

Fig. 3.17 shows the amount of power harvested by the PMU on the rooftop throughout a day. The most amount of power was 923 μW harvested at 15:00. The least amount of power was 738 μW harvested at 17:30. The average of the six values collected throughout the day was 822 μW. The rectifier output potential was 2.5 V when the maximum amount was collected and was 2.1 V when the minimum amount was collected. The average of the six trials was 2.3 V. The harvested power was enough to cold-start the PMU and to power the WSN without needing to periodically shut down. The WSN was able to communicate its temperature and orientation information via Bluetooth while being powered by the harvester.

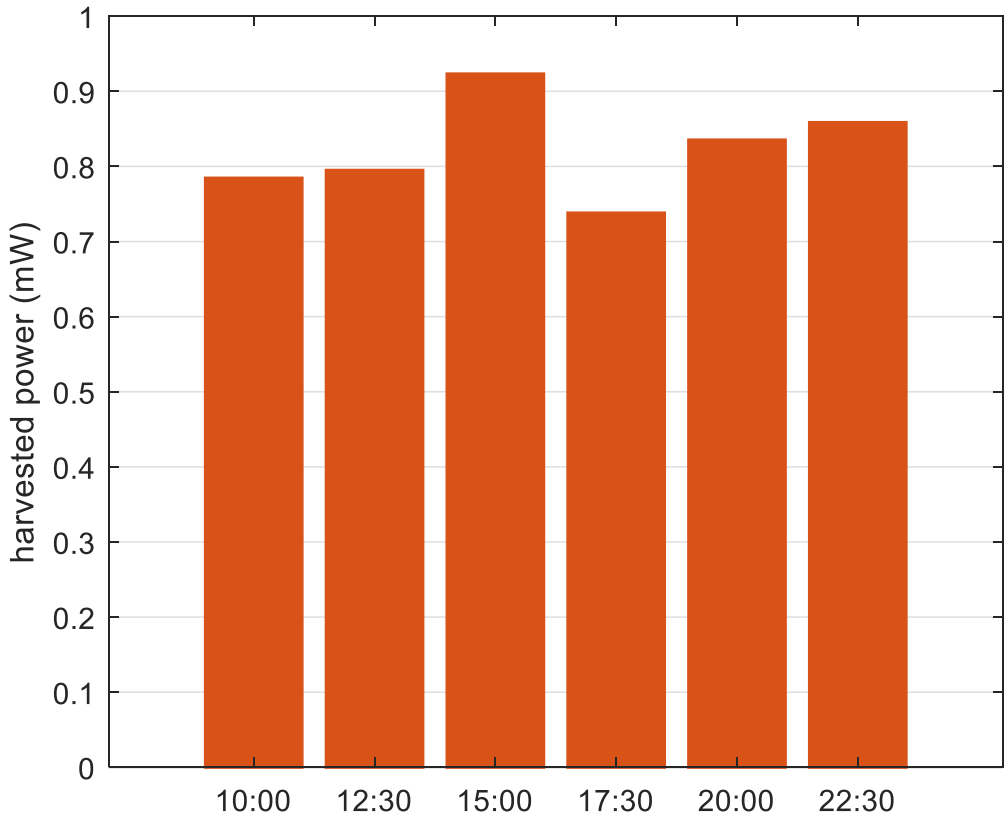

Figure 3.17: Power harvested by the FM harvester on the rooftop throughout a day.

The amount of power harvested by the PMU indoors was measured using the same method except that the measurement was taken on a different day at 15:00. The amount of power harvested indoors was 159 μW, and the rectifier output potential was 1.9 V. It should be noted that the MPPT (maximum power point tracking) feature of the PMU is one of the factors that determine the rectifier output potential and that the potential is not necessarily proportional to the amount of power harvested. Even indoors, the PMU was able to cold-start and power the WSN without needing to periodically shut down. Fig. 3.18 shows photographs of the rooftop (left) and indoor (right) field measurement configurations. It shows the WSN communicating its temperature and orientation information via Bluetooth while being powered by the harvester.

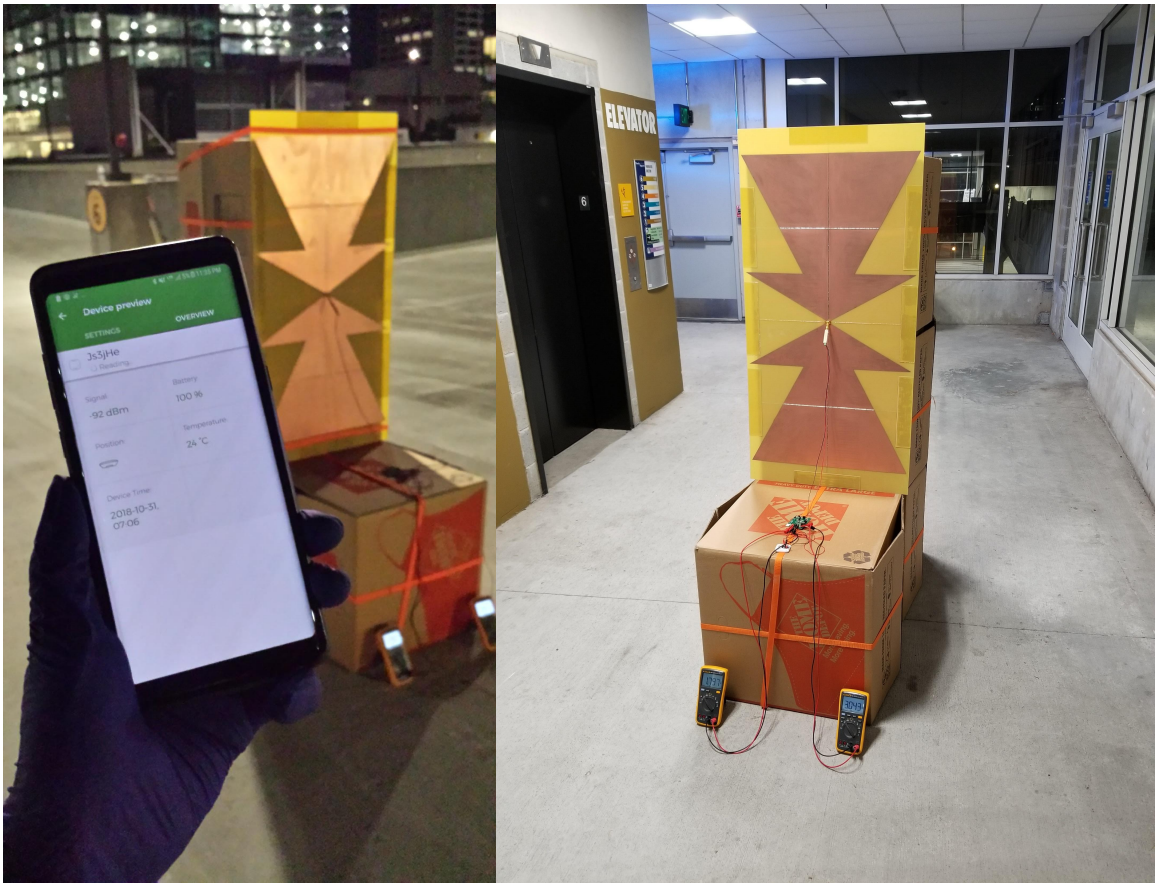

Figure 3.18: The FM harvester rooftop and indoor field measurement configurations.

3.6 Comparison to Related Work

Table 3.1 compares a list of ambient RF energy harvesting work [22, 10, 15, 17, 19, 20, 39]. This work is the only one in the list which achieves full -10 dB matching in the respective frequency band (for both the antenna and the matching circuit at the targeted power level). The FBW is as wide as 23 %, whereas the others only achieve single-digit FBWs. The proposed omnidirectional antenna enables simultaneous energy harvesting from all surrounding FM towers, whereas the others focus on harvesting from single sources using directional antennas. The system harvested as much as 923 μW at 1.54 km away from the broadcasting tower while retaining omnidirectionality. This is equivalent to harvesting 60 μW at 6.3 km away as Friis formula states that power received is inversely proportional to distance squared [53]. With or without taking distance into account, no other work in the table harvested as much power as this work. It achieves competitive RF-dc η and sensitivity while retaining wide-band operation rather than being specifically optimized to individual frequencies. This is due in part to minimizing the number of rectifier stages. The RF-dc η is higher than seven of the other work in the table (higher RF-dc η at lower input power). [17] and [19] respectively offer sensitivities of -14.6 dBm and -8.8 dBm. (These values are for configuration with which they achieved their best field test results as indicated in the table.) This work is more sensitive at -17 dBm, which translates to being as far as 10.6 km away from the broadcasting tower and still being able to harvest usable energy [53]. The proposed system (fabricated on low-cost FR4) harvested outside ambient energy indoors to power a WSN without needing to periodically shut down, which no other work in this list demonstrated, FM or otherwise, with or without periodic shut-down.

Table 3.1: Comparison of the FM energy harvester and other related work.

	region (MHz)	-10 dB match (FBW)	final load	antenna (gain)	harvested power	η (RF-dc)
[17]	400-600 band	partial TV (2 %)	μ-controller	log-periodic (7.3 dBi)	17 μW @ 6.3 km	21 % @ -4.74 dBm
[10]	400-600 band	partial TV (4 %)	WSN	horiz. dipole (1.33 dBi)	NA @ 6.3 km	40 % @ -5 dBm
[20, 39]	400-600 band	NA	sensor	log-periodic (5 dBi)	60 μW @ 4.1 km	30 % @ 0 dBm
[19]	400-600 band	NA	WSN	log-periodic (6 dBi)	NA @ 4.2 km	23 % @ -8.8 dBm
[15]	400-600 band	partial TV (7 %)	LED	loop (4.48 dBi)	3.6 μW @ NA	28 % @ -12.2 dBm
[15]	880-960	partial GSM (5 %)	LED	loop (4.73 dBi)	5.5 μW @ NA	18 % @ -15.2 dBm
[15]	1710-1880	partial GSM (1 %)	LED	loop (4.73 dBi)	2.4 μW @ NA	7 % @ -15.1 dBm
[15]	1920-2170	partial 3G (7 %)	LED	loop (4.76 dBi)	1.1 μW @ NA	40 % @ -25.4 dBm
[22]	76-95	partial FM (4 %)	capacitor	loop (1.83 dBi)	NA	26 % @ -18 dBm
this work	**88-108**	**full FM (23 %)**	**WSN**	**omnidirectional (2.0 dBi)**	**923 μW @ 1.54 km (rooftop)** **159 μW @ 1.54 km (indoor)** **60 μW @ 6.3 km (extrapolated)**	**56 % @ 0 dBm** **49 % @ -5 dBm** **33 % @ -13 dBm** **26 % @ -16 dBm**

CHAPTER 4

EXTENSION OF THE WORK ON THE FM ENERGY HARVESTER

4.1 FM Energy Harvesting Antenna Printed on a Window Glass

The usability of the FM energy harvesting antenna can be improved by making it more compact or by seamlessly integrating it into surroundings. One way to achieve the former is targeting a higher frequency band such as the UHF-TV band (Chapter 5). The latter is demonstrated by printing SNP (silver nano-particle) on a window glass to create the antenna [32].

Fig. 4.1 shows the dimensions of the antenna. The antenna is a triangular sheet dipole with rectangular ends for wider bandwidth. It consists of spokes rather than filled metal to conserve SNP and for better view through the window glass. The glass is $1400 \times 1620\,\text{mm}^2$, and the overall SNP outline is $1046 \times 1016\,\text{mm}^2$ ($0.34 \times 0.33\,\lambda^2$). The spokes are 2 mm wide (except for the center pieces, which are 4 mm wide) and 18 ° apart. The feed gap is $4 \times 4\,\text{mm}^2$. Impedance value of $50\,\Omega$ was chosen to allow the system to be compatible with characterization equipment designed to work with $50\,\Omega$ devices.

Fig. 4.2 shows a photograph of the antenna. The harvesting system powered the WSN for 16 min 40 s after every 19 min 36 s of charging. The amount of power harvested was 0.20 mW. Fig. 4.3 shows the power spectrum measured with the antenna at the test site located at (33.7759, -84.3898). Fig. 4.4 shows the simulated and measured S_{11} of the antenna. They achieve -10 dB and -5 dB matching across the entire FM frequency band, respectively.

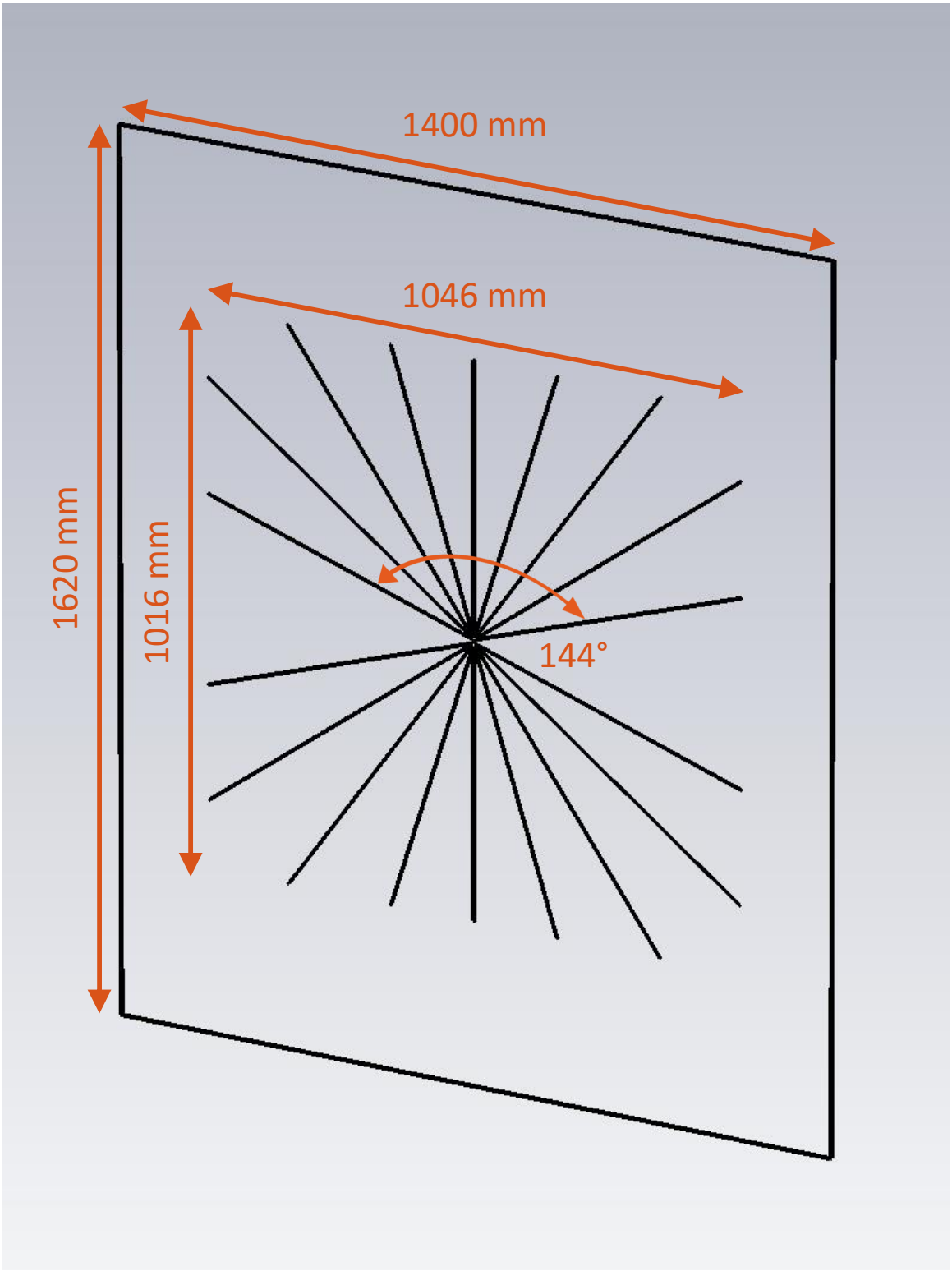

Figure 4.1: The dimensions of the SNP-on-glass antenna.

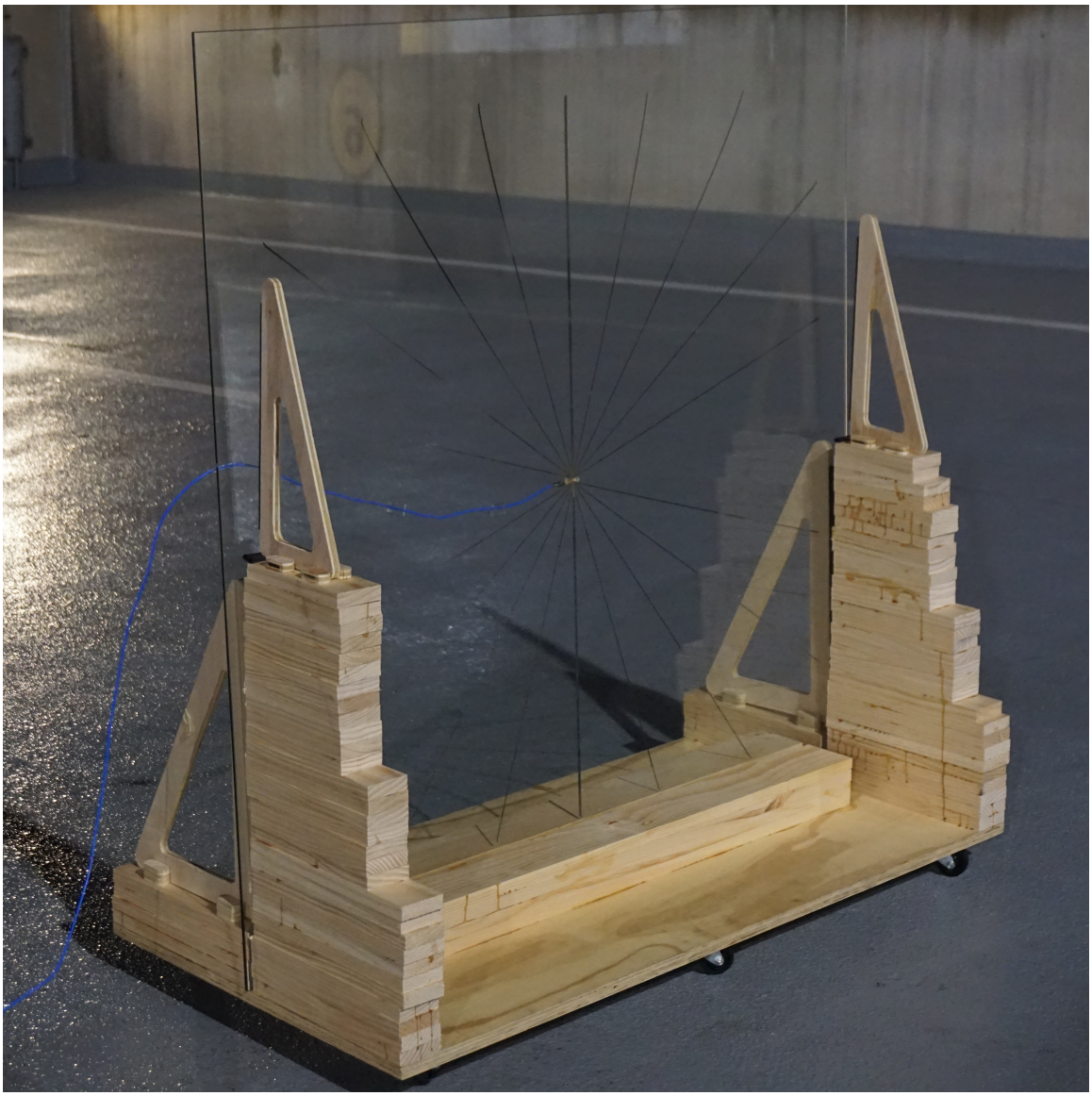

Figure 4.2: The SNP-on-glass antenna.

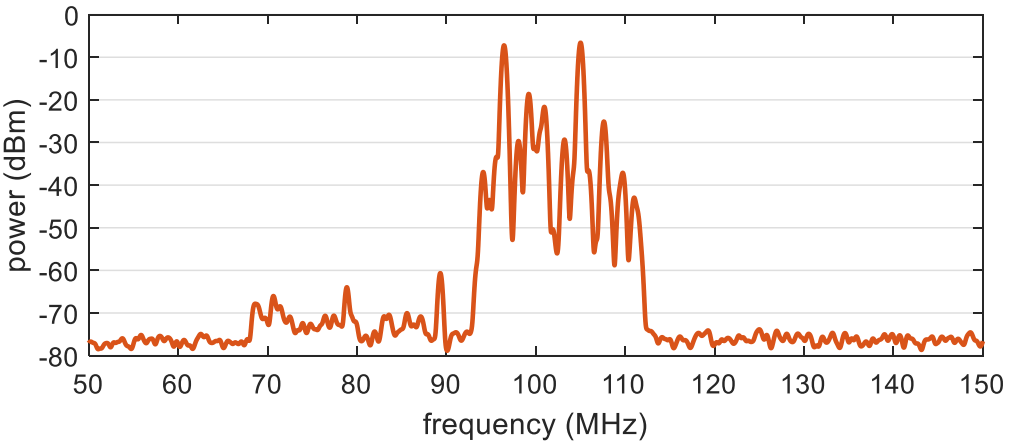

Figure 4.3: Spectrum measured with the SNP-on-glass antenna at the test site.

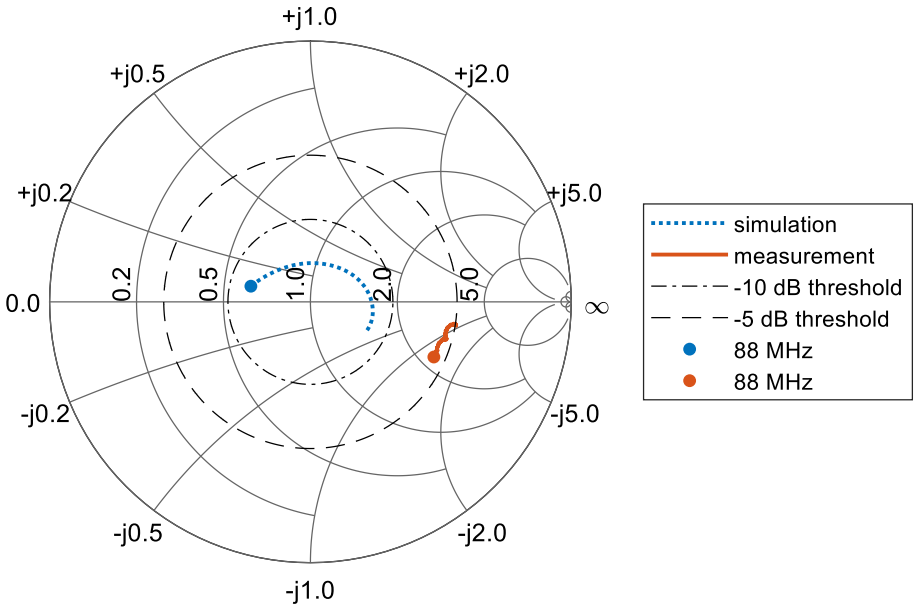

Figure 4.4: Simulated and Measured S_{11} of the SNP-on-glass antenna from 88 MHz to 108 MHz.

4.2 Effect of the FM Energy Harvesting Antenna on Neighboring Communication

Effect of the FM energy harvesting antenna on communication of neighboring antennas was investigated. Measuring isolation is the most straightforward method and has been performed as presented in Chapter 5. The experiment shown here provides additional intuition by directly observing the received power level. A signal generator and a spectrum analyzer are placed against the opposite walls of a $5 \times 5\,\mathrm{m}^2$ space as shown in Fig 4.5. The signal generator outputs 20 dBm at 97 MHz into a telescopic antenna, and the spectrum analyzer receives the signal through an identical telescopic antenna. The top and bottom of Fig. 4.6 show the spectrum analyzer display when the signal generator output is off and on, respectively. The former shows the ambient power level, and the latter shows the reference power level in the absence of the FM harvesting antenna.

Figure 4.5: The $5 \times 5\,\mathrm{m}^2$ space used for the experiment.

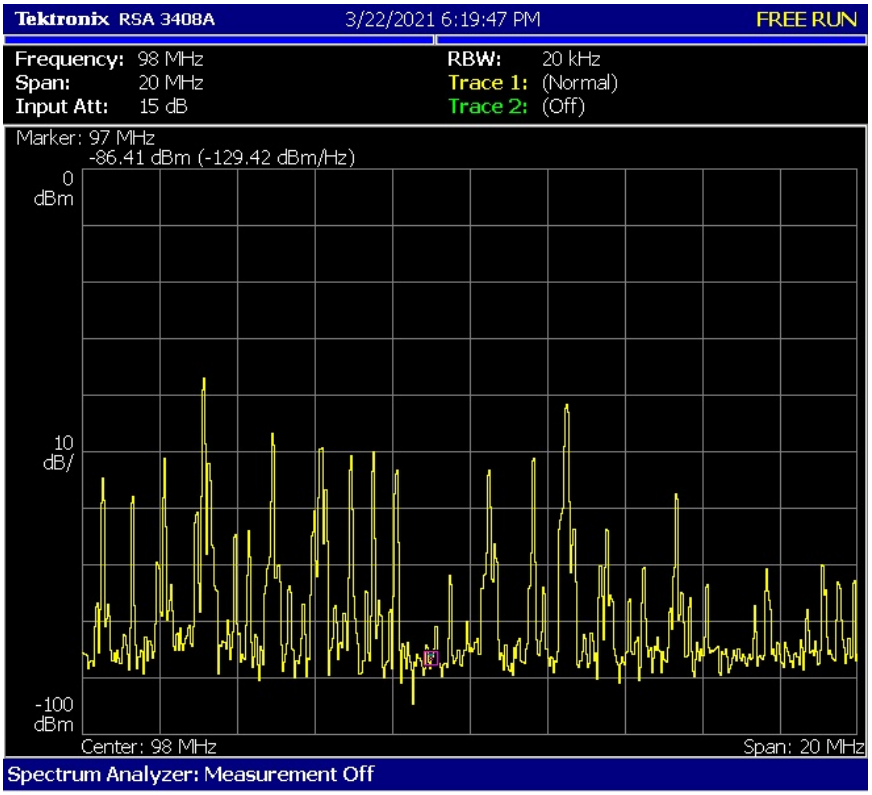

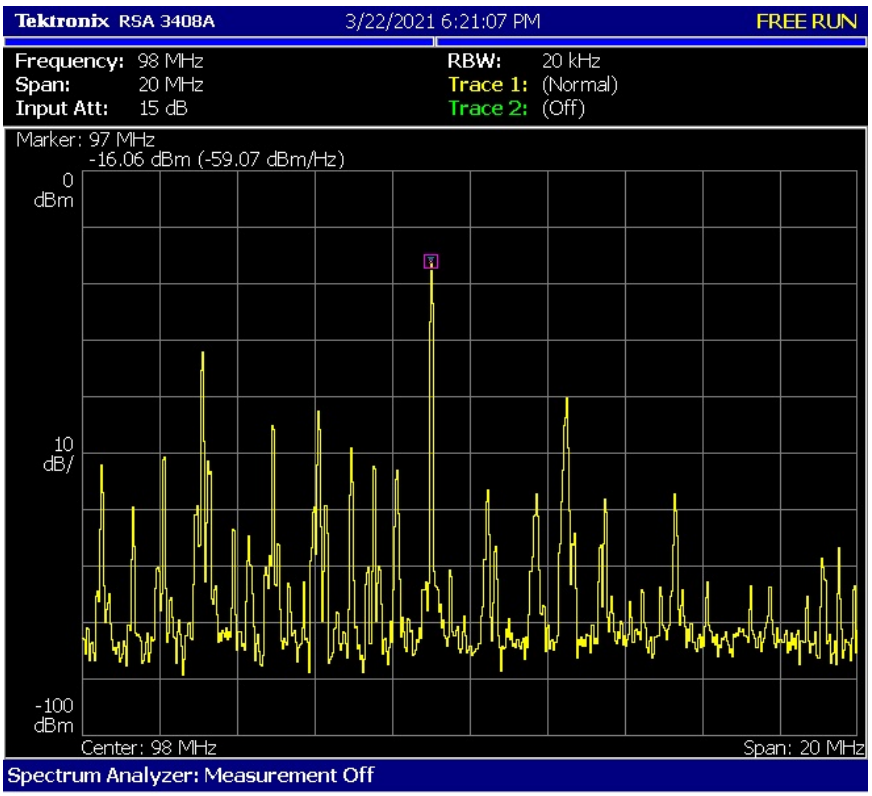

Figure 4.6: The ambient and the reference power level.

The FM harvesting antenna is situated between the signal generator and the spectrum analyzer at nine spots, one spot at a time, as shown in Fig. 4.7. Shown in Fig. 4.8 is the power received by the spectrum analyzer each time. The measurement was repeated at 0 dBm as shown in Fig. 4.9. The most deviation over the reference power level was 3.22 dBm and under the reference power level was 1.18 dBm.

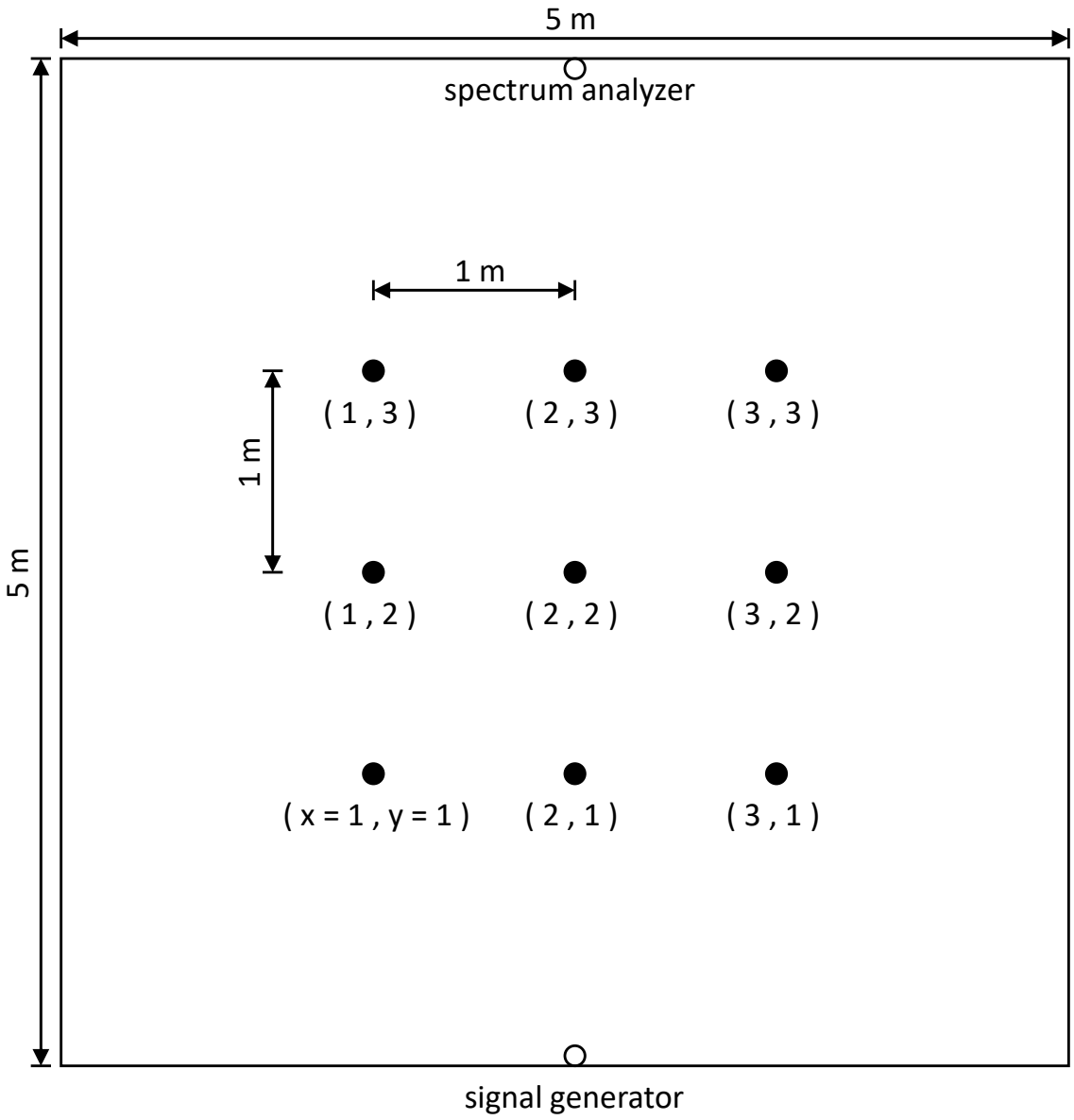

Figure 4.7: Placement of the FM energy harvesting antenna within the $5 \times 5\,\mathrm{m}^2$ space.

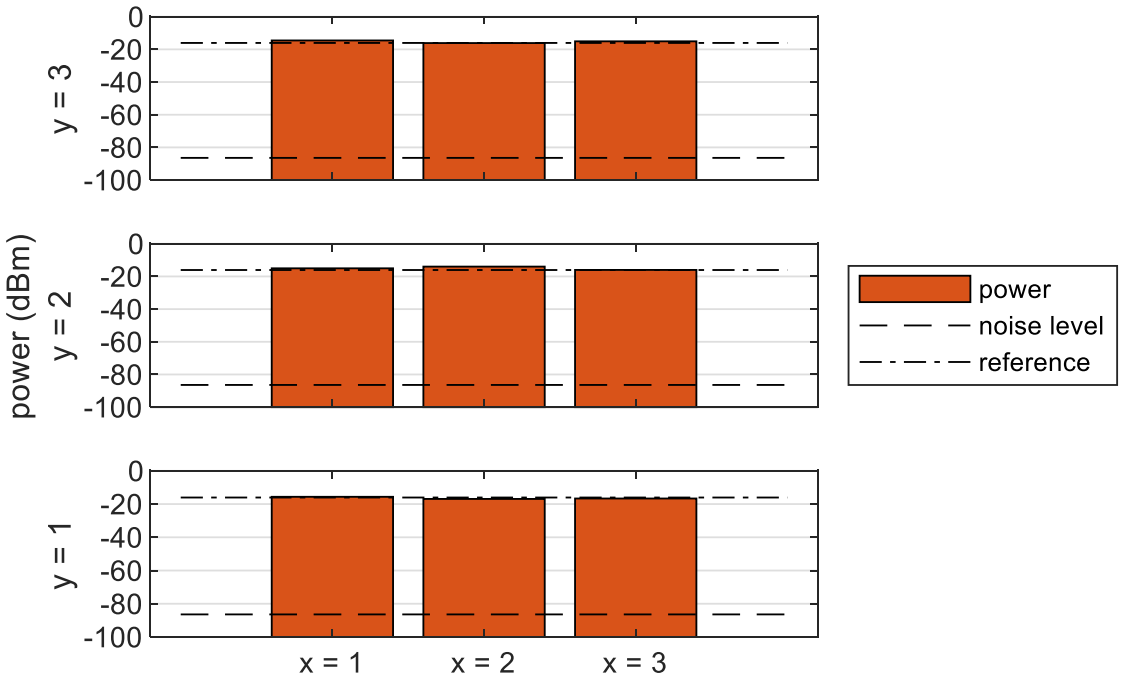

Figure 4.8: Power received while transmitting 20 dBm.

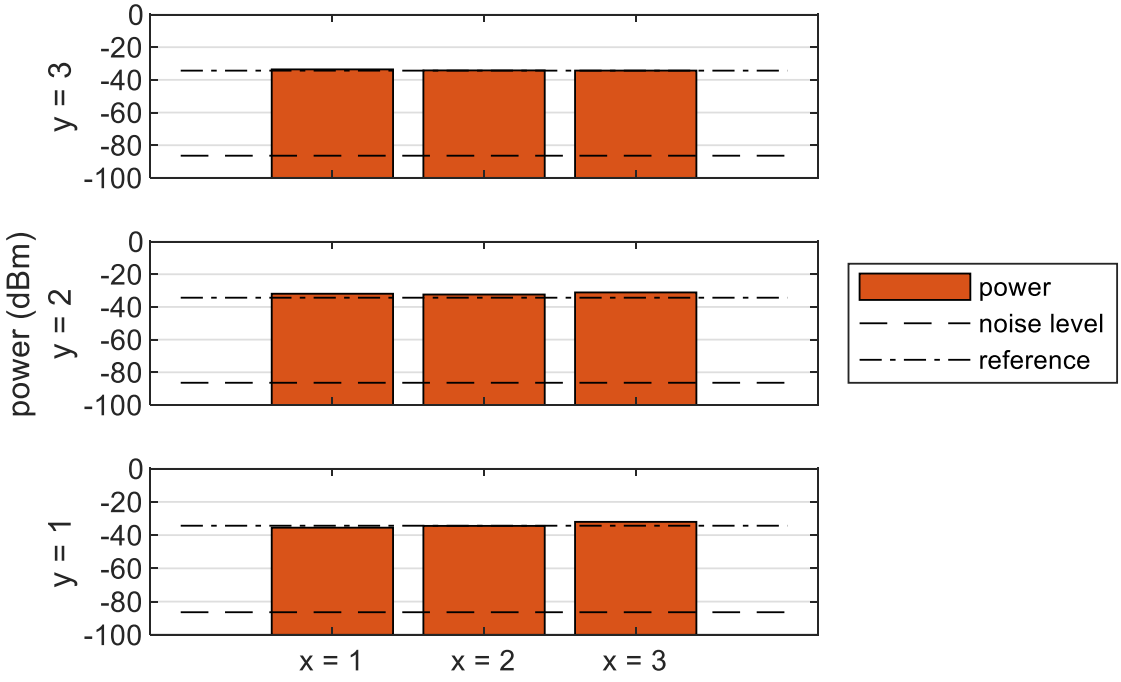

Figure 4.9: Power received while transmitting 0 dBm.

4.3 FM and UHF-TV Coverage Maps in the United States

The United States FCC (Federal Communications Commission) provides 1 mV/m contours of FM and UHF-TV broadcast signals in the United States. The data can be plotted as shown in Fig. 4.10 for FM and Fig. 4.11 for UHF-TV. The plots are framed to show the contiguous territories.

In a free space with $120\pi\,\Omega$ impedance, 1 mV/m approximately corresponds to -56 dBm/m^2. (Electric field squared then divided by impedance equates to surface power density.) The contours can be scaled according to received power being inversely proportional to distance squared [53], so that it can display contours corresponding to a desired level of surface power density. Fig. 4.12 and Fig. 4.13 show -30 dBm/m^2 contours of FM and UHF-TV broadcast signals, respectively. The information can be useful for estimating the areas in which an ambient RF energy harvesting system would be operational. For example, if the aperture of the antenna is 1 m^2 and the sensitivity of the system is -30 dBm, the harvester would operate in areas covered by -30 dBm/m^2 contours.

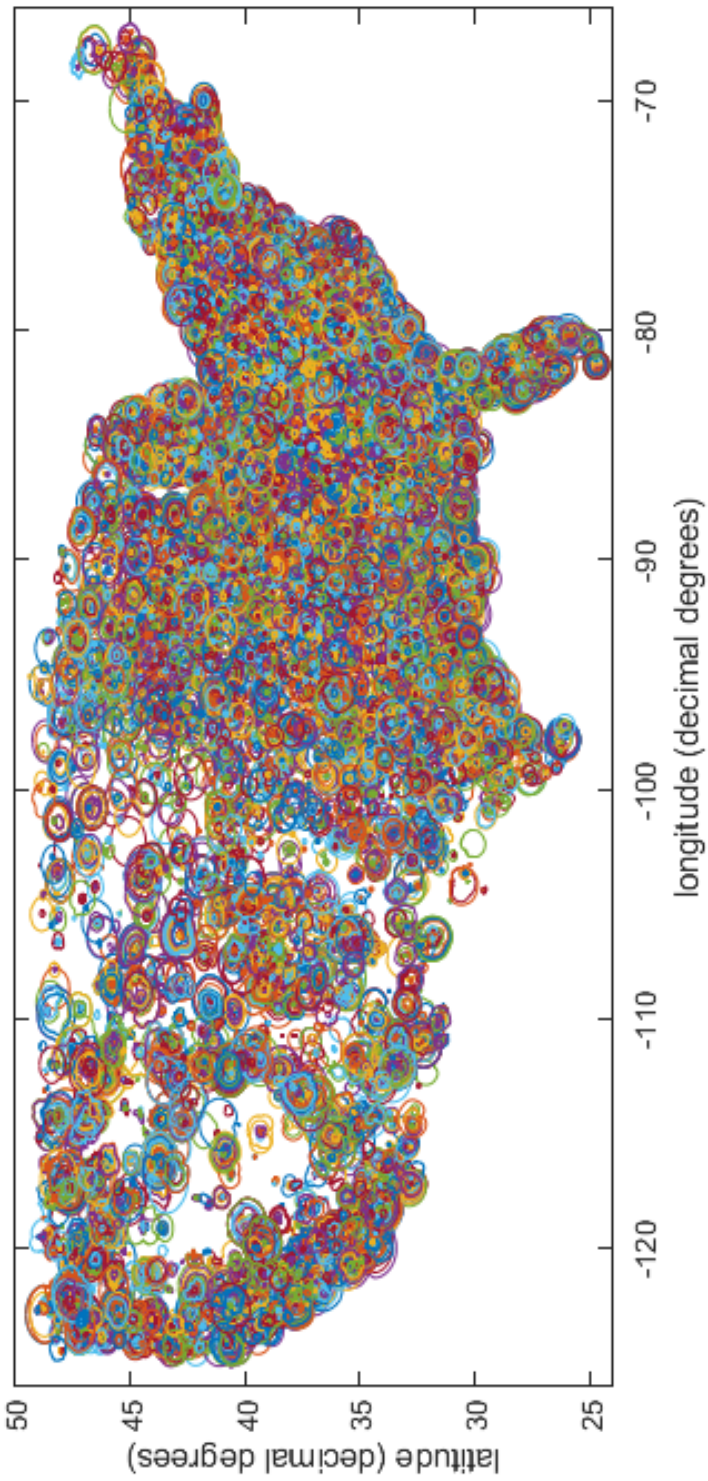

Figure 4.10: FM broadcast 1 mV/m contours in the contiguous United States.

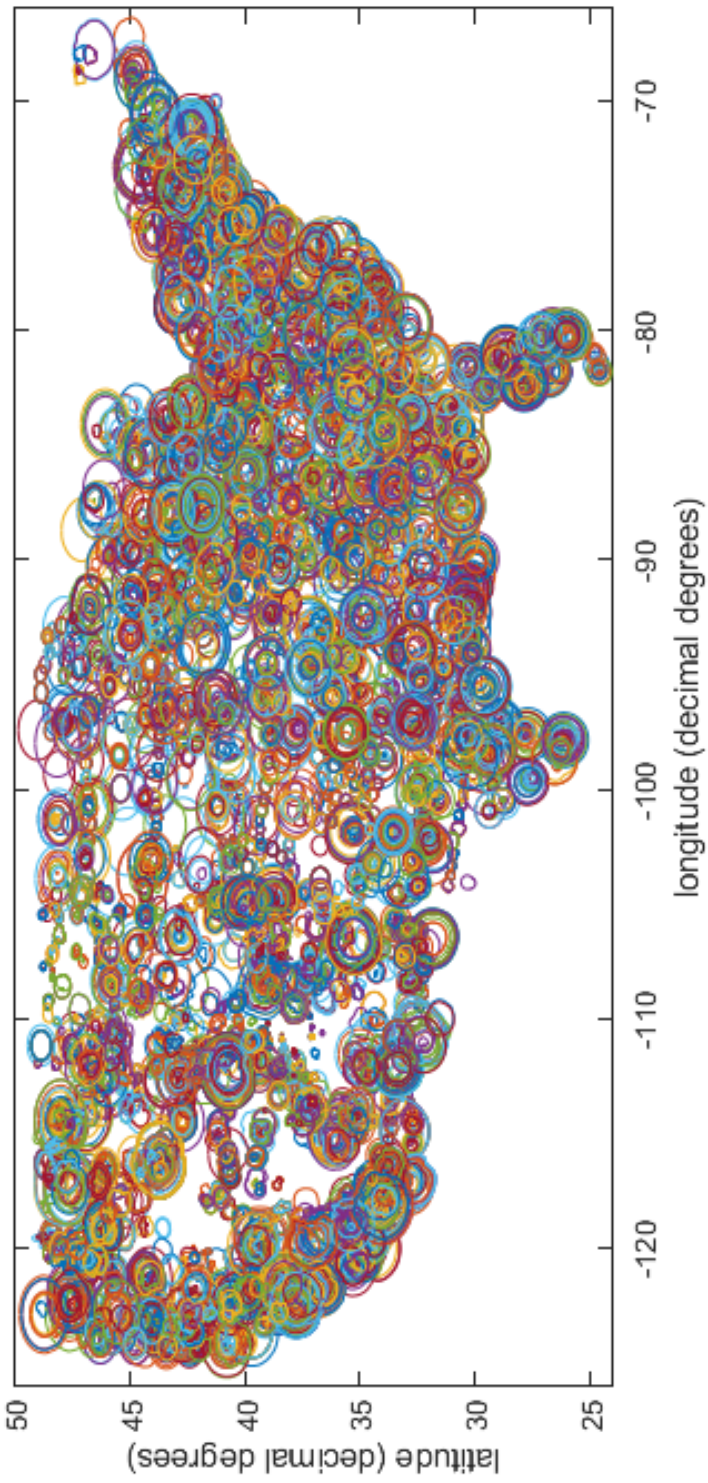

Figure 4.11: UHF-TV broadcast 1 mV/m contours in the contiguous United States.

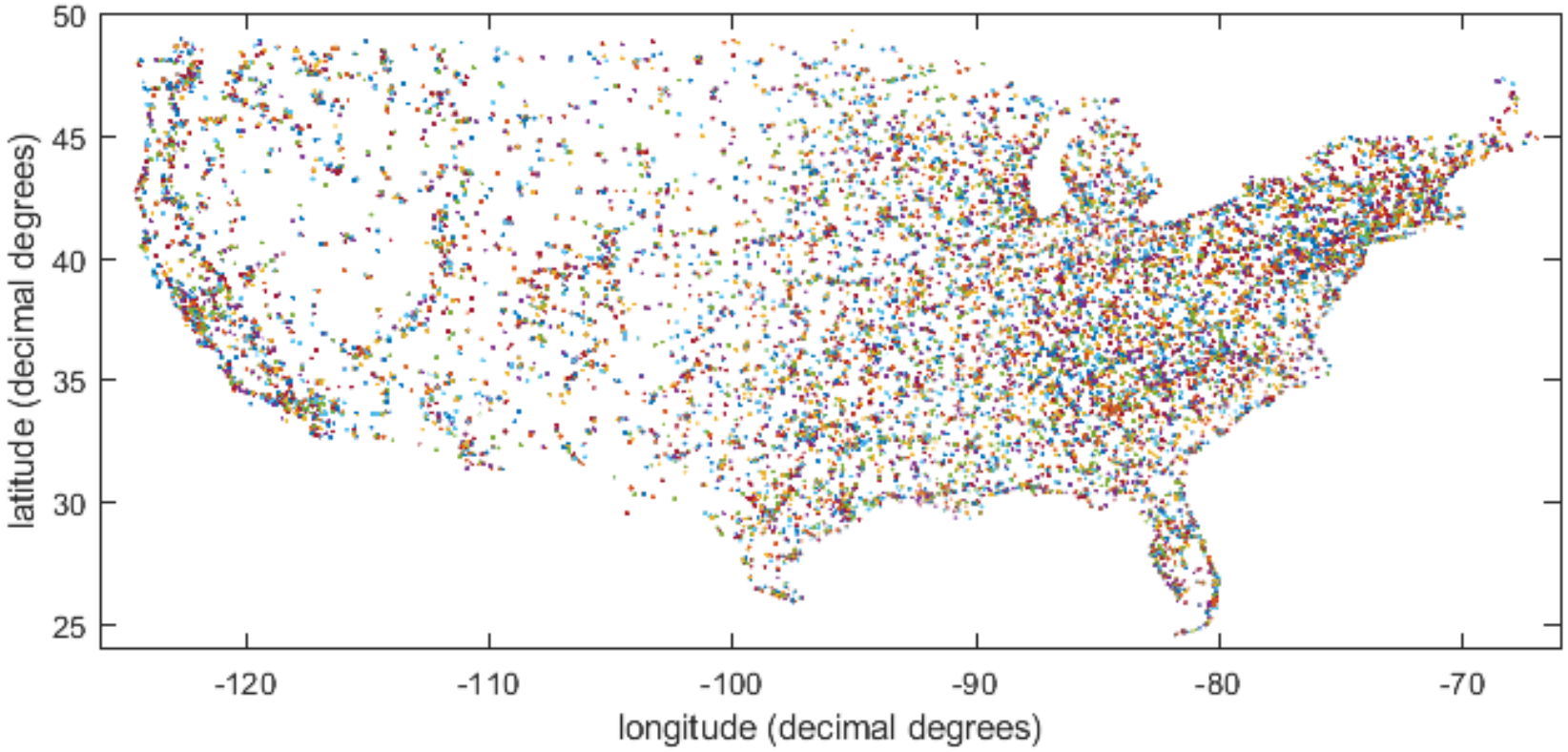

Figure 4.12: FM broadcast -30 dBm/m^2 contours in the contiguous United States.

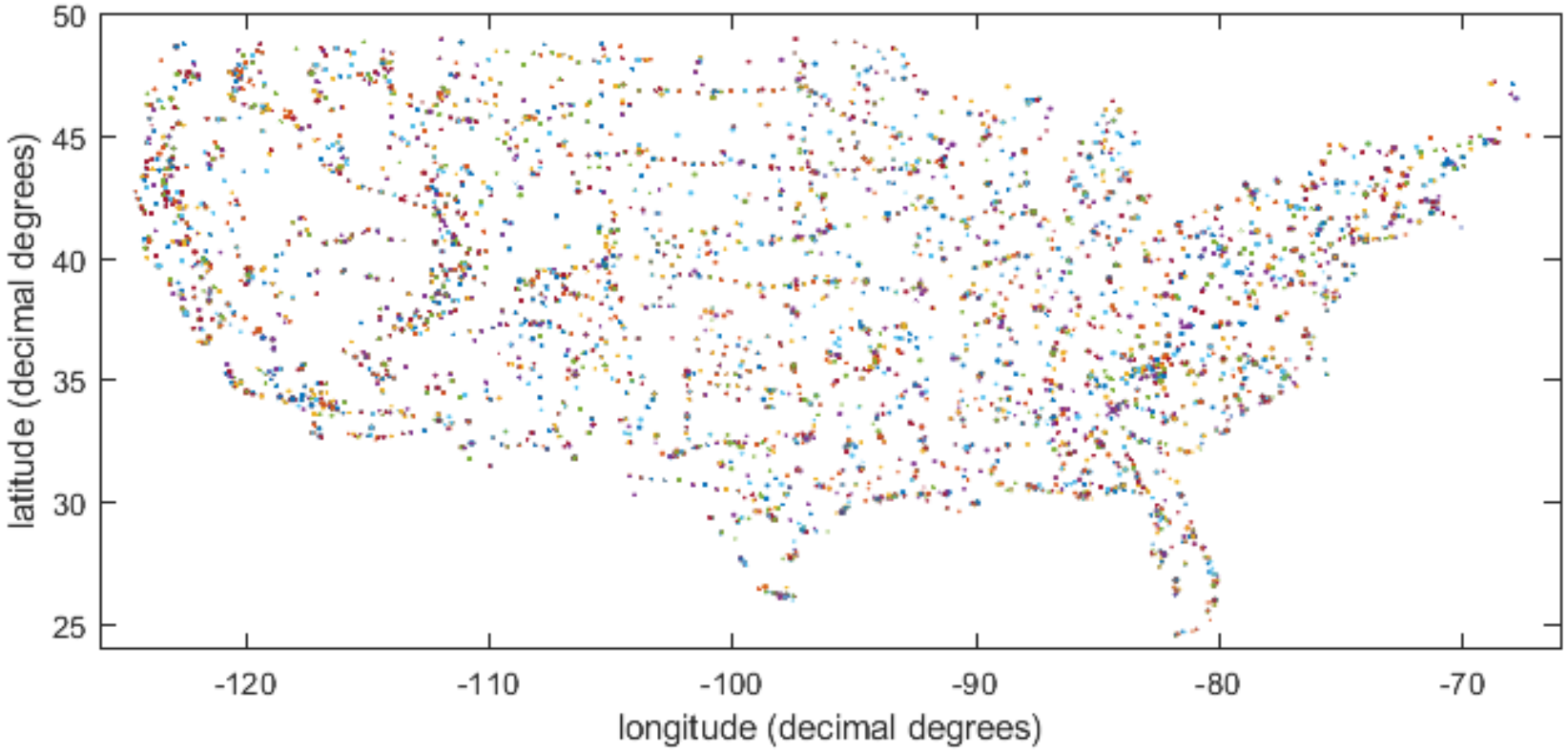

Figure 4.13: UHF-TV broadcast -30 dBm/m^2 contours in the contiguous United States.

CHAPTER 5
THE FULL-FM-AND-UHF-TV-BAND, QUASI-ISOTROPIC, AMBIENT RF ENERGY HARVESTER

5.1 Overview

UHF-TV signals are primarily horizontally polarized. This work combines energy harvested via north-south and east-west polarized UHF-TV antennas as well as one vertically polarized FM antenna by connecting multiple PMUs to one capacitor bank (Fig. 5.1). (Dual-band horizontal antennas would require more area.) The FM portion was detailed in Chapter 3. This Chapter details the UHF-TV portion (Fig. 5.2) and presents a combined full UHF-TV and FM band, quasi-isotropic, ambient RF energy harvester.

5.2 The UHF-TV Energy Harvester Antenna Design

Fig. 5.3 shows simulated and measured gain of the antennas fabricated on MG Chemicals 555 (35 μm copper, 1.6 mm FR4, $\epsilon = 4.2$ and $\delta = 0.015$ at 1 GHz). A triangular sheet dipole with rectangular ends for wider bandwidth is on each front and rear side. The overall metal outline is $210 \times 120\,\text{mm}^2$ ($0.38 \times 0.22\,\lambda^2$). The feeds are $50\,\Omega$ to allow the system to be compatible with characterization equipment. The dimensions were exhaustively swept in CST to balance S_{11} and gain. Front and rear antenna gains combined is 1 or greater across all θ and ϕ, allowing isotropic harvesting, i.e., $G_{front}(\theta, \phi) + G_{rear}(\theta, \phi) \geq 1$. If a horizontally polarized wave arrives from the $\phi = 45\,^\circ$ direction, half of the received power would be contributed by the front antenna and the other half by the rear antenna. These are not one individual antenna with an isotropic gain; such hypothetical antenna does not exist in real life. Fig. 5.4 shows simulated and measured radiation efficiency. The radiation efficiency is above 85 % across the entire UHF-TV band.

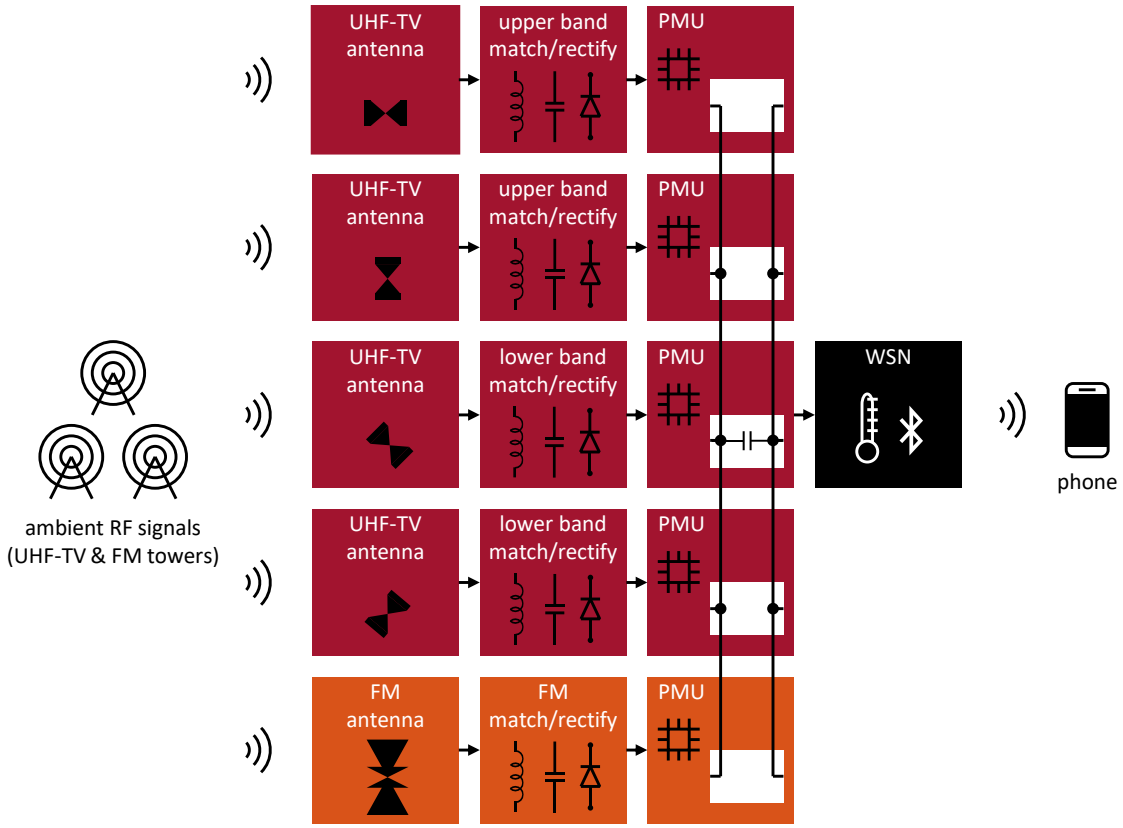

Figure 5.1: The harvester block diagram combining UHF-TV and FM.

Fig. 5.5 shows simulated and measured S_{11} while the antenna substrate is isolated from the rest of the harvester. The antenna achieves -10 dB matching across the entire UHF-TV band (of the United States) and FBW as wide as 36 %. Fig. 5.6 shows measured S-parameters while the harvester is assembled as depicted in Fig. 5.7 (which shows the combined UHF-TV and FM harvester powering the WSN). The top (port 1) and bottom (port 2) substrate antennas achieve -10 dB matching across the entire UHF-TV band. The substrates are 608 mm apart, separated by a copper-backed PMU/WSN plate, and rotated 45 ° relative to each other around the z axis for isolation (Fig. 5.2). The TV antennas are horizontally polarized, whereas the FM antenna (port 3) is vertically polarized. The antennas achieve 30 dB isolation among one another across the entire UHF-TV band.

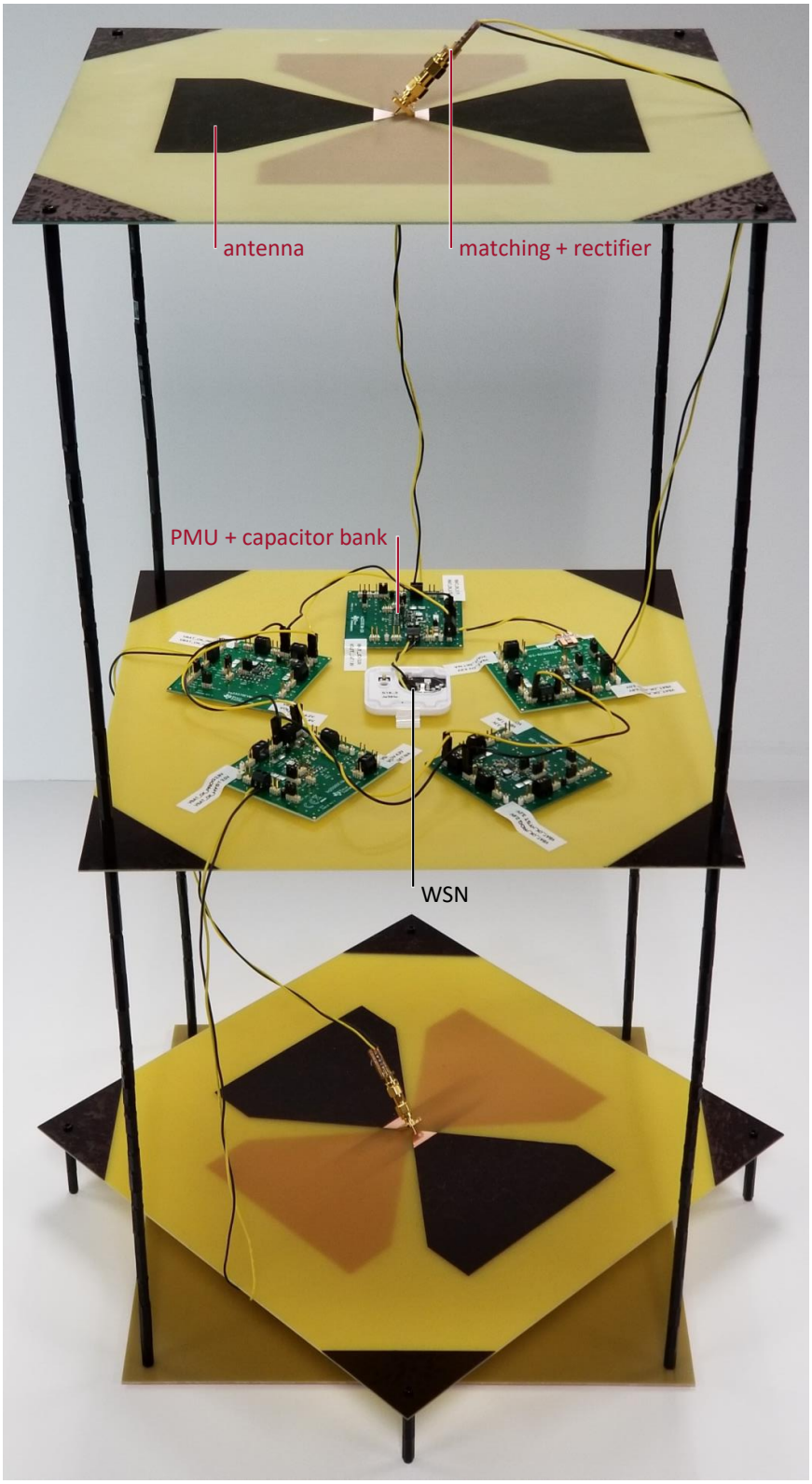

Figure 5.2: The UHF-TV harvester.

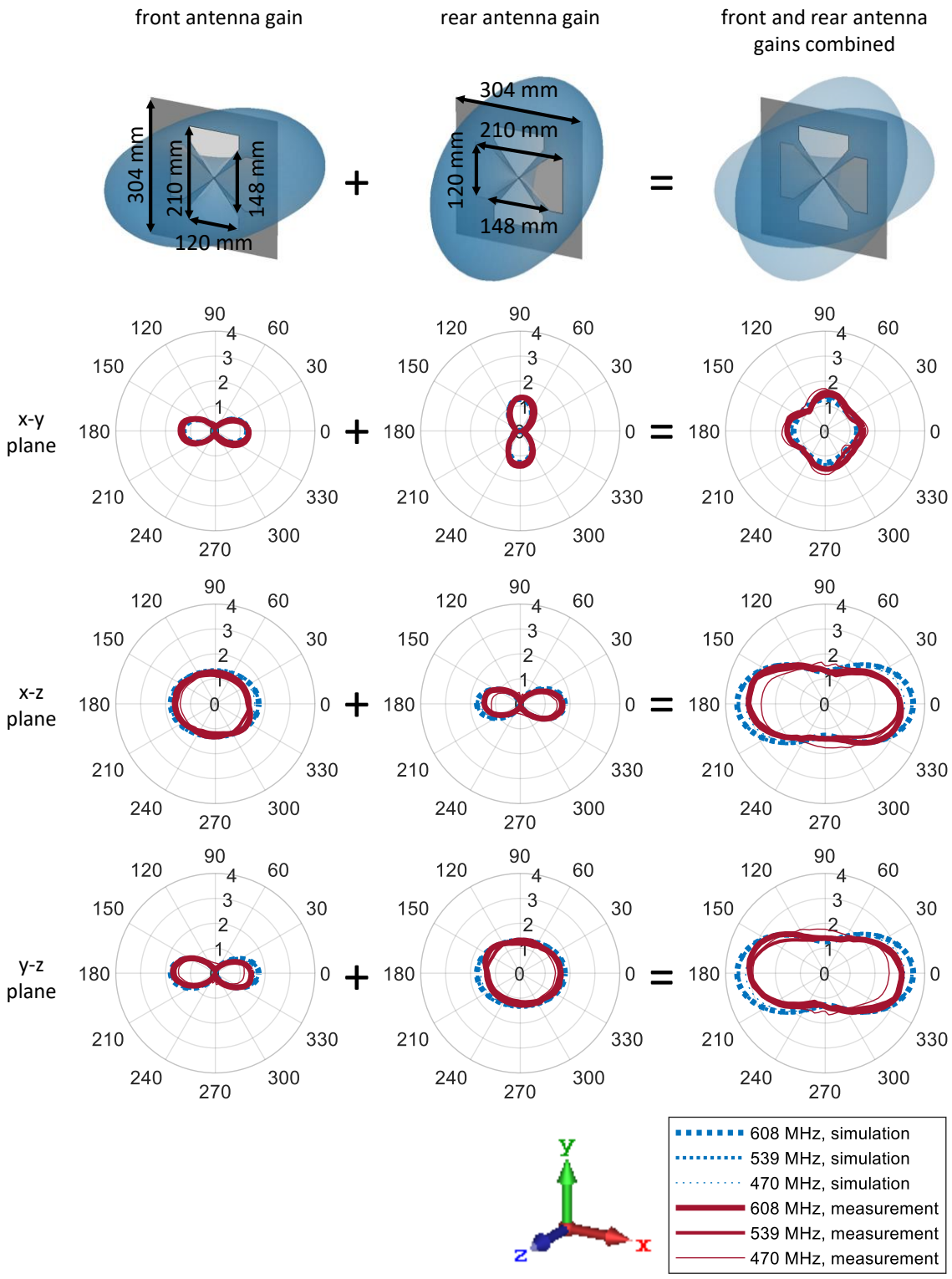

Figure 5.3: Realized gain of the UHF-TV antennas in linear scale, angle in degrees.

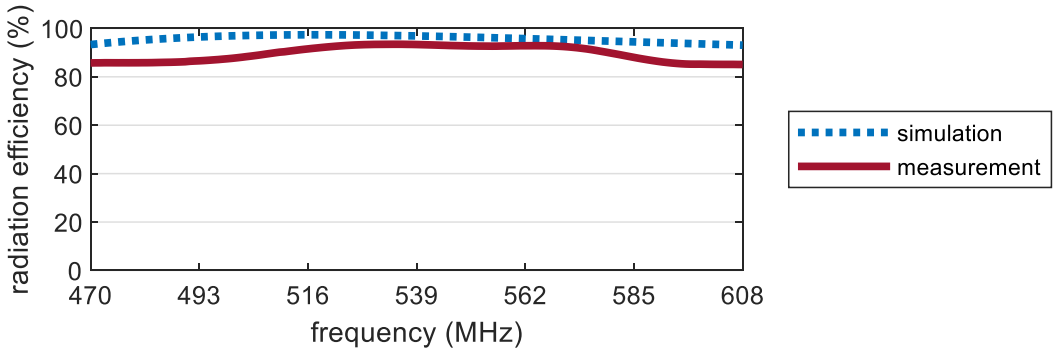

Figure 5.4: Simulated and measured radiation efficiency of the UHF-TV antenna.

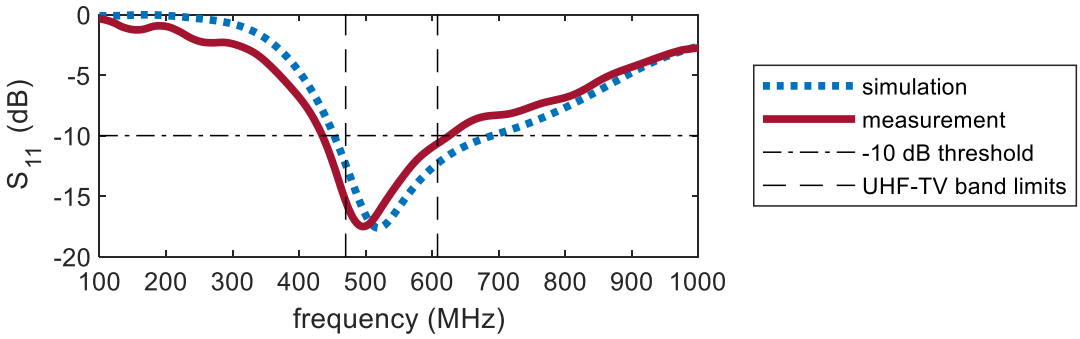

Figure 5.5: Simulated and measured S_{11} of the UHF-TV antenna in isolation.

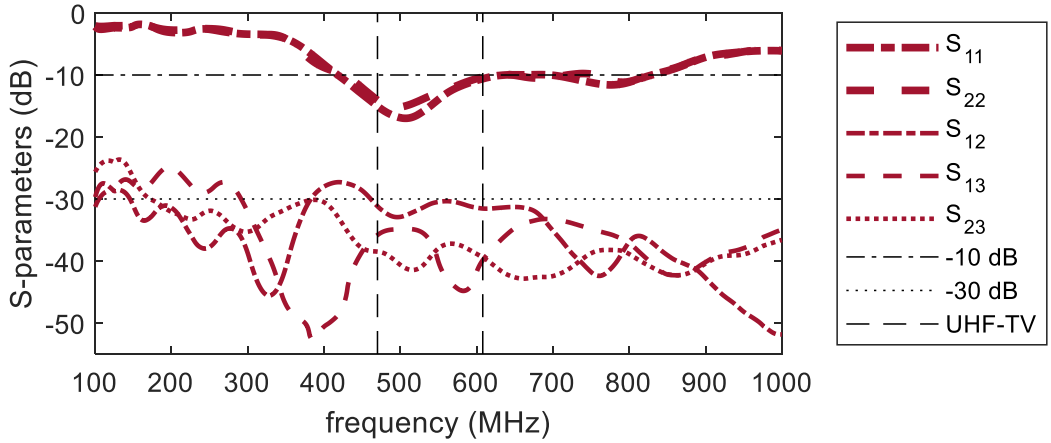

Figure 5.6: Measured S-parameters while the UHF-TV-and-FM harvester is assembled.

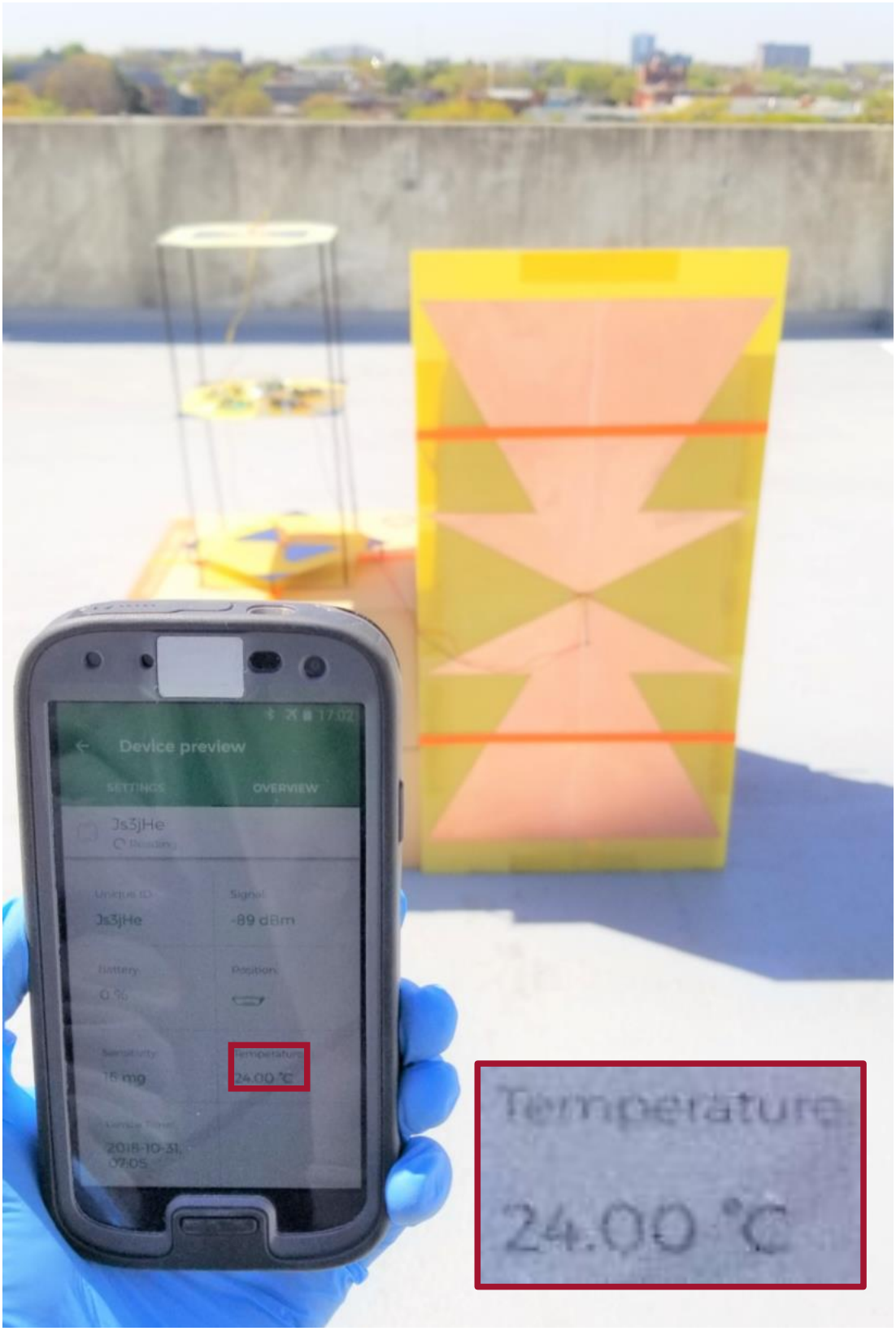

Figure 5.7: The UHF-TV-and-FM harvester powering the WSN at the test site.

5.3 The Matching and Rectifying Circuit Design

Fig. 5.8 shows schematics of the matching and rectifying circuits for the upper half (top) and the lower half (bottom) of the UHF-TV band. The rectifying circuit was fabricated on MG Chemicals 555. The impedance was measured, component values were exhaustively swept in ADS to match the impedance, the impedance was measured again after placing the component nearest to the rectifying circuit, and the process was repeated until the component nearest to the antenna was placed. Two matching network stages and one rectifying stage per circuit were used to minimize losses introduced by components, while FR4 was chosen for its low cost and mechanical robustness despite being relatively lossy. The PMU (Texas Instruments BQ25570) was represented by a 3.3 kΩ load. (The PMU has MPPT.) Fig. 5.9 shows simulated and measured S_{11}. The two circuits for the upper and lower half bands together achieve -10 dB matching across the entire UHF-TV band and across all power levels from -20 dBm to 0 dBm. The combined FBWs are 27 %, 31 %, and 31 % for -20 dBm, -10 dBm, and 0 dBm, respectively. The FBWs for upper and lower band circuits are 14 %, 21 %, 23 % and 17 %, 18 %, 15 %, respectively. Fig. 5.10 shows measured RF-dc η with varying loads (i.e, compatibility with various loads). Peak RF-dc η occurs at 4.7–5.6 kΩ. Fig. 5.11 shows RF-dc η across the UHF-TV band at 4.7 kΩ (i.e., compatibility with towers broadcasting in various UHF-TV frequencies). Fig. 5.12 shows measured RF-dc η with varying input power. As high as 70 % is achieved. Note that RF-dc η increasing with input power is a characteristic of Schottky diodes [44], [52]. Fig. 5.12 shows output potential with varying input power. As high as 2.3 V is achieved. The PMU requires 100 mV and 5 μW (330 mV and 15 μW for cold-start). Fig. 5.14 shows measured sensitivity and cold-start sensitivity. As low as -18 dBm and -13 dBm are achieved, respectively. Single-tone RF input was used for these measurements. Multi-tone RF inputs such as UHF-TV get added in time domain and yield higher output potential. Integration of the components from the antennas to the WSN on one substrate is discussed in section 6.5.

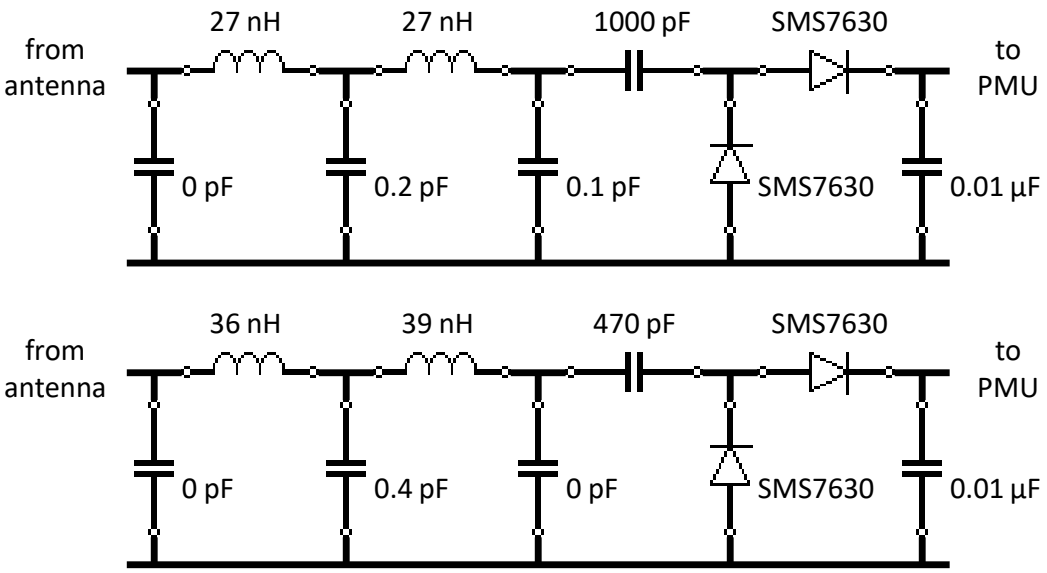

Figure 5.8: The matching and rectifying circuits for the upper and lower halves of the UHF-TV band.

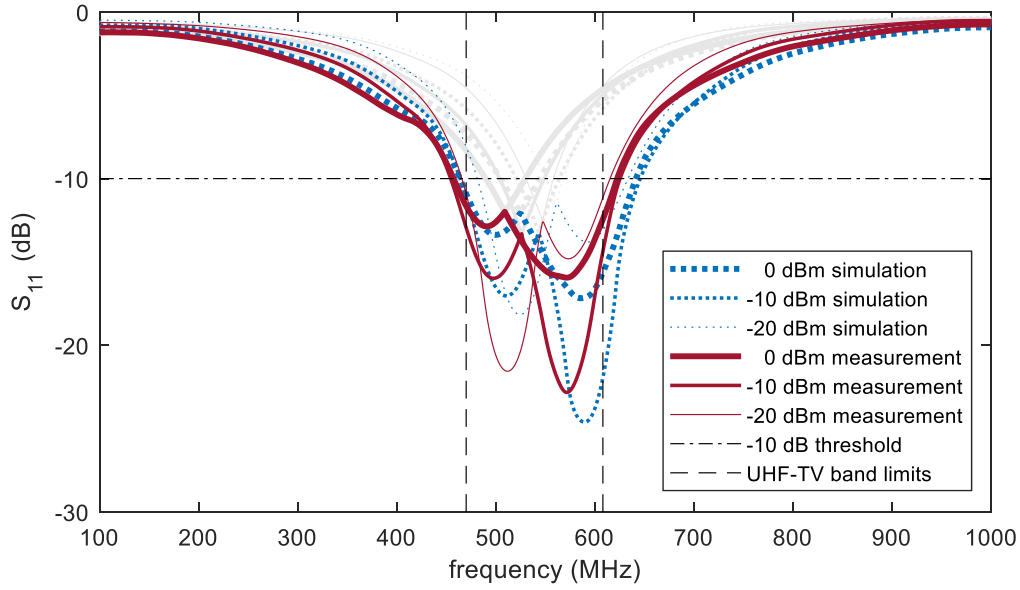

Figure 5.9: Simulated and measured S_{11} of the matching and rectifying circuits across the UHF-TV band.

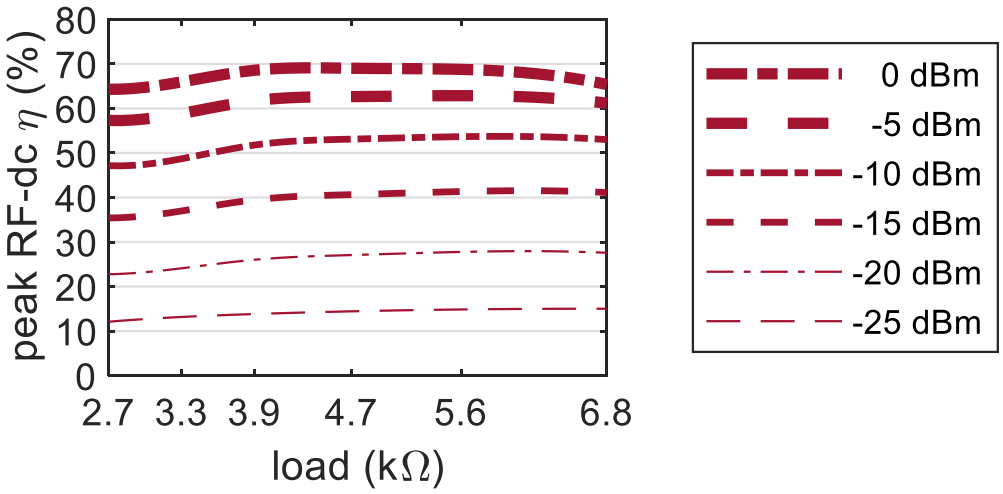

Figure 5.10: Measured RF-dc η of the UHF-TV harvester matching and rectifying circuits with varying load.

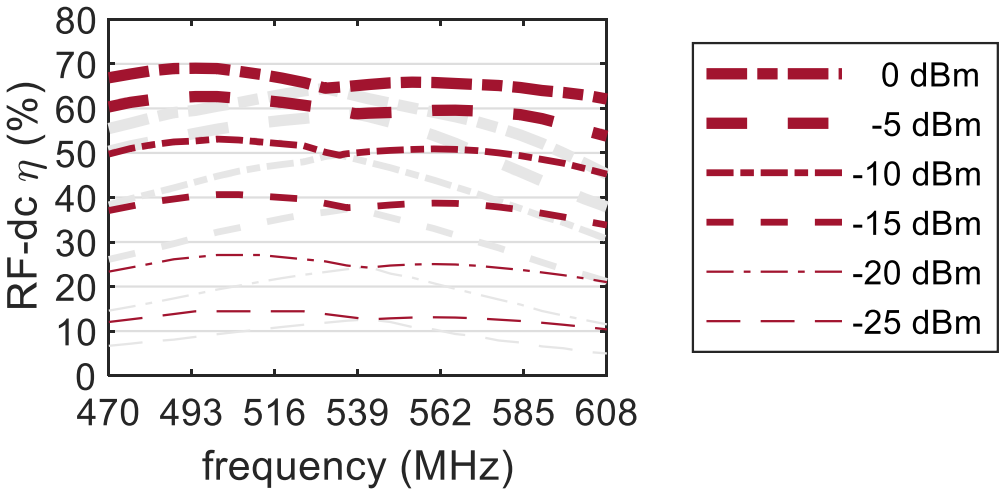

Figure 5.11: Measured RF-dc η of the matching and rectifying circuits across the UHF-TV band.

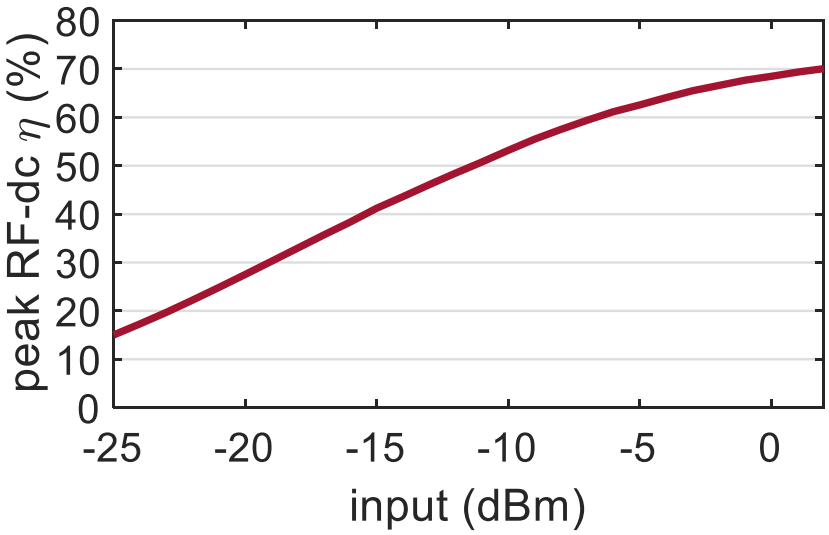

Figure 5.12: Measured RF-dc η of the UHF-TV harvester matching and rectifying circuits with varying input power.

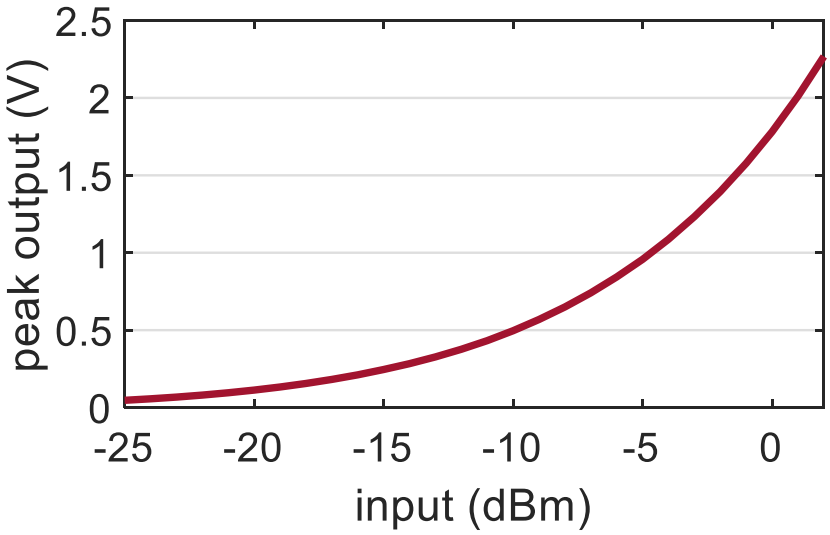

Figure 5.13: Measured output potential of the UHF-TV harvester matching and rectifying circuits with varying input power.

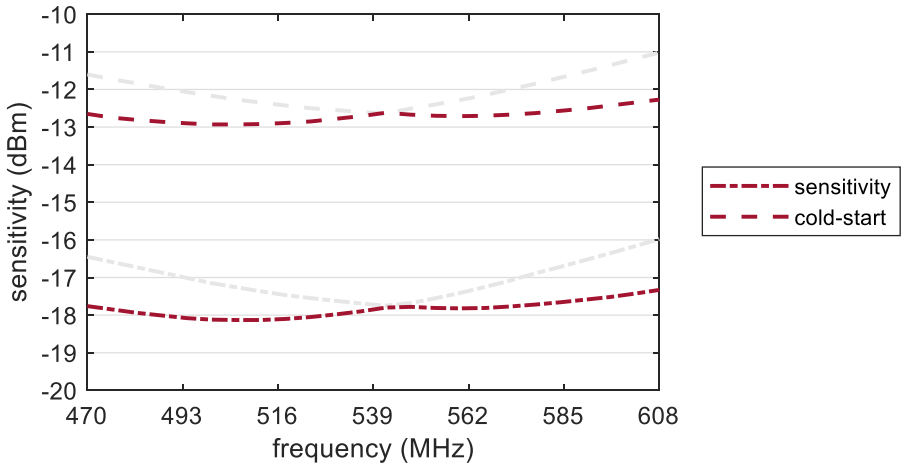

Figure 5.14: Measured sensitivity and cold-start sensitivity of the matching and rectifying circuits in the UHF-TV band.

5.4 System Demonstration

Fig. 5.15 shows a map of the broadcast towers within a 10 km radius of the test site (33.7759, -84.3898). Fig. 5.16 shows the power spectrum measured using the harvester antennas at the test site. The power density was measured to be 1.2 mW/m^2 for the UHF-TV band (3.1 mW/m^2 for the FM band). The highest contribution comes from channel 18 (494–500 MHz) located 5.83 km away for UHF-TV (91.1 MHz and 1.54 km for FM). Fig. 5.17 shows the power harvested throughout a day. The UHF-TV portion consistently harvested 200 μW or higher, reaching as high as 231 μW. High level of power could be harvested from the spectrum seemingly containing low power levels due to the fact that the UHF-TV spectrum contains multiple tones per channel [54]. Fig. 5.18 shows the UHF-TV harvester's charge cycle powering the WSN. The WSN (Kontakt.io S18-3) was powered for 16 min 40 s after every 26 min 40 s of charging. Measured RF-dc η was 40 %. Capacitance (three parallel Seiko CPH3225A) was chosen in order to provide enough current to turn on the WSN. Charge cycle measurement does not exist for combined UHF-TV and FM harvesting, because the FM harvester, even on its own, can power the WSN without periodically shutting down [30], [31].

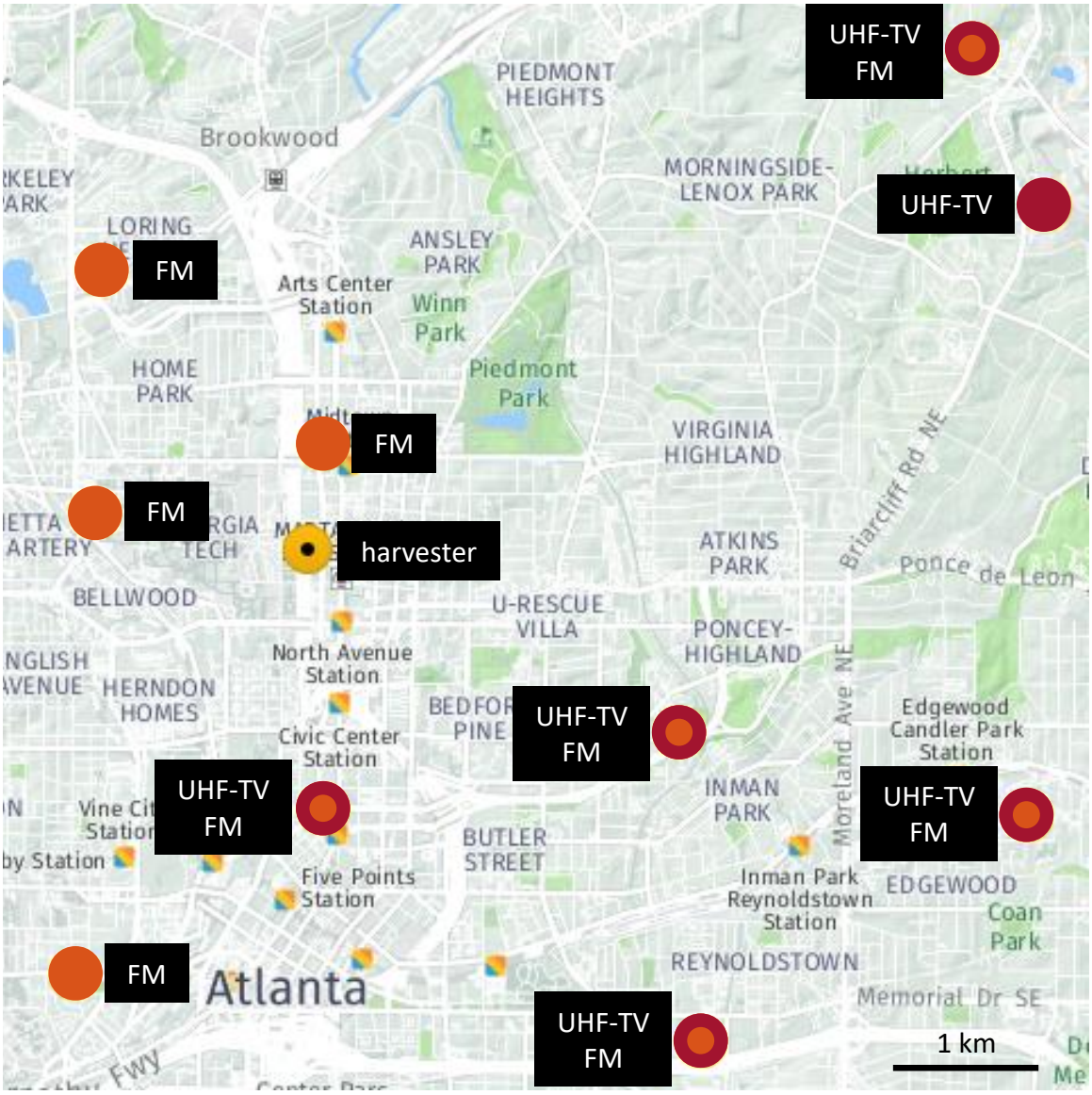

Figure 5.15: A map of the broadcast towers within a 10 km radius of the test site.

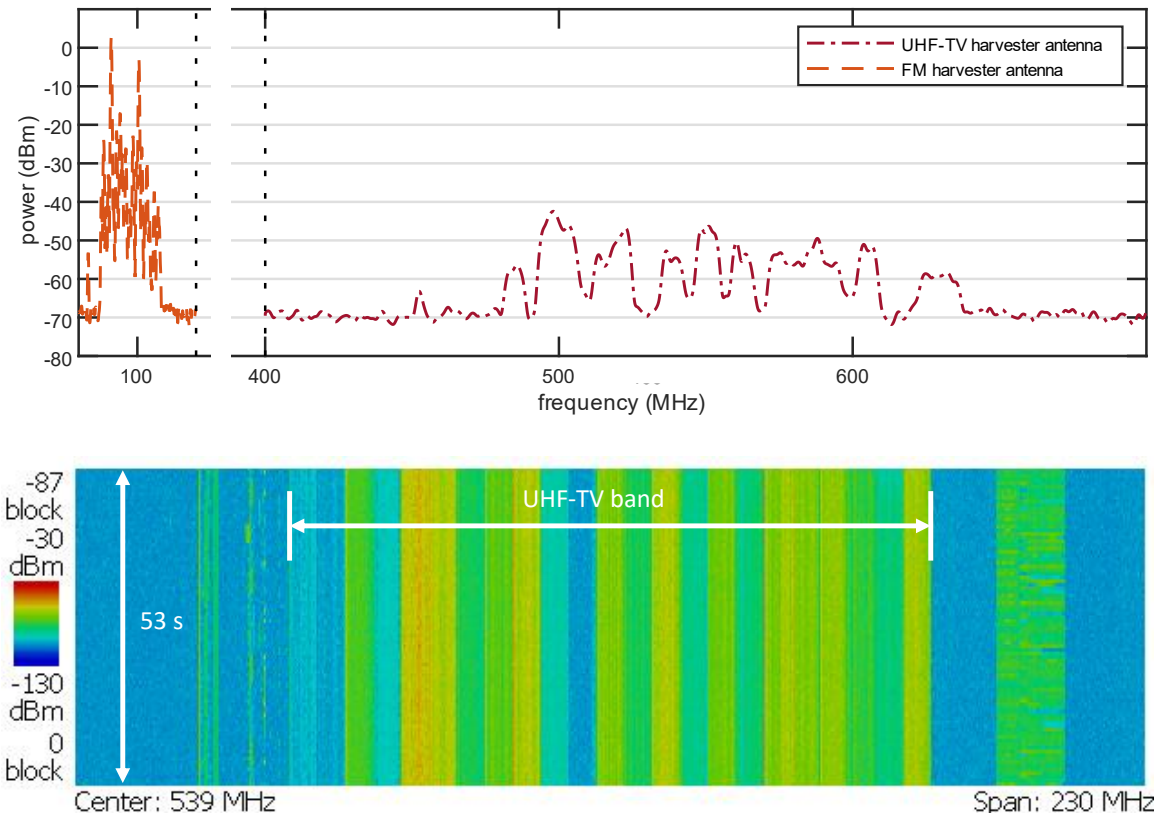

Figure 5.16: Spectrum measured using the harvester antennas at the test site.

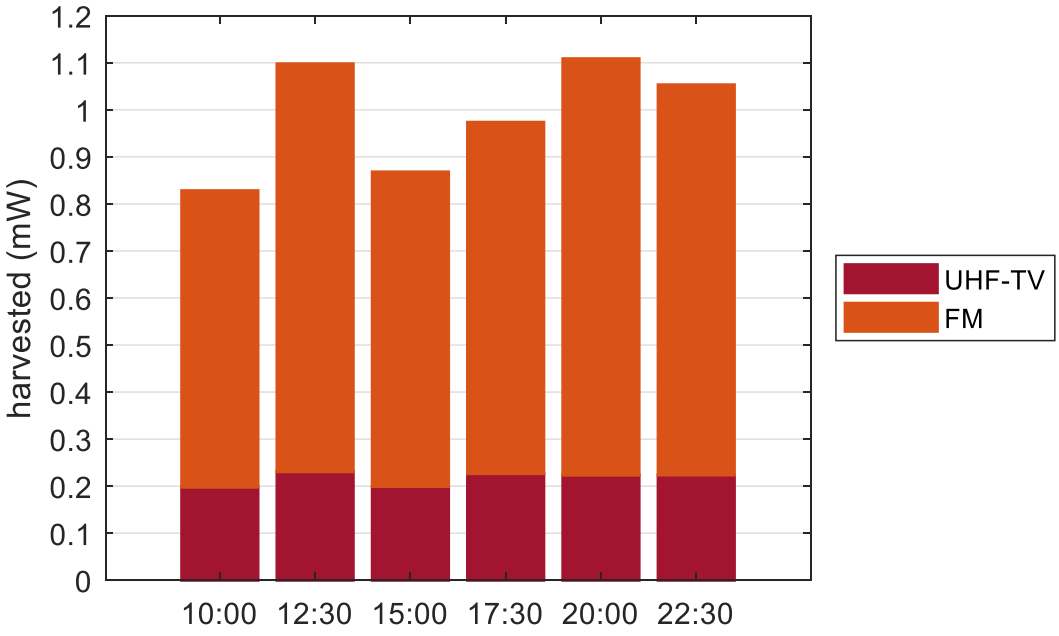

Figure 5.17: Power harvested throughout a day at the test site.

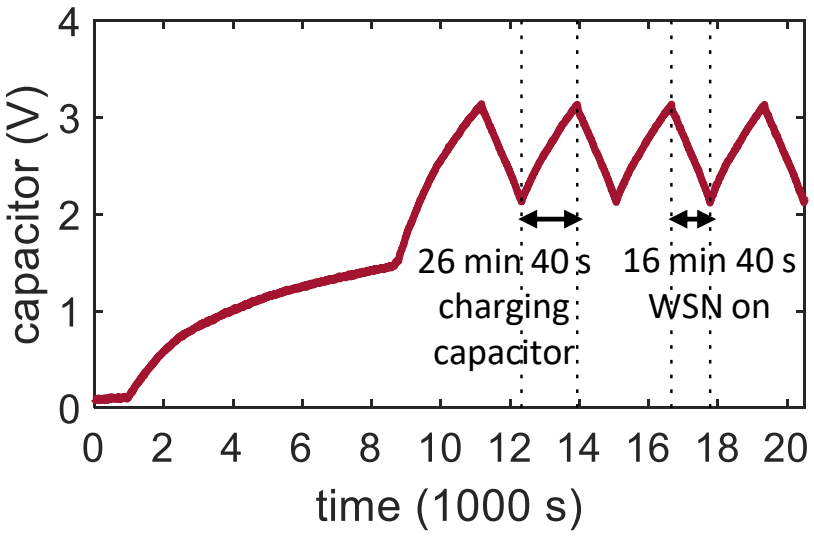

Figure 5.18: UHF-TV harvester charge cycle powering the WSN.

5.5 Comparison to Related Work

Table 5.1 compares ambient RF energy harvesting work [10, 12, 13, 15, 17, 19, 20, 39, 49, 50, 55, 56, 57, 58]. The frequency band showing the best performance was selected for each work. Only this work is capable of harvesting from all directions using its quasi-isotropic antenna setup. The antenna of this work has competitive size while achieving wide bandwidth. (Wider bandwidth requires larger antenna size [6].) Only this and one other work achieve double-digit -10 dB FBW at -20 dBm. The RF-dc η of this work is among the leaders, again, while achieving wide bandwidth. (Lower loss is easier to achieve with narrow-band matching.) No other work was able to harvest triple-digits of μW. This work is among the few that demonstrate powering a WSN. WSN/IoT devices have power and potential requirements for cold-start and for staying on. Without these constraints, wide bandwidth and high efficiency are easier to achieve and thus have diminished significance. Systems that do not demonstrate powering such load may not be capable of providing useful function.

Only this work allows harvesting from all surrounding towers simultaneously, whereas the others focus on harvesting from single sources at specific frequencies using directional antennas. Requiring careful alignment with calibration equipment prevents ambient RF energy harvesting from being adapted outside of the RF community. It is also impractical when deploying in mass scale, when towers are visually obstructed, or when it is unknown which tower provides the most power to a given location [14]. Only this work addresses these issues.

Table 5.1: Comparison of the UHF-TV energy harvester and other related work.

	band (center)	antenna radiation (area)	-10 dB FBW	RF-dc η	harvested power	final load
[10]	UHF-TV (540 MHz)	omnidirectional (0.012 λ^2)	4 % @ -10 dBm	5 % @ -20 dBm	NA @ 6.3 km	WSN
[12, 13]	GSM [a] (880 MHz)	bidirectional (0.17 λ^2)	32 % @ -20 dBm	30 % @ -20 dBm	67 μW @ NA	resistor
[15]	UHF-TV [a] (540 MHz)	bidirectional (NA)	7 % @ -20 dBm	NA	3.6 μW @ NA	LED
[17]	UHF-TV (540 MHz)	unidirectional (0.20 λ^2)	2 % @ -15 dBm	7 % @ -15 dBm	17 μW @ 6.3 km	μ-controller
[19]	UHF-TV (540 MHz)	unidirectional (NA)	NA	NA	NA @ 4.2 km	WSN
[20, 39]	UHF-TV (540 MHz)	unidirectional (NA)	NA	25 % @ -5 dBm	60 μW @ 4.1 km	sensor
[49]	UMTS (883 MHz)	omnidirectional (NA)	NA	0.8 % @ -20 dBm	0.3 μW @ 0.2 km	capacitor
[50]	UMTS [a] (2.14 GHz)	unidirectional (2.1 λ^2)	2 % @ -20 dBm	28 % @ -20 dBm	80 μW @ NA	resistor
[55]	GSM (882 MHz)	unidirectional (0.39 λ^2)	2 % @ -15 dBm	14 % @ -20 dBm	49 μW @ NA	WSN
[56]	UMTS [a] (2.14 GHz)	unidirectional (0.70 λ^2)	3 % @ -20 dBm	30 % @ -20 dBm	NA	open
[57]	GSM [a] (941 MHz)	unidirectional (0.09 λ^2)	33 % @ -15 dBm	15 % @ -20 dBm	15 μW @ 0.05 km	resistor
[58]	UMTS [a] (2.14 GHz)	bidirectional (0.25 λ^2)	9 % @ -10 dBm	32 % @ -20 dBm	6.2 μW @ NA	resistor
this work	UHF-TV [a] (540 MHz)	quasi-isotropic (0.30 λ^2)	27 % @ -20 dBm	28 % @ -20 dBm	231 μW @ 5.83 km	WSN

[a] multiband

GSM = Global System for Mobile communication™, UMTS = Universal Mobile Telecommunications System

CHAPTER 6

ADDITIONAL DETAILS ON THE UHF-TV ENERGY HARVESTER

6.1 Antenna Design Variable Sweeping Strategy

Without simulation, designers would have to begin by prototyping physical samples. They would have to measure the antenna's performance parameters, revise the designs based on the measurement results, and iterate the process until the measurement results satisfy the design goals. Simulation can perform this iterative process virtually and reduce the number of iterations that has to be done with physical samples. This section discusses a strategy for sweeping design variables to find optimal performance parameters in simulation.

Antenna design process begins by considering the constraints and the requirements. In the case of the UHF-TV harvester antenna presented in Chapter 5, the constraint was that the cost and the complexity had to be manageable so that the research could be carried out. The requirement was that it must achieve full-UHF-TV-band and isotropic reception. A set of copper-cladded FR4 triangular sheet antennas were chosen. The wavelength corresponding to the center frequency of the UHF-TV band (in the United States) is approximately 556 mm. A half-wave triangular sheet dipole would have a length in the vicinity of 278 mm. This information provided on intuition on how large the substrate needed to be. Thus, a 304 mm $\times$ 304 mm substrate was chosen.

Performance parameters can be described in terms of equations for standard types of antennas. However, equations can no longer be relied upon for antennas that deviate from the standard types. In the case of the UHF-TV harvester antenna, interaction between the front side and the back side antennas (among other design features) makes the antenna difficult to be described in terms of standard equations. Simulation becomes an important part of the design process.

One way to run simulation is to adjust design variables until performance parameters such as bandwidth and gain meet the design goals. Fig. 6.1 shows the three design variables of the UHF-TV harvester antenna. The idea is to find bandwidth and gain in simulation, adjust W, L, and F, and repeat until the design goals are satisfied. The design goals may be values that have been set in advance or may simply be the best values that can be achieved while adhering to the design constraints.

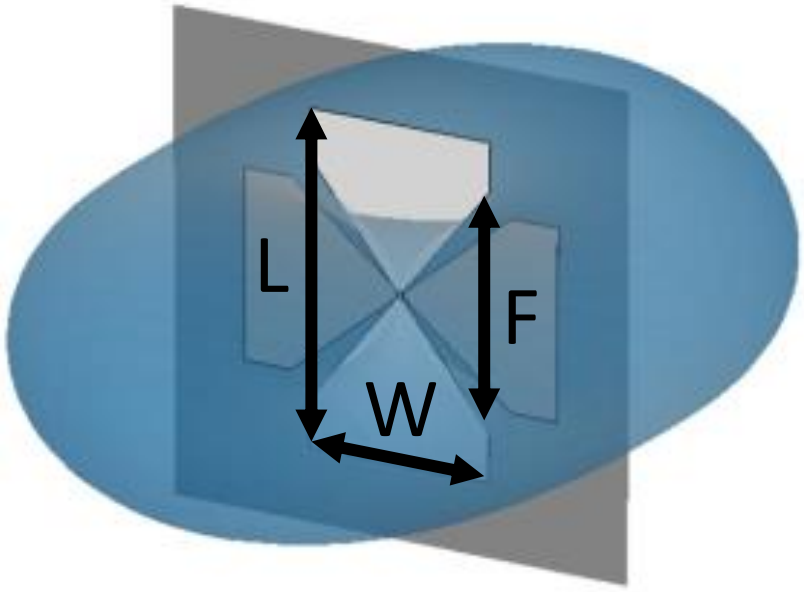

Figure 6.1: The design variables to sweep/optimize on the UHF-TV harvester antenna.

The designer can run a simulation, interpret the result, change a design variable based on theory (e.g., shortening an antenna to increase its frequency of operation), and repeat until design goals are satisfied. The essence is finding the design variable values that optimize the performance parameters.

Alternatively, each design variable can be swept, from one value to another value in increments. The simulation would present a set of results. The designer can then decide which design variable value yields the most desirable result. The designer can choose to sweep the design variable again in vicinity of the previous best design variable value with a smaller interval size. Sweeping can be considered as a method to automate the process of finding design variables that optimize performance parameters.

Another strategy is to use an optimization algorithm. The designer can specify which design variables to optimize. The simulation software generates results, adjusts the design variable values, and repeats in an attempt to yield performance parameters that come closest to, or meet, the design goals. Optimization algorithms can be considered as another method to automate the process of finding the design variable values that optimize the performance parameters.

An issue with these strategies is that they may arrive at local optima that may not be global optima. Suppose that a designer can adjust a physical dimension of a hypothetical antenna from 0 m to 10 m (the design variable), and that the performance is determined by its reflection coefficient (the performance parameter). Also suppose that the fabrication process has 1 m precision. Exhaustively sweeping the design variable would require 11 simulation trials and would guarantee finding the global optimum. To save time, the designer chooses to sweep the dimension with a 2 m interval size. After 6 trials, the designer discovers that -8.9 dB is achieved at 2 m and 4 m. The designer tries 1 m, 3 m and 5 m, which are in the vicinity of 2 m and 4 m. The designer finds the best result of -9.0 dB at 3 m. This is illustrated in the top part of Fig. 6.2. The designer was lucky that the relationship between the design variable and the performance parameter was simple and arrived at the global optimum after nine trials, saving time by running two fewer trials. However, the bottom part of Fig. 6.2 shows that the same strategy fails to arrive at the global optimum in the case of a more complicated relationship. The first six trials would lead the strategy to get stuck around the 8 m region and fail to find the global optimum located at 1 m.

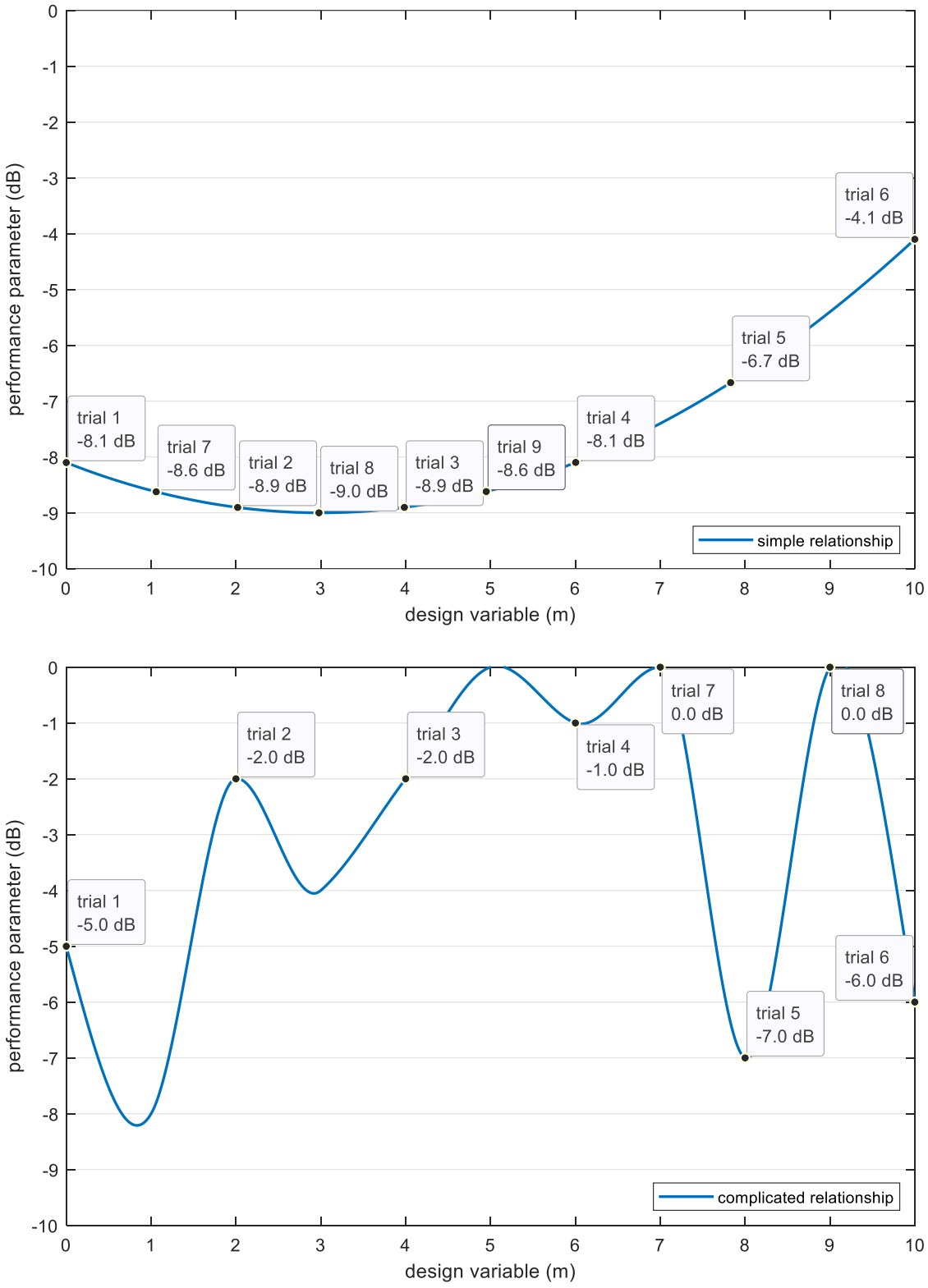

Figure 6.2: How a simple sweep strategy can fail to reach the global optimum.

Now consider an alternative scenario. The designer chooses to employ a basic optimization strategy that begins at 5 m (the middle of the range) and continues with the trials by moving to the neighboring design variable values until the performance parameter stops improving as shown in the top part of Fig. 6.3. The first three trials lets the designer know that decreasing the design variable value improves the performance parameter. The subsequent two trials discover that the best performance is achieved at 3 m and that decreasing the design variable value beyond this point degrades performance. The global optimum is found. This strategy fails to find the global optimum in the case of a more complicated relationship shown in the bottom part of Fig. 6.3. The first three trials lets the designer know that decreasing the design variable value improves the performance parameter. The subsequent two trials discover that the best performance is achieved at 3 m and that decreasing the design variable value beyond this point degrades performance. However, it fails to reach the global optimum located at 1 m. The strategy gets stuck in the local optimum at 3 m, because it does not have enough "energy" to "climb out" of its "stable, low-energy" state.

These examples show that exhaustive sweep is the only certain method to reach the best achievable performance parameter. However, exhaustive sweep increases simulation time. In the previous examples, the basic sweeping strategy required eight to nine trials, the basic optimization strategy required five trials, and the exhaustive sweep would have required eleven trials. In a hypothetical scenario, if a designer can afford one week of design time and exhaustive sweep takes one month, exhaustive sweep would not be a viable strategy.

The strategy outlined below has been formulated to move as closely to the global optimum as possible while staying within an allowed design time. The essence is to sweep as exhaustively as possible while minimizing the number of sweep trials that increases sweep interval size beyond the fabrication precision.

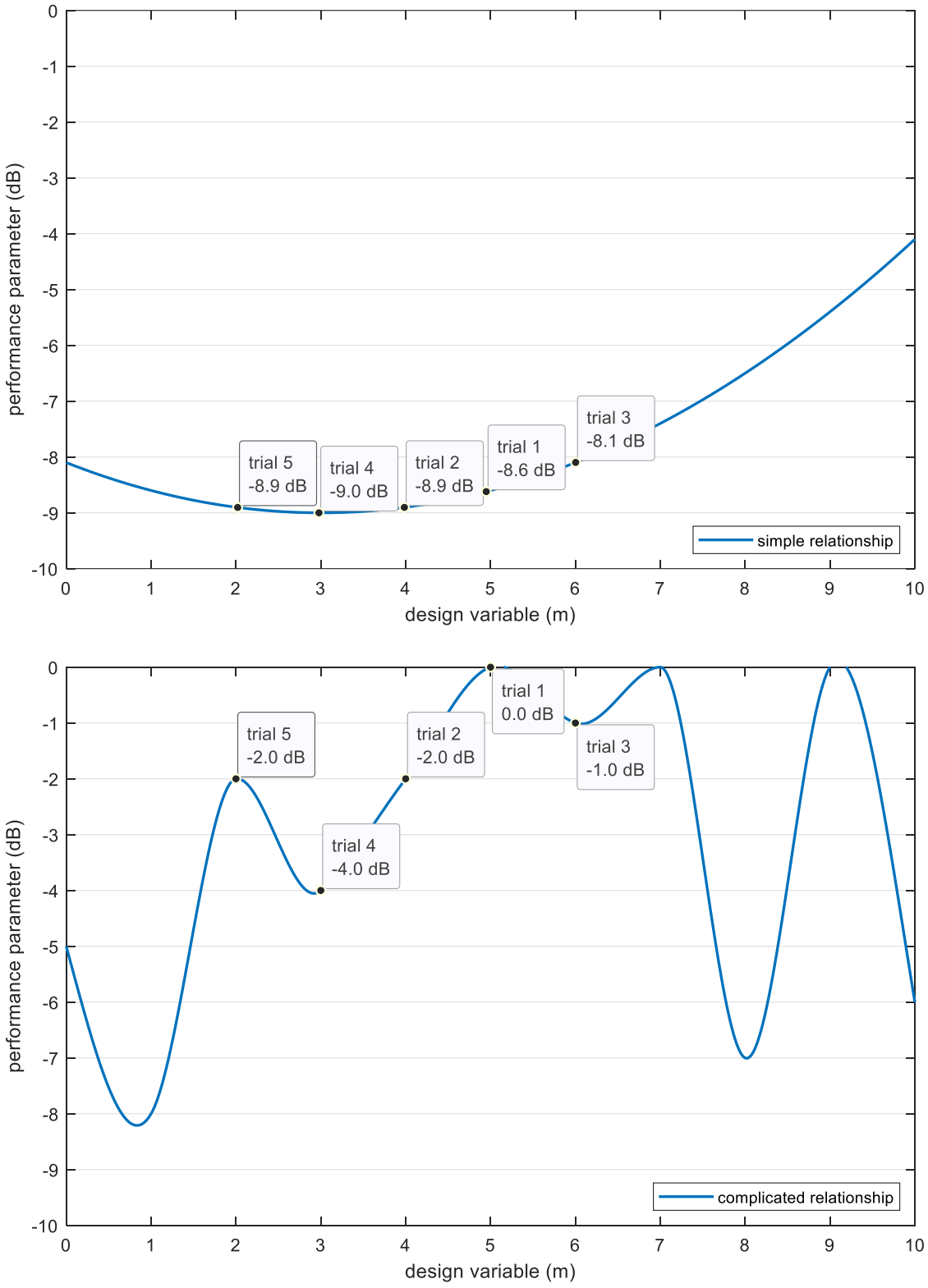

Figure 6.3: How a simple optimization strategy can fail to reach the global optimum.

1. Utilize the fastest computer hardware that can be sourced. Faster hardware reduces simulation time, allowing to sweep as exhaustively as possible.

2. Determine the design variables and their ranges. For the UHF-TV harvester antenna, the design variables are W, L, and F. Their lower bound is the size of the square feed opening (4 mm), and their upper bound is the size of the square substrate (304 mm).

3. Determine the fabrication precision. This defines the smallest interval size. Sweeping with the smallest interval size constitutes exhaustive sweep. For the UHF-TV harvester antenna, it is considered to be 1 mm.

4. Discard unnecessary combinations of design variable values. One example in the case of the UHF-TV harvester antenna is that the simulation results would be identical for all values of F when W is at its minimum. The duplicates can be discarded to reduce the number of simulation trials.

5. Sweep exhaustively if the run time of the sweep fits within the allowed design time. The run time can be estimated from the duration of a single trial and the number of trials. Otherwise, increase the interval size. It should not be increased to be more than the amount necessary to fit the run time within the design time.

6. If necessary, repeat step 5, sweeping in the vicinity of the previous best combination of design variable values.

This strategy was used to design the UHF-TV antenna discussed in Chapter 5. Note that this strategy has no loss of generality. The strategy can be used to simulate any design in general and is not limited to antennas. The strategy is most effective when the exhaustive sweep run time is comparable to the allowed design time.

6.2 Antenna Performance Parameter Weighting Strategy

Fig. 6.4 shows the gain pattern and the coordinate system of the UHF-TV harvester antenna. The gain is lowest in the ϕ = 45 °, -45 °, 135 °, and -135 ° directions in the *x*-*y* plane. The UHF-TV harvester antenna is designed to be alignment-free. To be alignment-free, the realized gain in these directions must be 0.5 or greater, so that the combined gain of the front and the rear antennas would be 1 or greater across all θ and ϕ. The minimum realized gain in the UHF-TV band was a performance parameter that needed to be considered while executing the sweeping strategy.

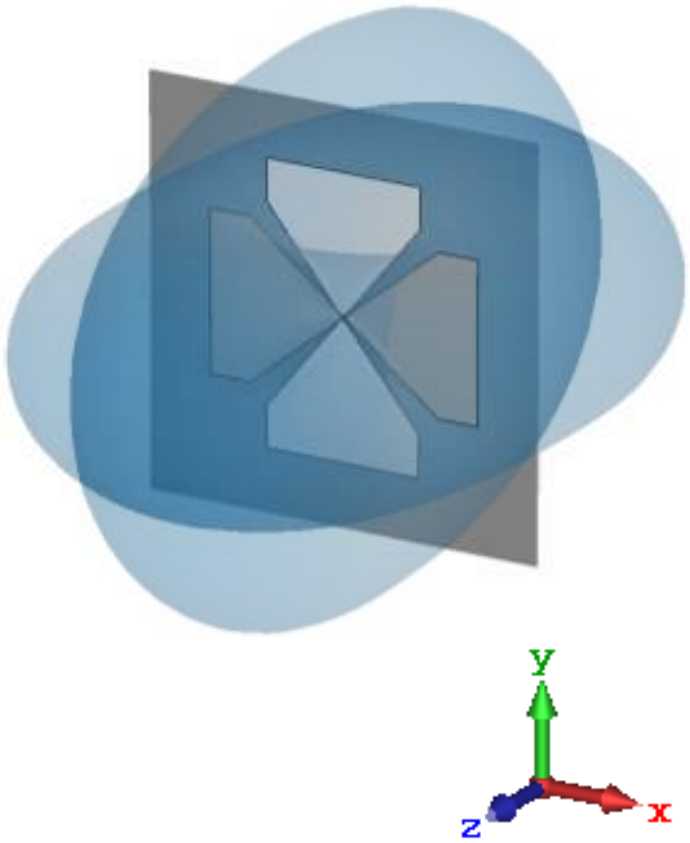

Figure 6.4: The gain pattern and the coordinate system of the UHF-TV harvester antenna.

The UHF-TV harvester antenna is also designed to be channel-agnostic. To be channel-agnostic, the antenna's bandwidth must cover the entire UHF-TV band. $S_{11} <$ -10 dB was used to define bandwidth throughout this research. The maximum S_{11} in the UHF-TV band was another performance parameter that needed to be considered while executing the sweeping strategy.

Imagine that while executing the sweeping strategy, two optima are found. One optimum has a minimum realized gain of 1 and a maximum S_{11} of -30 dB. The other optimum has a minimum realized gain of 1.5 and a maximum S_{11} of -20 dB. Which is more optimal? One optimum has to be chosen as the final design or as the focus point for the next sweep trial.

One way to decide is the following. The first optimum has a minimum realized gain that is a twofold improvement over the design goal and a maximum S_{11} that is a hundred-fold improvement over the design goal. The second optimum has a minimum realized gain that is a threefold improvement over the design goal and a maximum S_{11} that is a tenfold improvement over the design goal. The improvement is at least twofold for the first optimum and at least threefold for the second optimum. The second optimum can be chosen as being more optimal in this case. The same principle can be applied for optima that do not satisfy design goals. If one performance parameter is more important than another, the metrics can be multiplied by weighting factors, and their relative importance can be reflected.

It becomes more complicated if, for example, the minimum realized gain of the second optimum was only slightly (almost negligibly) better than the first optimum. Using the strategy just described, the second optimum would still have been the better optimum, but the first optimum would intuitively have been the better optimum. A better strategy is necessary.

A weighting function was used for designing the UHF-TV harvester antenna. The minimum realized gain variation and the maximum S_{11} variation relative to the design goals were fitted into weighting functions involving arctangent, so that variations near the design goals would have more weight, but variations away from the design goals would still influence the decision.

Fig. 6.5 illustrates the performance parameters of the UHF-TV harvester antenna. The minimum realized gain is 0.57 as can be seen in the top plot. The maximum S_{11} is -12.3 dB as can be seen in the bottom plot.

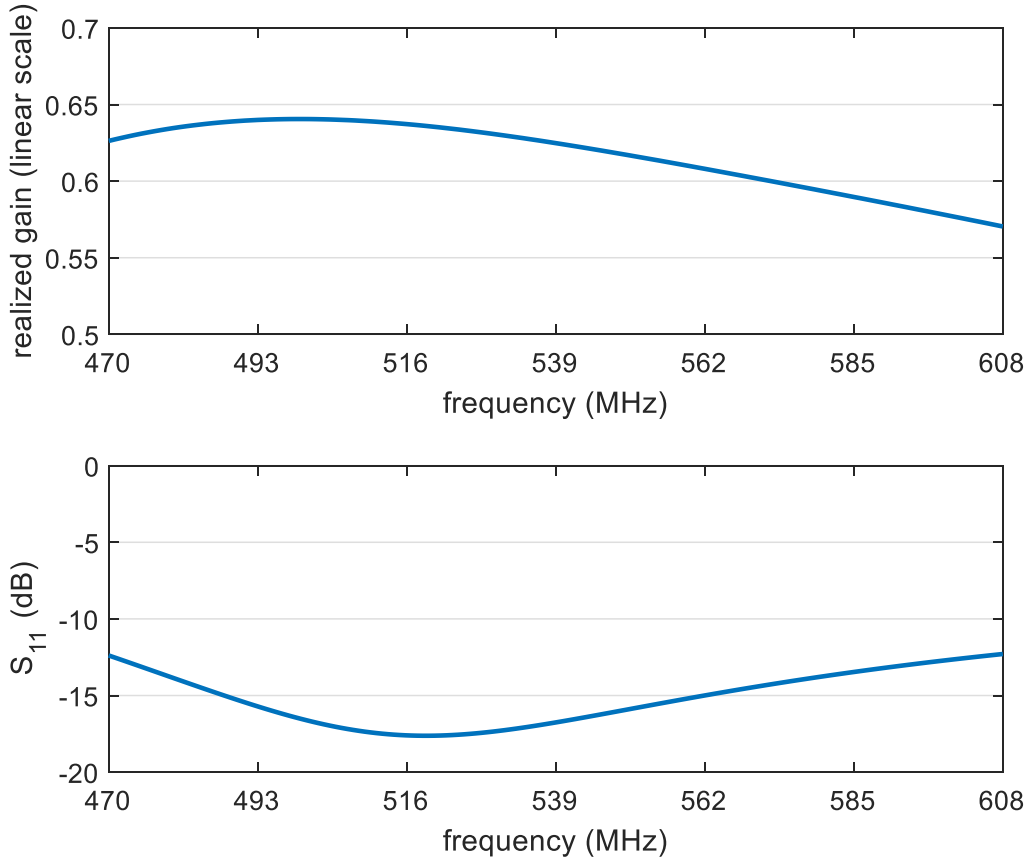

Figure 6.5: Performance parameters of the UHF-TV harvester antenna.

6.3 Matching Network Optimization Strategy

A matching circuit topology must first be chosen before the circuit can be optimized. Lumped-element matching rather than distributed-element matching was used, because transmission lines are not as compact as discrete components in designs that target long wavelengths (sub-GHz). A combination of series inductors and shunt capacitors was used. Shunt inductors and series capacitors could have also been used, but this would have increased the number of design variations which would have increased the simulation time. One-, two-, three-, and four-stage matching networks were considered and simulated. Increasing the number of stages allows wider bandwidth but has diminishing return, and the increased number of components introduces additional losses.

Voltage multiplier topology was used for the rectifying circuit. They provide higher output potential than single-diode topologies and have been used without additional dc-blocks or RF-chokes in numerous previous work [22, 12, 21, 28, 38, 43]. Increasing the number of stages allows higher output potential but has diminishing return and introduces additional losses, similarly to the case of matching networks.

The load impedance at the output of the matching network is determined by the rectifying circuit. The diodes can be modeled in simulation. However, the accuracy of the simulation results can suffer from inaccurate models, and ensuring the accuracy of the models can be extremely time consuming. Instead, physical samples were fabricated, and their input impedances were measured. Shorted series connections and opened parallel connections were used in the matching network during the initial measurement. A potential issue with this method was that the diodes may not be operating at the power level outputted by the VNA due to the impedance mismatch between the VNA and the rectifying circuit.

This issue was addressed by allowing the diodes to get gradually closer to operating at the intended power level. Matching network component values that match the measured impedance were found via ADS simulation, the component nearest to the rectifying circuit was placed on to the physical sample, the new impedance was measured, and the process was repeated. Measuring the impedance each time effectively "resets" the design process, so that any inaccuracy in simulating each component would not accumulate.

The idea of avoiding the risk of inaccurate modeling was also applied with component and PCB (printed circuit board) parasitics. S-parameter models of inductors and capacitors provided by component manufacturers could have been used, but they introduce a risk of inaccurate modeling if they are not carefully verified. The inductor and capacitor models built into ADS were used for the UHF-TV harvester matching network design. Keysight Momentum software could have been used for PCB parasitic modeling, but it also introduces a risk of inaccurate modeling if it is not carefully verified. ADS simulation without Momentum was used for the UHF-TV harvester design. It must be noted that these methods can potentially be beneficial if extensive amount of design time is invested to adequately verify their accuracy.

As mentioned at the end of section 6.1, the design variable sweeping strategy outlined in that section can be applied to simulating all designs in general. But as was mentioned, the strategy becomes less effective if the exhaustive sweep takes considerably longer than the allowed design time. This was the case when simulating higher number of matching networks stages, having to handle as many as ten design variables (inductors and capacitors), each having around 60 possible values (available inductor and capacitor values), in the case of a four-stage design. The design process of iteratively placing one physical component at a time reduces the number of design variables after each iteration and eventually allows to sweep exhaustively. Optimization algorithms built into ADS were used to simulate higher number of design variables until the number of design variables was reduced to allow exhaustive sweep.

As stated in Section 6.1, the smallest sweep interval size should be set to equal the fabrication precision. The idea is that even if performance can improve by varying a design variable value by a fraction of the fabrication precision, such physical sample capable of discerning the performance improvement would be impossible to fabricate anyway. This means that even if performance can improve by using unattainable inductor and capacitor values, such matching network would be impossible to fabricate anyway.

Similarly to the case of antenna design, the maximum S_{11} in the UHF-TV band was used as the performance parameter for designing the UHF-TV harvester matching network. Another option was to use RF-dc η as advocated by [42, 43, 46], but only the maximum S_{11} in the UHF-TV band was used as the performance parameter for designing the UHF-TV harvester matching network. This is because the harvester's ability to harvest in all UHF-TV frequencies becomes less convincing if it fails to impedance match (e.g., in terms of -10 dB) regardless of whether it has an arguably adequate an RF-dc η.

Fig. 6.6 shows example results of the UHF-TV harvester matching network optimization. The top plot shows the best result. Two circuits for the upper and the lower half bands together achieve -10 dB matching across the entire UHF-TV band and across all power levels from -20 dBm to 0 dBm. The load was represented by a 3.3 kΩ resistor. The bottom plot shows a result of a configuration that does not achieve these same design goals. It achieves -10 dB matching across the entire UHF-TV band and across all power levels from -20 dBm to -10 dBm, but it falls slightly short of achieving -10 dB matching across the entire UHF-TV band at 0 dBm. It uses three-stage matching network designs, whereas the former example uses two-stage designs.

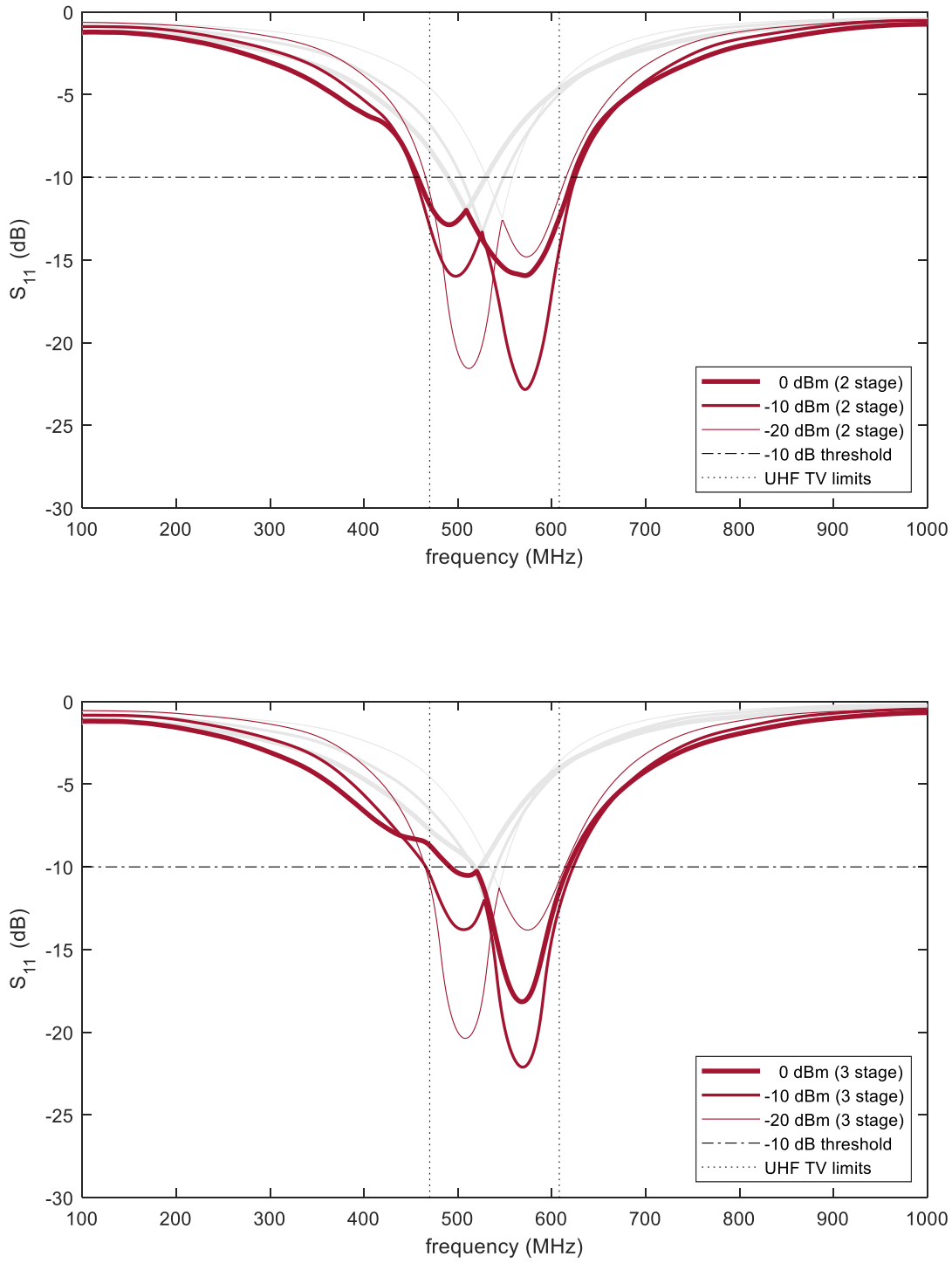

Figure 6.6: Example results of the UHF-TV harvester matching network optimization.

6.4 Benchmarking the Amount of Harvested Power Among Related Work

Comparing the performance of ambient RF energy harvesting systems proposed in literature is difficult for a number of reasons. They have varying design approaches (e.g., high directivity of [17] versus wide beam-width of this work) and characterization methods (e.g., using a resistor load to measure the amount of harvested power as demonstrated by [57] versus using a functioning WSN/IoT device as demonstrated by this work). Many simply do not provide comprehensive enough data for comparison.

The amount of harvested power is a key metric of ambient RF energy harvesting systems. Fig. 6.7 shows the amount of harvested power among related work. The power levels have been extrapolated in terms of distance to make the comparison make sense. Testing the systems under an identical condition would have been more ideal but would have been unfeasible. The systems do not even target the same frequency band. Extrapolation was performed according to Friis formula which describes received power as being inversely proportional to distance squared [53]. Four other related work were selected for comparison, a significant amount considering the scarcity of work that report the amount harvested power along with distance information. The furthest reported distance (6.3 km) was chosen as the common distance for extrapolation, so that arguably the most significant data would not be altered. Considering the difficulty of facilitating a fair and accurate comparison, this method serves well to provide intuition as to how performances of the related work compare.

The UHF-TV harvester shows the highest performance followed by the FM harvester, respectively showing -7.0 dBm and -12.6 dBm. At -17.7 dBm and -15.9 dBm, [17] and [20, 39] respectively show that they would harvest more than -20 dBm, which is considered to be enough power for Schottky diodes and PMUs to operate and provide useful function. The distance appears to be too far for [49] and [57] to harvest enough power to cross this threshold, respectively showing -65.2 dBm and -60.2 dBm.

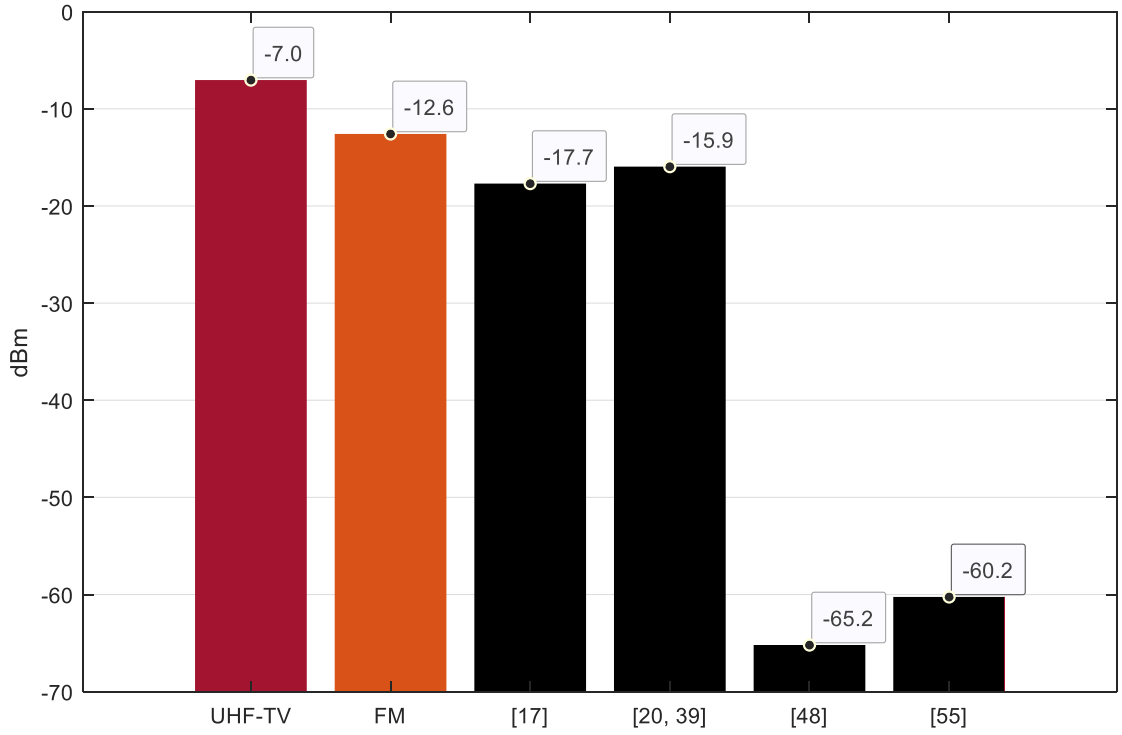

Figure 6.7: Comparison of power harvested at 6.3 km (extrapolated) among related work.

6.5 Future Work

One aspect of this work that can benefit from improvement most significantly and immediately is the form factor. The system currently consists of antennas, matching and rectifier circuits, and PMUs all on separate substrates. Integrating on to a single substrate would vastly improve the usability of the system. Rather than the current practice of utilizing the PMU evaluation boards, only the necessary components of the PMUs would be integrated on to the single substrate.

The reason why this was not done from the beginning was to ensure that the research produces presentable results in timely manner. Setting a more challenging initial goal decreases the chance of obtaining presentable results within the allowed time. Publishing results invites feedback from other scholars in the field which can be used to improve the research as opportunities arise.

A single-piece matching circuit (as opposed to having two circuits for the upper and lower half bands) would allow a single pair of UHF-TV antennas to be used. The system would be integrated on to a single substrate more easily this way and yield a more compact form factor.

Due to the orientations of the UHF-TV and the FM antennas, it would be unnatural to combine them on to a single planar substrate without altering their operating principle. To achieve this, a north-south and east-west polarized dual band (UHF-TV and FM) set of antennas can be designed. Designing a full-UHF-TV-and-FM-band matching circuit would be a formidable challenge. UHF-TV and FM harvesters can also instead be separate systems, which would allow the systems to be more compact.

6.6 Applications

Potential applications for UHF-TV and FM energy harvesting are described in Chapter 1. In addition, the design aspects unique to this work makes it suitable for a number of applications that are worth mentioning.

The large antenna sizes that correspond to long wavelengths (sub-GHz) allow the harvesters to receive more power. Smart agriculture and structural monitoring (buildings, bridges, etc.) span across large areas and may comfortably accommodate the UHF-TV and FM energy harvesting antennas. Users in these fields may not necessarily be RF experts, so they may appreciate or even necessitate the alignment-free and channel-agnostic nature of the system. The ability to operate indefinitely without needing to replace batteries would increase safety in structural monitoring applications by not requiring users to frequently climb large structures. As demonstrated with the antenna printed on window glass described in Chapter 4, the antennas and the systems can be seamlessly integrated into structures.

CHAPTER 7
CONCLUSION

7.1 Presented Outcome

This research demonstrates an ambient RF energy harvesting system (fabricated on low cost FR4) capable of harvesting from all surrounding UHF-TV and FM towers across km ranges in all UHF-TV and FM frequencies simultaneously to perpetually power a WSN. For UHF-TV, front and rear antenna gains combined is 1 or greater across all θ and ϕ, allowing isotropic harvesting (omnidirectional for FM). The system achieves -10 dB matching across the entire frequency bands. The RF-dc η is as high as 70 %. The system is as sensitive as -18 dBm. The UHF-TV portion harvested as much as 231 μW across 5.83 km (885 μW across 1.53 km for FM). The alignment-free, channel-agnostic nature of this work demonstrates the potential for widespread adaption of ambient RF energy harvesting.

7.2 Publications / Contributions

- E. M. Jung et al., "A wideband, quasi-isotropic, kilometer-range FM energy harvester for perpetual IoT," *IEEE Microw. Wireless Compon. Lett.*, vol. 30, no. 2, pp. 201–204, Feb. 2020.

  This paper demonstrates an alignment-free, channel-agnostic, km-range, ambient RF FM energy harvester capable of harvesting triple-digit μW from outside while indoors to cold-start and to perpetually power a WSN without needing to periodically shut down [30].

- Y. Cui, E. M. Jung, A. O. Adeyeye, C. Lynch, X. He and M. Tentzeris, "Additively manufactured RF devices for 5G, IoT, RFID, WSN, and smart city applications," *Int. J. High Speed Electron. Syst.*, vol. 29, no. 01n04, 2020.

  This paper discusses the design, fabrication, and measurement details of the FM energy harvester's additively manufactured matching and rectifying circuit [31].

- T. Cheng et al., "DUCO: Autonomous large-scale direct-circuit-writing (DCW) on vertical everyday surfaces using a scalable hanging plotter," *Proc. ACM Interact. Mob. Wearable Ubiquitous Technol.*, vol. 5, no. 3, Sep. 2021.

  This paper extends the FM energy harvester work by printing SNP on a window glass to seamlessly integrate the antenna into everyday surroundings [32].

- E. M. Jung, W.-S. Lee, R. J. Vyas, and M. M. Tentzeris, "A wideband, quasi-isotropic, ambient RF energy harvester combining UHF-TV and FM," *IEEE Antennas and Wireless Propag. Lett.*, vol. 20, no. 10, pp. 1854–1858, Oct. 2021.

  This paper demonstrates an alignment-free, channel-agnostic, km-range, ambient RF UHF-TV energy harvester capable of supplying triple-digit μW to cold-start and to perpetually power a WSN. It incorporates the FM energy harvester from the previous work by dc combining [34].

- E. M. Jung, W.-S. Lee, and M. M. Tentzeris, "Far-field wireless charging technologies for widespread adaption," *IEEE Access*, submitted for publication.

  This paper surveys commercial and academic efforts to bring far-field charging towards widespread adaption. It compares the merits of published work in the field. It advocates focusing on low-power industrial WSN/IoT applications as well as testing for practical usability with load devices that provide actual function [59].

REFERENCES

[1] S. Kim *et al.*, "Ambient rf energy-harvesting technologies for self-sustainable standalone wireless sensor platforms," *Proceedings of the IEEE*, vol. 102, no. 11, pp. 1649–1666, 2014.

[2] A. Collado and A. Georgiadis, "Conformal hybrid solar and electromagnetic (em) energy harvesting rectenna," *IEEE Transactions on Circuits and Systems I: Regular Papers*, vol. 60, no. 8, pp. 2225–2234, 2013.

[3] K. Niotaki, A. Collado, A. Georgiadis, S. Kim, and M. M. Tentzeris, "Solar/electromagnetic energy harvesting and wireless power transmission," *Proceedings of the IEEE*, vol. 102, no. 11, pp. 1712–1722, 2014.

[4] J. Bito, R. Bahr, J. G. Hester, S. A. Nauroze, A. Georgiadis, and M. M. Tentzeris, "A novel solar and electromagnetic energy harvesting system with a 3-d printed package for energy efficient internet-of-things wireless sensors," *IEEE Transactions on Microwave Theory and Techniques*, vol. 65, no. 5, pp. 1831–1842, 2017.

[5] Y. Zhang, S. Shen, C. Y. Chiu, and R. Murch, "Hybrid rf-solar energy harvesting systems utilizing transparent multiport micromeshed antennas," *IEEE Transactions on Microwave Theory and Techniques*, pp. 1–13, 2019.

[6] L. J. Chu, "Physical limitations of omni-directional antennas," *Journal of Applied Physics*, vol. 19, no. 12, pp. 1163–1175, 1948. eprint: `https://doi.org/10.1063/1.1715038`.

[7] F. Yildiz, "Potential ambient energy-harvesting sources and techniques.," *Journal of technology Studies*, vol. 35, no. 1, pp. 40–48, 2009.

[8] C. A. Balanis, *Antenna theory: analysis and design*. John wiley & sons, 2016.

[9] F. Congedo, G. Monti, L. Tarricone, and M. Cannarile, "Broadband bowtie antenna for rf energy scavenging applications," in *Proceedings of the 5th European Conference on Antennas and Propagation (EUCAP)*, 2011, pp. 335–337.

[10] R. Shigeta *et al.*, "Ambient rf energy harvesting sensor device with capacitor-leakage-aware duty cycle control," *IEEE Sensors Journal*, vol. 13, no. 8, pp. 2973–2983, 2013.

[11] C. Mikeka, H. Arai, A. Georgiadis, and A. Collado, "Dtv band micropower rf energy-harvesting circuit architecture and performance analysis," in *2011 IEEE International Conference on RFID-Technologies and Applications*, 2011, pp. 561–567.

[12] C. Song, Y. Huang, J. Zhou, and P. Carter, "Improved ultrawideband rectennas using hybrid resistance compression technique," *IEEE Transactions on Antennas and Propagation*, vol. 65, no. 4, pp. 2057–2062, 2017.

[13] C. Song *et al.*, "A novel six-band dual cp rectenna using improved impedance matching technique for ambient rf energy harvesting," *IEEE Transactions on Antennas and Propagation*, vol. 64, no. 7, pp. 3160–3171, 2016.

[14] Y. Hu, S. Sun, H. Xu, and H. Sun, "Grid-array rectenna with wide angle coverage for effectively harvesting rf energy of low power density," *IEEE Transactions on Microwave Theory and Techniques*, vol. 67, no. 1, pp. 402–413, 2019.

[15] M. Piñuela, P. D. Mitcheson, and S. Lucyszyn, "Ambient rf energy harvesting in urban and semi-urban environments," *IEEE Transactions on Microwave Theory and Techniques*, vol. 61, no. 7, pp. 2715–2726, 2013.

[16] Y. Liu, X. Liu, X. Yang, and D. Xie, "Log-periodic antenna with interdigital structure for energy harvesting from tv broadcast tower," in *2015 Asia-Pacific Microwave Conference (APMC)*, vol. 2, 2015, pp. 1–3.

[17] R. J. Vyas, B. B. Cook, Y. Kawahara, and M. M. Tentzeris, "E-wehp: A battery-less embedded sensor-platform wirelessly powered from ambient digital-tv signals," *IEEE Transactions on Microwave Theory and Techniques*, vol. 61, no. 6, pp. 2491–2505, 2013.

[18] A. N. Parks and J. R. Smith, "Sifting through the airwaves: Efficient and scalable multiband rf harvesting," in *2014 IEEE International Conference on RFID (IEEE RFID)*, 2014, pp. 74–81.

[19] A. N. Parks, A. P. Sample, Y. Zhao, and J. R. Smith, "A wireless sensing platform utilizing ambient rf energy," in *2013 IEEE Topical Conference on Biomedical Wireless Technologies, Networks, and Sensing Systems*, 2013, pp. 154–156.

[20] A. Sample and J. R. Smith, "Experimental results with two wireless power transfer systems," in *2009 IEEE Radio and Wireless Symposium*, 2009, pp. 16–18.

[21] A. Georgiadis, G. Vera Andia, and A. Collado, "Rectenna design and optimization using reciprocity theory and harmonic balance analysis for electromagnetic (em) energy harvesting," *IEEE Antennas and Wireless Propagation Letters*, vol. 9, pp. 444–446, 2010.

[22] A. Noguchi and H. Arai, "Small loop rectenna for rf energy harvesting," in *2013 Asia-Pacific Microwave Conference Proceedings (APMC)*, 2013, pp. 86–88.

[23] X. Wang and A. Mortazawi, "High sensitivity rf energy harvesting from am broadcasting stations for civilian infrastructure degradation monitoring," in *2013 IEEE International Wireless Symposium (IWS)*, 2013, pp. 1–3.

[24] T. Ajmal, V. Dyo, B. Allen, D. Jazani, and I. Ivanov, "Design and optimisation of compact rf energy harvesting device for smart applications," *Electronics Letters*, vol. 50, no. 2, pp. 111–113, 2014.

[25] J. A. Hagerty, F. B. Helmbrecht, W. H. McCalpin, R. Zane, and Z. B. Popovic, "Recycling ambient microwave energy with broad-band rectenna arrays," *IEEE Transactions on Microwave Theory and Techniques*, vol. 52, no. 3, pp. 1014–1024, 2004.

[26] J. Zbitou, M. Latrach, and S. Toutain, "Hybrid rectenna and monolithic integrated zero-bias microwave rectifier," *IEEE Transactions on Microwave Theory and Techniques*, vol. 54, no. 1, pp. 147–152, 2006.

[27] S. Daskalakis, A. Georgiadis, A. Bletsas, and C. Kalialakis, "Dual band rf harvesting with low-cost lossy substrate for low-power supply system," in *2016 10th European Conference on Antennas and Propagation (EuCAP)*, 2016, pp. 1–4.

[28] D. Masotti, A. Costanzo, M. D. Prete, and V. Rizzoli, "Genetic-based design of a tetra-band high-efficiency radio-frequency energy harvesting system," *IET Microwaves, Antennas Propagation*, vol. 7, no. 15, pp. 1254–1263, 2013.

[29] B. L. Pham and A. Pham, "Triple bands antenna and high efficiency rectifier design for rf energy harvesting at 900, 1900 and 2400 mhz," in *2013 IEEE MTT-S International Microwave Symposium Digest (MTT)*, 2013, pp. 1–3.

[30] E. M. Jung *et al.*, "A wideband, quasi-isotropic, kilometer-range fm energy harvester for perpetual iot," *IEEE Microwave and Wireless Components Letters*, vol. 30, no. 2, pp. 201–204, 2020.

[31] Y. Cui, E. M. Jung, A. Adeyeye, C. Lynch, X. He, and M. Tentzeris, "Additively manufactured rf devices for 5g, iot, rfid, wsn, and smart city applications," *International Journal of High Speed Electronics and Systems*, vol. 29, no. 01n04, p. 2 040 016, 2020. eprint: `https://doi.org/10.1142/S0129156420400169`.

[32] T. Cheng *et al.*, "Duco: Autonomous large-scale direct-circuit-writing (dcw) on vertical everyday surfaces using a scalable hanging plotter," *Proc. ACM Interact. Mob. Wearable Ubiquitous Technol.*, vol. 5, no. 3, Sep. 2021.

[33] A. Desai and P. Nayeri, "A multi-linear polarization reconfigurable plus shaped dipole antenna for wireless energy harvesting applications," in *2018 International Applied Computational Electromagnetics Society Symposium (ACES)*, 2018, pp. 1–2.

[34] E. M. Jung, W.-S. Lee, R. J. Vyas, and M. M. Tentzeris, "A wideband, quasi-isotropic, ambient rf energy harvester combining uhf-tv and fm," *IEEE Antennas and Wireless Propagation Letters*, vol. 20, no. 10, pp. 1854–1858, 2021.

[35] R. Rhea, "The yin-yang of matching: Part 1—basic matching concepts," *High Frequency Electronics*, vol. 5, no. 3, pp. 16–25, 2006.

[36] R. Rhea, "The yin-yang of matching: Part 2—practical matching techniques," *High Frequency Electronics*, vol. 5, no. 4, pp. 28–40, 2006.

[37] S. D. Assimonis, S. Daskalakis, and A. Bletsas, "Efficient rf harvesting for low-power input with low-cost lossy substrate rectenna grid," in *2014 IEEE RFID Technology and Applications Conference (RFID-TA)*, 2014, pp. 1–6.

[38] D. Masotti, A. Costanzo, P. Francia, M. Filippi, and A. Romani, "A load-modulated rectifier for rf micropower harvesting with start-up strategies," *IEEE Transactions on Microwave Theory and Techniques*, vol. 62, no. 4, pp. 994–1004, 2014.

[39] A. P. Sample, D. J. Yeager, P. S. Powledge, A. V. Mamishev, and J. R. Smith, "Design of an rfid-based battery-free programmable sensing platform," *IEEE Transactions on Instrumentation and Measurement*, vol. 57, no. 11, pp. 2608–2615, 2008.

[40] H. Sun, Y. Guo, M. He, and Z. Zhong, "Design of a high-efficiency 2.45-ghz rectenna for low-input-power energy harvesting," *IEEE Antennas and Wireless Propagation Letters*, vol. 11, pp. 929–932, 2012.

[41] Z. Liu, Z. Zhong, and Y. Guo, "Enhanced dual-band ambient rf energy harvesting with ultra-wide power range," *IEEE Microwave and Wireless Components Letters*, vol. 25, no. 9, pp. 630–632, 2015.

[42] F. Bolos, D. Belo, and A. Georgiadis, "A uhf rectifier with one octave bandwidth based on a non-uniform transmission line," in *2016 IEEE MTT-S International Microwave Symposium (IMS)*, 2016, pp. 1–3.

[43] J. Kimionis, A. Collado, M. M. Tentzeris, and A. Georgiadis, "Octave and decade printed uwb rectifiers based on nonuniform transmission lines for energy harvesting," *IEEE Transactions on Microwave Theory and Techniques*, vol. 65, no. 11, pp. 4326–4334, 2017.

[44] B. R. Marshall, M. M. Morys, and G. D. Durgin, "Parametric analysis and design guidelines of rf-to-dc dickson charge pumps for rfid energy harvesting," in *2015 IEEE International Conference on RFID (RFID)*, 2015, pp. 32–39.

[45] S. Hemour and K. Wu, "Radio-frequency rectifier for electromagnetic energy harvesting: Development path and future outlook," *Proceedings of the IEEE*, vol. 102, no. 11, pp. 1667–1691, 2014.

[46] S. D. Assimonis, S. Daskalakis, and A. Bletsas, "Sensitive and efficient rf harvesting supply for batteryless backscatter sensor networks," *IEEE Transactions on Microwave Theory and Techniques*, vol. 64, no. 4, pp. 1327–1338, 2016.

[47] A. Costanzo, A. Romani, D. Masotti, N. Arbizzani, and V. Rizzoli, "Rf/baseband codesign of switching receivers for multiband microwave energy harvesting," *Sensors and Actuators A: Physical*, vol. 179, pp. 158 –168, 2012.

[48] K. Gudan, S. Shao, J. J. Hull, J. Ensworth, and M. S. Reynolds, "Ultra-low power 2.4 ghz rf energy harvesting and storage system with -25 dbm sensitivity," in *2015 IEEE International Converence on RFID (RFID)*, 2015, pp. 40–46.

[49] S. Kitazawa, H. Ban, and K. Kobayashi, "Energy harvesting from ambient rf sources," in *2012 IEEE MTT-S International Microwave Workshop Series on Innovative Wireless Power Transmission: Technologies, Systems, and Applications*, 2012, pp. 39–42.

[50] S. Shen, Y. Zhang, C. Chiu, and R. Murch, "A triple-band high-gain multibeam ambient rf energy harvesting system utilizing hybrid combining," *IEEE Transactions on Industrial Electronics*, vol. 67, no. 11, pp. 9215–9226, 2020.

[51] R. Fano, "Theoretical limitations on the broadband matching of arbitrary impedances," *Journal of the Franklin Institute*, vol. 249, no. 1, pp. 57 –83, 1950.

[52] C. H. P. Lorenz *et al.*, "Breaking the efficiency barrier for ambient microwave power harvesting with heterojunction backward tunnel diodes," *IEEE Transactions on Microwave Theory and Techniques*, vol. 63, no. 12, pp. 4544–4555, 2015.

[53] H. T. Friis, "A note on a simple transmission formula," *Proceedings of the IRE*, vol. 34, no. 5, pp. 254–256, 1946.

[54] R. Vyas, "An embedded, wireless-energy-harvesting platform (e-wehp) for powering sensors using existing, ambient, wireless signals present in the air," Ph.D. dissertation, Georgia Institute of Technology, 2014.

[55] U. Muncuk, K. Alemdar, J. D. Sarode, and K. R. Chowdhury, "Multiband ambient rf energy harvesting circuit design for enabling batteryless sensors and iot," *IEEE Internet of Things Journal*, vol. 5, no. 4, pp. 2700–2714, 2018.

[56] H. Sun, Y. Guo, M. He, and Z. Zhong, "A dual-band rectenna using broadband yagi antenna array for ambient rf power harvesting," *IEEE Antennas and Wireless Propagation Letters*, vol. 12, pp. 918–921, 2013.

[57] V. Kuhn, C. Lahuec, F. Seguin, and C. Person, "A multi-band stacked rf energy harvester with rf-to-dc efficiency up to 84%," *IEEE Transactions on Microwave Theory and Techniques*, vol. 63, no. 5, pp. 1768–1778, 2015.

[58] C. Song, Y. Huang, J. Zhou, J. Zhang, S. Yuan, and P. Carter, "A high-efficiency broadband rectenna for ambient wireless energy harvesting," *IEEE Transactions on Antennas and Propagation*, vol. 63, no. 8, pp. 3486–3495, 2015.

[59] E. M. Jung, W.-S. Lee, and M. M. Tentzeris, "Far-field wireless charging technologies for widespread adaption," *IEEE Access*, submitted for publication.

VITA

Jung moved from Korea to study in the United States in 1999. He received his B.S. in 2008 and M.S. in 2009 from the University of Michigan with focuses on microelectromechanical systems and semiconductor fabrication. He worked as a translator for two years during his military service before proceeding to work in the industry for three years as an analog and digital circuit designer. He received his Ph.D. in 2021 from the Georgia Institute of Technology for his research in electromagnetics.